UNIVERSITY OF BIRMINGHAM

University of Birmingham

School of Biosciences

How does the expression of phospholipase B influence the host pathogen relationship between *Cryptococcus neoformans* and the macrophage? And an investigation into the properties of two *Bdellovibrio bacteriovorus* C-di-GMP metabolism proteins – Bd2325 and Bd1971

A research Thesis submitted by:

Robert J. Evans

As part of the requirement for the degree of:

MRes in Molecular and Cellular Biology

Under the supervision of:

Dr Robin May

And

Dr Andrew Lovering

Robert Evans

Dear Reader

The following thesis is a composite of two separate research projects which were undertaken by the author for the award of an MRes in Molecular and Cellular Biology within the School of Biosciences at the University of Birmingham.

Due to the different nature of each project it is hard to draw similarities between the two, although it is true that both may be of interest to a microbiologist as they both focus on microorganisms – *Cryptococcus neoformans* and *Bdellovibrio bacteriovorus* respectively. In addition to this both projects examine important proteins expressed by each organism which appear to contribute to their respective life cycles.

Part one of this thesis will detail the first research project which sought to characterise the contribution of the enzyme phospholipase B to the intracellular lifecycle employed by the pathogenic fungus *Cryptococcus neoformans* which has the ability to survive within the phagolysosome of immune cell macrophages.

Part two of this thesis switches kingdoms to detail the second project which examined the predatory bacterium *Bdellovibrio bacteriovorus.* This bacterium has a unique lifecycle which involves predation of other gram negative bacteria resulting in prey cell invasion and an interperiplasmic growth and replication phase. The aim of this project was to characterise the nature of two *B. bacteriovorus* proteins which alter the levels of the bacterial secondary messenger C-di-GMP which is thought to control aspects of the bacteria's predatory lifecycle.

As each part is so different in its target organism and methodologies it is understandable that the entire thesis may not be of professional interest to you, however it is hoped an appreciation of the thesis as a whole can nonetheless be found through a love of science and pursuit of new knowledge.

Yours faithfully

Robert Evans

University of Birmingham

Robert Evans

ABSTRACT - PART ONE

How does the expression of phospholipase B influence the host pathogen relationship between *Cryptococcus neoformans* and the macrophage?

Supervisor - Dr Robin C. May

Cryptococcus neoformans is a pathogenic fungus that can cause fatal meningoencephalitis disease in immune compromised individuals. Fatal disease occurs when *C. neoformans* disseminates from the initial site of infection in the lungs to the central nervous system. Among the virulence factors which contribute to cryptococcal disease phospholipase B is the least understood. Phospholipase B is a phospholipid modifying enzyme, it currently has three confirmed enzymatic functions – phospholipase A_1 activity, phospholipase A_2 activity and lysophospholipase activity. Previous studies have revealed that phospholipase B is essential for full cryptococcal virulence. Phospholipase B has been implicated in multiple stages of cryptococcosis pathogenesis including intracellular survival within alveolar macrophages, escape from macrophages and dissemination to the central nervous system. In this study we sought to further characterise the phenotypes that phospholipase B deficiency produces in *Cryptococcus neoformans*. To do this we infected J774 murine macrophages with a phospholipase B knockout *Cryptococcus neoformans var. grubii* strain called PLB and compared the resulting infection phenotype with that of the wild type parent strain – H99. We found that phospholipase B is required for intracellular proliferation within macrophages. Phospholipase B deficiency also produces *Cryptococcus* cells which are larger in diameter than wild type cells. In this study we also report the first application of high throughput lipidomic analysis of *Cryptococcus* infected macrophages and identify a potential eicosanoid modifying treatment for *Cryptococcus* infection.

Robert Evans

ABSTRACT- PART TWO

An investigation into the properties of two *Bdellovibrio bacteriovorus* C-di-GMP metabolism proteins – Bd2325 and Bd1971

Supervisor – Dr Andrew Lovering

Bdellovibrio bacteriovorus is a small motile bacterium with a unique lifecycle; it has evolved to predate gram negative bacteria intracellularly, growing inside the prey cell periplasm. The predatory lifecycle of *B. bacteriovorus* is multifaceted and involves many distinct stages including prey cell recognition, attachment, cellular invasion, modification of prey cell structure, cellular replication and finally escape from the prey cell; each stage in the lifecycle appears to be tightly controlled by bacterial signalling cascades. At least some of the regulation within *B. bacteriovorus* is mediated by the small secondary messenger molecule C-di-GMP which has come to prominence in the last few years as an important universal regulator of bacterial life processes such as controlling adhesion to surfaces, motility and the expression of virulence factors. The cytosolic level of C-di-GMP is controlled by the actions of two groups of opposing enzymes – guanylate cyclase GGDEF domain proteins synthesise C-di-GMP while phosphodiesterase EAL or HD-GYP domain proteins degrade C-di-GMP. In this study we attempt to discover the mechanism of signalling for two *B. bacteriovorus* phosphodiesterase proteins Bd2325 and Bd1971 – these proteins are a HD-GYP phosphodiesterase, and a EAL phosphodiesterase respectively. Determination of a crystal structure for these proteins would be invaluable to discover the function of these proteins and would aid *B. bacteriovorus* research and C-di-GMP signalling research greatly. Herein we report the refinement of recombinant expression and purification of each protein followed by preliminary biochemical analysis.

ACKNOWLEDGEMENTS

First and foremost I would like to thank my two project supervisors Robin May and Andrew Lovering for their advice and enthusiasm throughout the project. I'm looking forward to the next three years with both of you as PhD supervisors.

Secondly I would like to thank Simon Johnston, Nicola Cumley, Kerstin Voelz, Leanne Smith, Wilber Sabiiti and Rhiannon Pursall for welcoming me so warmly into the May Lab and helping me with my project. I feel very lucky to have worked with such nice people.

Finally I would like to thank Andy Southam for his help with the mass spectrometry analysis and sample preparation.

PART ONE

INTRODUCTION 1

1.1 The *Cryptococcus* family 1

1.2 *Cryptococcus* neoformans pathogenesis 2

1.3 *Cryptococcus* neoformans virulence factors 4

1.4 Phospholipase B and *Cryptococcus neoformans* pathogenesis 8

1.5 Project aims 10

MATERIALS AND METHODS 11

2.1 Cells and strains 11

2.2 Intracellular proliferation assay 11

2.3 Cell size assay 14

2.4 Lipidomics study 15

RESULTS 20

3.1 Phospholipase B is required for in vitro cryptococcal intracellular growth. 20

3.2 *PLB1* knockout produces a distinct, much larger cellular morphology in PLB. 29

3.3 A high throughput lipidomic analysis of *C. neoformans* infected macrophages 38

3.4 Cryptococcal intracellular proliferation can be modulated with eicosanoid modifying treatments 50

DISCUSSION 54

INTRODUCTION 66

1.1 Bdellovibrio bacteriovorus 66

1.2 – Bdellovibrio bacteriovorus lifecycle 68

1.3 Bdellovibrio bacteriovorus and C-di-GMP signalling 74

1.4 Project aims 79

MATERIALS AND METHODS 87

2.1 Bdellovibrio bacteriovorus protein expression 87

2.2 Pre purification lysate preparation 89

2.3 Protein purification 90

2.4 Analysis of purified protein 92

2.5 Inclusion body resolubilisation and refolding 94

RESULTS.....96

3.1 – Bd2325 expression.....96

3.2 Recombinant Bd2325^{SF} appears to be sequestered in insoluble inclusion bodies following expression in E. coli. 97

3.3 Bd2325^{SF} inclusion bodies can be solubilised in highly denaturing conditions. 99

3.4 Bd2325SF protein refolding shows varying success using different methods 99

3.5 An autoinduction expression protocol allows the expression of Bd2325^{LF} and improves the solubility of Bd2325^{SF}.....107

3.6 – Bd1971 expression.....113

3.7 An alternatively positioned His-tag does not improve the stability of Bd1971.....113

3.8 Autoinduction expression of Bd1971 significantly improves protein stability 115

3.9 Bd1971 – purified protein analysis.....119

3.10 Preliminary AUC analysis of Bd1971 shows possible oligomeric state changes in the presence of cAMP.....121

DISCUSSION 125

4.1 Bd2325.....125

4.2 Bd1971.....130

4.3 Conclusion 134

BIBLIOGRAPHY 135

Robert Evans

ABREVIATIONS

Part one

15d-PGJ$_2$ - 15 deoxy$\Delta^{12, 14}$ prostaglandin J$_2$

AA – Arachidonic acid

AIDS – Acquired immunodeficiency syndrome

AML – Acute myeloid leukemia

BAP – Bezafibrate and Medroxyprogesterone acetate combination treatment

BEZ - Bezafibrate

CD4 – Cluster of differentiation 4

CFU – Colony forming unit

CNS – Central nervous system

COX-1 – Cyclooxygenase 1

COX-2 – Cyclooxygenase 2

DMEM – Dulbecco's modified eagle medium

DMSO – Dimethyl sulfoxide

DPPC - Dipalmitoylphosphate

FBS – Fetal bovine calf serum

FT-ICR – Fourier transform ion cyclotron resonance

GalXm - Galactoxymannan

GxM - Glucuronoxymannan

H99 – *Cryptococcus neoformans* wild type strain H99 – serotype A

HIV – Human immunodeficiency virus

HPLC – High performance liquid chromatography

IL-12 – Interleukin -12

IL-13 – Interleukin -13

IL-4 – Interleukin - 4

IPR – Intercellular proliferation rate

LP - Lipoxin

LPL - Lysophospholipase

LPTA – Lysophospholipid transacetylase

LT - Leukotriene

m/z – Mass charge ratio

MPA – Medroxyprogesterone acetate

PA - Glycerophosphate

PBS – Phosphate buffered saline

PCA – Principle component analysis

PGA_3 – Prostaglandin A_3

PGD_2 – Prostaglandin D_2

PGE_2 – Prostaglandin E_2

PGH_2 – Prostaglandin H_2

PGJ_3 – Prostaglandin J_3

PI - Glycerophosphoinisitol

Pla1 – Phospholipase A1

Pla2 – Phospholipase A2

Plb – Phospholipase B

PLB – *Cryptococcus neoformans* H99 strain with *PLB1* knockout

PLB1 - *Cryptococcus neoformans* PLB strain with *PLB1* rescue version 1

PLB2 - *Cryptococcus neoformans* PLB strain with *PLB1* rescue – version 2

PMA – Phorbol myristate acetate

SF-DMEM – Serum free DMEM

Th1 – T helper cell type 1

Th2 – T helper cell type 2

YPD – Yeast peptone dextrose media

Robert Evans

Part two

Ala – Alanine

Asn - Asparagine

Asp – Aspartic acid

AUC – Analytical ultra centrifuge

BBCF – Birmingham Biophysics Characterisation Facility

BSA – Bovine serum albumin

cAMP – Cyclic adenosine 3',5' monophosphate

C-di-GMP – Bis- (3'5')- cyclic dimeric guanosine monophosphate

cGMP – Cyclic guanosine monophosphate

CRP – cAMP receptor protein

FPLC – Fast protein liquid chromatography

FT – Flow through

Gln - Glutamine

GMP – Guanosine monophosphate

GTP – Guanosine triphosphate

Gu-Hcl – Guanosine hydrochloride

HI – Host independant

Ile - Isoleucine

IMAC – Immobilised metal affinity chromatography

IPTG – Isopropyl β – D – 1 thiogalactopyranoside

LB – Lysogeny broth

MCP – Methyl accepting chemotactic protein

Met - Methionine

OD – Optical density

OT - Onto

PBP – Class C penicillin binding protein

PEG – Polyethylene glycol

PGpG – 5' – phosphoguanyl – (3'-5')- guanosine

SDS-PAGE – Sodium dodecyl sulphate polyacrylamide gel electrophoresis

Ser - Serine

Thr - Threonine

Tyr - Tyrosine

UV - Ultraviolet

Val - Valine

PART ONE

How does the expression of phospholipase B influence the host pathogen relationship between *Cryptococcus neoformans* and the macrophage?

Supervisor - Dr Robin C. May

INTRODUCTION

1.1 The *Cryptococcus* family

Cryptococcus neoformans is a pathogenic fungus belonging to the Basidiomycota phylum. *C. neoformans* is unusual among fungi in that it can cause serious disease in humans. Cryptococcal disease (also known as cryptococcosis) was first described over 100 years ago, but for many years remained relatively obscure as serious disease only occurred in individuals with existing immune deficiencies - which themselves were rare. In recent decades however the occurrence of cryptococcosis has risen. This is due mainly to the emergence and rapid spread of HIV AIDs as well as the growing use of immune suppressive drugs following organ transplant. These factors have contributed to a worldwide increase in the number of immune compromised hosts which *C. neoformans* can infect (Idnurm et al., 2005). A recent study estimated that cryptococcosis caused by *C. neoformans* could affect up to one million people worldwide annually and in sub-Saharan Africa where the HIV epidemic is most severely felt it could account for approximately 13-44% of HIV related deaths (Park et al., 2009). Recent years have also seen the emergence of a new cryptococcal species along the western seaboards of North American and Canada called *Cryptococcus gatti* which can cause fatal cryptococcosis in healthy, immune competent individuals (Bartlett et al., 2008).

There are two sub varieties of *Cryptococcus neoformans*: *C. neoformans var. neoformans* and *C. neoformans var. grubii*, both *C. neoformans* varieties cause fatal cryptococcosis in immune compromised hosts. Although *C. neoformans* infects humans it is primarily an environmental organism which can be isolated from the soil, bird guano and rotting wood (Kronstad et al., 2011). Due to its yeast like nature *C. neoformans* is often compared to the laboratory yeast model *Saccharomyces cerevisiae* even though the two organisms are only distantly related evolutionary. *C. neoformans* can reproduce both sexually and asexually. Unlike asexual reproduction which occurs by budding, sexual reproduction involves a telomorph (a

taxonomical term used to define the sexual form of a normally asexual fungi) form called *Filobasidiella neoformans*. This telomorph state can form under certain environmental and nutritional conditions, genetic recombination occurs between two distinct mating types designated ‘a’ and ‘α’. This mating produces basidiospores which are thought to be the main infective vectors in cryptococcosis (Giles et al., 2009, Hull and Heitman, 2002) .

1.2 *Cryptococcus* neoformans pathogenesis

The pathogenesis of cryptococcosis begins in the lung following inhalation of live *Cryptococcus* cells or infectious spores (Giles et al., 2009). Infection most often occurs when individuals with an existing immune deficiency encounter *C. neoformans* in the environmental or come into contact with infected wild animals. Following inhalation the fungus colonises the lungs - in immune compromised hosts it then disseminates to the central nervous system (CNS) via the blood where it causes fatal meningoencephalitis. Healthy individuals who come into contact with *C. neoformans* can develop a latent infection which is confined to the lungs, if the infected hosts goes on to develop an immune deficiency in later life for example by contracting HIV then *C. neoformans* is able to emerge from its semi dormant state within the lungs and cause fatal disease (Garcia-Hermoso et al., 1999).

The first immune defence *C. neoformans* encounters inside the lungs is the innate immune response. This response is characterised by activation of the complement cascade and the influx of innate phagocytic cells such as macrophages and neutrophils to the site of infection. Rather than being detrimental to *C. neoformans* survival in the lungs, the recruitment of alveolar macrophages to the site of cryptococcal infection is an important event in the life cycle of *Cryptococcus* infection. Following phagocytosis *C. neoformans* is able to tolerate the destructive conditions inside alveolar macrophage and can even able replicate within the phagolysosome (Feldmesser et al., 2000).

Infection of the alveolar space by *C. neoformans* can manifest in both healthy and immune compromised hosts. In infected hosts who possess a working immune system *C. neoformans* is usually cleared from the lungs by the innate and later adaptive immune responses. However it is also possible for the infection to become chronic and remain within the lungs inside granulomatous formations similar to tuberculoid pathologies. The granulomas seen during cryptococcosis consist of clumps of alveolar macrophages which surround a core of extracellular cryptococci. Granuloma formation during *C. neoformans* infection is dependent on a $CD4^+$ Th1 adaptive immune response (Hill, 1992). This may partly explain why HIV co infection correlates with poor granuloma formation and increased dissemination as HIV depletes a host's $CD4^+$ T cells. Although granuloma mediated trapping of *C. neoformans* can prevent dissemination to the CNS it also produces disease latency and could be responsible for the aforementioned observations that latent infections in healthy hosts can emerge as fatal cryptococcosis if an immune deficiency later develops. Evidence of this effect in a rat model of cryptococcosis showed that healthy rats infected with *C. neoformans* did not develop disseminated disease, instead the fungi was contained within alveolar granulomas. The *Cryptococcus* within the granulomas remained viable for up to 18 months post infection, when immune deficiency was mimicked using immune suppressive glucocorticoid steroids C. *neoformans* emerged from the granulomas and could disseminate to the CNS (Goldman et al., 2000).

It is still not entirely clear how *C. neoformans* is able to disseminate from the lungs, into the blood and across the blood brain barrier into the brain. It is thought however that its ability to persist inside macrophages contributes in some way. Observations from our group (Ma et al., 2006) as well as others (Alvarez and Casadevall, 2006) have noted that *Cryptococcus* has a unique method which it uses to escape from the macrophage. This mechanism termed

'vomocytosis' or 'phagosomal extrusion' allows *Cryptococcus* to jump out of the macrophage without any harm being done to itself or the host cell.

The discovery of phagosomal extrusion supports the 'Trojan horse' hypothesis of cryptococcal dissemination which hypothesises that following phagocytosis in the lungs *C. neoformans* can survive and replicate within alveolar macrophages while using the niche to hide from immune detection. Infected macrophages from the lungs move to other parts of the body whereupon newly multiplied *Cryptococcus* cells jump from the macrophage into the extracellular space. As this escape does not harm the host cell it produces little inflammation, ensuring continued immune evasion. It is possible that *C. neoformans* emerge from their macrophage 'Trojan horses' when they are in circulation in the blood, the free *C. neoformans* cells can then cross the blood brain barrier themselves; which they have been seen to do (Chang et al., 2004). It is also possible however that some infected macrophages may cross into the CNS and deliver their cargo directly to their destination.

1.3 *Cryptococcus* neoformans virulence factors

Cryptococcus neoformans possesses several virulence factors which help it survive within the human body. These are production of a polysaccharide capsule, production of the pigment melanin, the ability to grow at human body temperature and secretion of environment modifying enzymes such as phospholipase B.

Capsule expression

The polysaccharide capsule surrounding *C. neoformans* is unusual for a fungus to possess. The capsule is implicated in virulence as capsule negative strains of *Cryptococcus neoformans* are avirulent (Fromtling et al., 1982, Chang and Kwon-Chung, 1994). The thickness of the capsule is dependent on strain genotype as well as growing conditions such as

environmental pH and CO_2 levels (Granger et al., 1985). Synthesis of the capsule is controlled by at least four genes designated *CAP64*, *CAP59*, *CAP10* and *CAP60* (Buchanan and Murphy, 1998, Ma and May, 2009) . Deletion of each gene produces un encapsulated mutant which lack virulence (Chang et al., 1996, Chang and Kwon-Chung, 1994, Chang and Kwon-Chung, 1999, Chang and Kwon-Chung, 1998).The capsule is composed of two key polysaccharide components: glucuronoxylomannan (GXM) and galactoxymannan (GalXM) (Bose et al., 2003), with a ratio of approximately 9:1 by mass in favour of GXM (Idnurm et al., 2005).

A number of survival benefits have been attributed to the possession of a capsule during cryptococcosis, for example it has been shown that the capsule can protect *Cryptococcus neoformans* from phagocytosis under certain conditions (Kozel and Gotschlich, 1982). Encapsulated *Cryptococcus* can be phagocytosed if they become opsonised however (Kozel and Gotschlich, 1982); but once phagocytosed the capsule is able to protect the yeast from destruction within the phagolysosome. Following phagocytosis *C. neoformans* cells produce thicker capsules; this adaption is thought to infer protection against intracellular conditions (Ma and May, 2009). During infection *C. neoformans* capsule size is at its largest in the lungs and becomes smaller in the brain (Rivera et al., 1998). *Cryptococcus neoformans* has also been reported to shed capsule polysaccharides such as GXM into the extracellular space. The polysaccharides are contained with vesicles which are expelled from the *Cryptococcus* in the extracellular space (Rodrigues et al., 2007). This GXM is thought to interfere with the generation of immune responses (Monari et al., 2006)

37^{o}C growth

The ability to tolerate and even thrive at the human body temperature of 37 ^{o}C is important for any pathogen to cause long term infection. There are over 30 cryptococcal species which have

been identified but only two species *Cryptococcus neoformans* and *Cryptococcus gatti* are able to infect enough hosts to be considered serious threats to human health, one of the reasons for this is that these two species are able the only ones which can grow well at human body temperature e.g. 37 ^{o}C (Ma and May, 2009). In other words humans most likely come into contact with many other species of *Cryptococcus* but only *C. neoformans* and *C. gatti* have adaptations such as being able to grow at 37 ^{o}C which are required to colonise the human body.

Melanin production

C. neoformans has been found to produce the pigment melanin during *in vivo* infection (Rosas et al., 2000). Melanin synthesis has also been observed in strains isolated from pigeon guano (Nosanchuk et al., 1999). The study of un melanised *Cryptococcus* strains has revealed that melanin production has a role in virulence (Kwon-Chung and Rhodes, 1986). Melanisation is mainly thought to protect the fungus from macrophage killing as melanised cells are more resistant to radical oxygen species produced by macrophages. Melanisation also makes *C. neoformans* less susceptible to phagocytosis (Ma and May, 2009).

Phospholipase B

C. neoformans produces a secretory phospholipase called phospholipase B (Plb) which has been identified in several studies as an essential factor in cryptococcal virulence (Chayakulkeeree et al., 2011, Noverr et al., 2003, Chen et al., 1997a, Cox et al., 2001). Plb is a lipid modifying enzyme that has multiple catalytic functions. Plb possesses the catalytic functions of phospholipase A_1 (Pla1) and phospholipase A_2 (Pla2). Pla1 and Pla2 cleave the ester bonds which link the two fatty acid chains to the glycerol head in phospholipids at the sn1 and sn2 positions respectively; this produces a free fatty acid and a lysophospholipid. As

well as Pla1 and Pla2 activities Plb also has lysophospholipase (LPL) and lysophospholipid transacetylase (LPTA) activity. The LPL and LPTA activities both modify the lysophospholipid products of sn1 or sn2 cleavage. LPL removes the remaining fatty acid from the lysophospholipid to give a second free fatty acid and a glycerylphosphatidate whereas LPTA catalyses the formation of new phospholipid molecules by regenerating ester linkages between free fatty acids and lysophospholipids (Shea et al., 2006).

The gene which codes for Plb is called *PLB1*; the gene is 2218 base pairs (bp) in length and is composed of 6 introns. *PLB1* codes for a protein 637 amino acids in size. Homologous gene sequences to *PLB1* have been found in other pathogenic yeasts such as *Candida albicans* (Cox et al., 2001) . The first complete purification and in-depth analysis of the Plb protein was published in by Chen et al. (Chen et al., 2000). The single protein they purified possessed all three enzymatic activities previously described. The mass of the protein was estimated to be around 160 kDa and was hypothesised to be composed of two equally weighted subunits. They also determined that its optimum pH for activity was in the acidic range; around 4.0 to 5.0 pH and that the enzyme could function at 37 ^{o}C i.e. human body temperature. Substrate analysis found that purified Plb could use a broad range of phospholipids as a substrate but dipalmitoylphosphates (DPPC) and phosphatidylglycerols (PG) were identified as preferred substrates (Chen et al., 2000). These properties suggest that Plb is bioactive within the body and more specifically within acidified phagolysosomes. When the *PLB1* gene was isolated from C. neoformans it was speculated that the product was a secretory protein due to a stretch of hydrophobic amino acids which can indicate an extracellular localisation signature (Cox et al., 2001). This initial hypothesis has proved to be correct as secretion of Plb has been detected in clinical cases (Santangelo et al., 2005) as well as in vitro studies (Chen et al., 1997b).

1.4 Phospholipase B and *Cryptococcus neoformans* pathogenesis

Plb has been implicated as a contributor to *C. neoformans* virulence. For instance experiments from a murine cryptococcosis model found that mice infected with a Plb knockout strain of *C. neoformans* lived significantly longer than mice infected with a wild type H99 strain, in addition to this the Plb knockout strain produced a lower fungal burden in the lungs suggesting reduced survival and proliferation and a lower rate of dissemination to the brain, this final observation might correlate to a reduced rate of vomocytosis in Plb knockout strains which was also observed (Chayakulkeeree et al., 2011). These observations agree with other studies which have also noted that Plb deficient *C. neoformans* strains have reduced growth, dissemination and subsequent lethality in mice (Noverr et al., 2003, Chen et al., 1997a).

There is some speculation over how Plb contributes to *C. neoformans* virulence. Plb can breakdown membrane lipids so potentially the enzyme could be secreted to destabilise the phagosome and outer membrane of the host cell, this explanation is unsatisfactory however because *C. neoformans* is able to survive and grow sufficiently well inside the phagosome and does not disrupt phagosome maturation (Levitz et al., 1999). Furthermore vomocytosis from the macrophage does not cause harm to macrophage (Ma et al., 2006) which probably would occur if its cell membrane was damaged in any way in the process.

Another theory is that Plb activity metabolises either *Cryptococcus* or macrophage derived phospholipids and produces arachidonic acid (AA). This lipid metabolite sits at the top of the eicosanoid synthesis pathway. Members of the eicosanoid family include prostaglandins (PG), leukotrienes (LT) and lipoxins (LP). Eicosanoids are lipid derived signalling molecules which have roles in cell signalling. These signalling molecules are of special note in the case of *C. neoformans* parasitism of host immune cells as there is in depth and conclusive evidence that eicosanoids are key modulators of the host immune response (Harizi et al., 2008).

Each eicosanoid subtype is produced by the modification of AA via a specific enzyme, for example the PG pathway specific precursor PGH_2 is produced by the oxidation of AA by the cyclooxygenase enzymes COX-1 and COX-2 whereas LT and LP specific precursors are produced by two different lipoxygenases. Eicosanoid production is unregulated during inflammation, especially PG synthesis via the up regulation of COX-2 (Harizi et al., 2008). In the model proposed arachidonic acid is liberated by Plb from possibly the cryptococcal membrane, phagosomal membrane, macrophage outer cell membrane or possibly other membrane bound organelles in the macrophage. The increased amount of arachidonic acid consequently contributes to increased eicosanoid production. The proposed origin of these extra eicosanoids is as unknown as the site of arachidonic acid liberation. Both macrophages (Harizi et al., 2008) and *C. neoformans* itself (Noverr et al., 2001) can produce eicosanoids so either or both may contribute. Eicosanoids exert their effects largely on the cells which produce them via autocrine signalling and to a lesser extent via paracrine signalling so the production of eicosanoids by infected macrophages likely influences only these cells or cells in close proximity (Harizi et al., 2008).

Eicosanoids might aid *C. neoformans* survival by attenuating or suppressing the antimicrobial mechanisms of the infected macrophage, but they may also influence the nature of the broader immune response produced during cryptococcosis. For example PGE_2 which is one of the most ubiquitous prostaglandins during inflammation can produce a Th2 $CD4^+$ biased immune response by down regulating IL-12 release from macrophages (van der Pouw Kraan et al., 1995). With this in mind previous findings from our group have shown that *C. neoformans* inside J774 macrophages in the presence of Th2 cytokines such as IL-4 and IL-13 show increased proliferation and cellular escape compared to untreated macrophages and those treated with Th1 cytokines (Voelz et al., 2009).

1.5 Project aims

Studies from our group and others have shown that knockout strains of *C. neoformans* deficient in Plb show reduced virulence. We wish to further characterise this attenuation in the hope that we can further understand the role that Plb plays in cryptococcosis. We will assess how well a *PLB1* knockout of *C. neoformans* var. grubii (H99) can survive within a murine J774 macrophage cell line. We will compare this knockout strain to a wild type H99 and a knockout strain which has had the PLB1 gene artificially reconstituted via a plasmid vector. As well as these virulence assays we will also start to unravel the complex network of lipid metabolism found inside a macrophage infected with *Cryptococcus*. In what we believe to be the first application of high throughput lipidomic technology to analyse macrophages infected with *Cryptococcus* we will utilise electrospray Fourier transport ion cyclotron resonance (FT-ICR) mass spectrometry to analyse whole cell lipid extractions from macrophages infected with wild type H99 and Plb knockout *C. neoformans*. From the lipid identity profiles produced we hope to begin to deduce what lipids Plb may be modifying during infection.

MATERIALS AND METHODS

2.1 Cells and strains

As an *in vitro* macrophage model we used a murine J774 macrophage cell line.

C. neoformans var. grubii strain H99 was the wild type *Cryptococcus* strain used in our study; PLB, PLB1 and PLB2 are genetic mutants derived from H99. The creation of PLB, PLB1 and PLB2 has been described in detail previously (Cox et al., 2001). Briefly the PLB knockout strain was created by disrupting the *PLB1* gene using insertion while the two rescue strains – PLB1 and PLB2, both had Plb activity restored with a plasmid vector containing an intact *PLB1* gene. PLB1 and PLB2 represent the two most successful transformant strains created e.g. they showed restored Plb activity and otherwise almost identical behaviour to the wild type strain.

Cryptococcus neoformans strains (H99, PLB, PLB1, PlB2) from our strain library which is stored at -80 ^{o}C were streaked onto YPD agar (1 % Yeast extract – MP cat no# 103303, 1 % peptone - Melford cat no# GP1328, 2 % dextrose – Fisher Scientific cat no# G/0500/53, 2 % Agar – Melford cat no# m1002) and grown for 48 hours at 25 ^{o}C and then stored until needed at 4 ^{o}C to halt further growth. Before experimentation liquid cultures were grown from these stock plates in 2 ml YPD growth medium (1 % yeast extract, 1 % peptone, 2 % dextrose)) in 14 ml PP test tubes (Greiner BioOne cat no# 187261) for 24 hours at 25 ^{o}C while constantly being rotated to ensure complete cell suspension during growth.

2.2 Intracellular proliferation assay

J774 preparation

J774 cells were grown to approximately 70 % confluence in T75 tissue culture flasks (Cat no# 178905, Nunc – Thermo Scientific) with complete DMEM (Dulbecco's Modified Eagle

medium, low glucose, Sigma Aldrich Cat no# D5546, supplemented with 10 % FBS - Invitrogen, 1% 10,000 units Penicillin / 10 mg streptomycin – Sigma cat no# 4333-100ml , 1 % 200 mM L – glutamine – Sigma cat no# G7513) before being re-plated into 2 cm^2 24 well tissue culture plates (Greiner BioOne Cell Star – cat no# 662160) at a density of $1x10^5$ cells per well in 1 ml complete DMEM. The plates were then incubated for 24 hours at 37 ^oC, 5 % CO_2.

C. neoformans cells preparation

Overnight 2 ml cultures of each *C. neoformans* strain were grown as previously described. After 24 hours of growth the 14 ml tubes were vortexed to ensure complete resuspension of cells before aliquoting 1 ml from each culture into separate autoclaved 1.5 ml Eppendorf tubes. To wash the cells each tube was centrifuged for 2.5 minutes at 6500 rpm (MSE centrifuge), following centrifuging the supernatant was discarded. The pellet containing the *Cryptococcus* cells was then resuspended in 1ml sterile PBS (Sigma Aldrich cat no# P4417). The number of cells for each strain was calculated by counting with a haemocytometer before making dilutions of $1x10^6$ cells per 100 µl PBS in 1.5 ml Eppendorf tubes, making enough dilution to give 100 µl per well required in the IPR. An hour before infection 0.1µl opsonising antibody (18B7, an IgG capsular polysaccharide monoclonal antibody – kindly provided by Arturo Casadevall, Albert Einstein College of Medicine, New York , USA) per 100 µl was added to each tube. The tubes were then left for 1 hour in a rotator at room temperature.

J774 activation and infection

Unless otherwise stated the J774 macrophages were activated before infection via treatment with PMA (phorbol myristate acetate). Briefly the medium from each well was removed and replaced with 1ml fresh serum free DMEM supplemented with 15 µl 10 µg/L phorbol 12-

myristate 13-acetate (PMA) (Sigma Aldrich cat no# P1585 , stock concentration 1 mg/L resuspended in DMSO (dimethyl sulfoxide – Sigma Aldrich cat no# D454400-100 ml) diluted from stock concentration with sterile PBS. After 45 minutes of exposure the PMA supplemented medium was removed from each well and replaced with serum free DMEM (SF DMEM) (The same composition as complete DMEM but without 10 % FBS)

Following a two hour incubation the medium from each well was aspirated away. To remove any remaining un-phagocytosed *Cryptococcus* each well was washed 4 times. To do this 1ml of sterile PBS was added to each empty well before gently tapping the sides of the culture plate to agitate any non adherent cells; the PBS was then quickly aspirated away. This wash was repeated at least four times for each well. Between each was the number of remaining extracellular yeast cells was assessed under a microscope. Four washes was usually sufficient to remove all extracellular yeast, however more washes were applied if needed. Following the last wash the PBS in each was replaced with 1 ml SF DMEM.

Counting

Before counting the medium was removed from the wells for the corresponding time point. Each well was washed twice with 1 ml PBS agitating in between washes to remove extracellular yeast. To lyse the macrophages and release the intracellular *Cryptococcus* for counting 200 µl distilled water was pipetted into each well, the plate was then incubated for 25 minutes. Following cell lysis the bottom surface of each well was scraped with the end of a pipette tip before removing the distilled water and transferring it to a 1.5 ml Eppendorf tube. Each well was washed out with an addition 200 µl of distilled water to ensure all the yeast was collected. The cells were then counted by eye using a haemocytometer.

2.3 Cell size assay

Setup for the cell size assay was identical to the intracellular assay. J774 cells were plates at a concentration of $1x10^5$ cells per well, activated with PMA for 45 minutes, infected with 100 µl opsonised *C. neoformans* ($1x10^6$ cells) , incubated for 2 hours at 37 ^oC, washed four times with PBS and refreshed with 1ml SF DMEM as previously described.

The plate was placed in an environmentally controlled stage (Okolabs) set to 30 ^oC, 5 % CO_2. The cells were imaged using a Nikon TE2000 microscope attached to a Digital Sight DS-Qi1MC camera. Bright field microscopy was used with a 20 x objective lens (Ph1 PLAN APO). Three positions were chosen for each experimental condition and a time lapse movie was created from each position. Frames were recorded every 4 minutes for 20 hours. Image acquisition and analysis was performed using the Nikon Elements software package (Nikon).

Cell size was measured using the ellipse area tool found on Nikon Elements (Nikon), a perfect circle was drawn from the centre of each *Cryptococcus* cell, the size of the circle was determined by the first edge of the area circle to hit the edge of the cryptococcal cell boundary – *Cryptococcus* cells are normally circular but are not always perfect circles, this regime sought to standardise measurement of irregular shaped cells. Cell diameter was recorded in pixels; this measurement was converted to µm using the appropriate calibration for the 20x lens (1 pixel → 0.461 µm).

Statistical analysis

A non parametric Mann Whitney U test was performed to calculate the significance of size distribution shift for each experiment (e.g. StrainX 0 hour vs. StrainX 18 hour). The analysis was performed using an online tool (http://faculty.vassar.edu/lowry/utest.html). A measurement of significance was given as a Z value. The α value was 0.05 meaning that any

Z value below -1.95 or above 1.95 was considered to be significant. A two tailed T test was also calculated to give a P value.

2.4 Lipidomics study

Cell preparation

The preparation of infected J774 cells for the lipid extraction was similar to the preparation of the intracellular proliferation and vomocytosis assays previously described but on a larger scale. Instead of growing macrophages in 2 cm^2 24 tissue culture plate wells the cells for each experimental condition were grown in T75 flat bottomed tissue culture flasks. Before the start of the study the cells were grown to around 80 % confluence which we estimated would give a total cell number in the flask of around $4x10^6$ per flask. The macrophages were activated with PMA 45 minutes before infection with $4x10^7$ opsonised *Cryptococcus*. After two hours un phagocytosed cells were washed away and the medium was replaced with serum free DMEM. The flasks were then incubated for 24 hours at 37 ^oC, 5 % CO_2.

Cell quenching

Following a 24 hour incubation period each flask was taken in turn from the incubator and washed twice with 10 ml PBS to remove any extracellular cryptococcal cells which may have emerged due to macrophage lysis or cellular escape. All of the PBS between washes was removed using a glass Pasteur pipette, making sure to tilt the flask so that all of the remaining PBS collected in one corner before removing.

Next 2 ml of the extraction solution (60 % HPLC grade methanol, 40 % HPLC grade distilled water) which had been chilled in dry ice for at least 15 minutes was added to each flask. After addition the adherent cells in the flask were scraped from the surface of the flask using a cell scraper. To ensure low temperatures at this stage the flasks were placed on a thin layer of dry

ice during the scraping. The cells were transferred to pre chilled (at least 15 minutes in dry ice) 2 ml Eppendorf tubes using a clean glass Pasteur pipette. Until all of the flasks were processed each tube was kept chilled in dry ice to prevent metabolic activity. The tubes were then centrifuged with a fixed angle rotor (Thermo Scientific cat) for 5 minutes at 2500 g (Heraeus Biofuge primo R, Thermo Scientific). To keep the temperature of this stage under 0 ^{o}C the centrifuge was pre-chilled to -9 ^{o}C and the fixed angle rotor was placed in a -20 ^{o}C freezer for at least an hour before use. In addition to pre-chilling the centrifuge care was taken not to overcrowd and potentially heat the centrifuge – a limit of 10 tubes per spin was imposed.

The supernatant was removed from the tubes using a glass Pasteur pipette and discarded and the remaining pellets were stored at -80 ^{o}C until extraction.

Lipid extraction

The weight of each cell pellet was calculated by subtracting the weight of the 2 ml Eppendorf tube pre experiment from the final weight. 8 µl methanol (HPLC grade) per mg of the cell pellet weight was added to each tube. 8 µl chloroform (HPLC grade) per pellet mg was added to clean 1.8 ml glass vials, the resuspended contents of each 2 ml Eppendorf tube were then transferred to these vials using a clean glass Pasteur pipette for each transfer. Following transfer the methanol and chloroform mix was taken back up into the pipette and ejected into the vial twice to rinse out any remaining residue within the pipette. 7.2 µl distilled water (HPLC grade) per mg was then added to each vial. The vials were then vortexed for 30 seconds each and left on ice for 10 minutes. After 10 minutes the samples were loaded into a spinning bucket centrifuge (Heraeus, Thermo Scientific) and spun for 10 minutes at 1500 g, 4 ^{o}C. After centrifugation the vials were carefully removed from the centrifuge and left to rest for 5 minutes. After the samples have settled there should be three distinct layers, the upper

layer containing polar metabolites, the middle interface layer proteins and the lower layer non polar lipids.

Using a Hamilton syringe (Hamilton) two 200 µl aliquots from the top polar layer were removed into 1.5 ml Eppendorf tubes, washing before each use with methanol. The syringe was then washed out with chloroform and as much of the lower non polar was removed and transferred to a clean 1.8 ml glass vial. Care was taken not to disturb the interface layer. The syringe was washed with chloroform between each use. The polar and non polar samples as well as the original vials with the remaining interface were stored until needed at -80 ^{o}C.

Non polar sample mass spectrometer analysis

Before analysis 60 µl aliquots of each non polar sample were made from the vials in -80 ^{o}C storage into clean 1.8 ml glass vials. The samples were dried under liquid nitrogen before being resuspended with 120 µl of a methanol and chloroform mixture (2:1 ratio respectively) supplemented with 5 mM ammonium acetate. Each sample was then vortexted for 30 seconds to fully re suspend.

Just before the loading of the 96 well sample plate the samples were centrifuged for 10 minutes at 4 ^{o}C to remove particulate contamination. Being careful not to disturb the samples after centrifuging 11 µl aliquots were pipetted into each well of the 96 well sample plate.

Data Collection

To analyse the samples and process the raw data we were kindly assisted by Dr Andy Southam, a post doctoral research assistant who works with Professor Chris Bunce, School of Biosciences, Birmingham University.

In total 6 non polar samples were analysed for the pilot study. This sample set included two strains – H99 and PLB and there were three repeats for each strain. In addition to the six samples a blank sample was analysed. This blank sample was composed of just the solvents used in the previous non polar sample preparation step (e.g. 2:1 ratio methanol and chloroform with 5 mM ammonium acetate.

The samples were analysed in triplicate using a high resolution FT-ICR mass spectrometer (model: LTQ-FT ultra, Thermo Scientific) attached to a nano electrospray sample infuser (Model: Triversa, Advion Biosciences). The raw data was collected as transient scans of the detected signals.

Data pre-processing

Following sample analysis the raw transient scan data was averaged and was converted into a conventional mass spectrum dataset (e.g. m/z vs. intensity) using a Fourier transform algorithm with the MATLAB software package.

Data Processing

To process the data it was first filtered so that only peaks which were found in at least 2 out of 3 triplicate samples were counted as real, any peaks failing this criteria were discarded as noise. A matrix was generated to display the triplicate filtered samples data, comparing m/z with the relative intensity reading for each sample, only peaks which had an intensity > 0 in at least 50% of the samples were included within the matrix. In addition to this any peaks which were detected within the sample set as well as the blank were considered contamination and as such were omitted from the matrix. Finally the matrix was normalised using PQN normalisation.

Bezafibrate (BEZ) and medroxyprogesterone (MPA) combination treatment

The intracellular proliferation assay itself was performed as previous described; however the assay used only H99 and PLB strains. The two strains were split into two treatment groups, H99 and PLB without BAP treatment and H99 and PLB with BEZ and MPA (BAP) treatment. Time points were measured at 0 hour, 18 hour and 24 hour time points.

BEZ (stock concentration 0.05 M, diluted in DMSO) and MPA (stock concentration 0.5 mM, diluted in ethanol) was added to each treatment well following infection with *Cryptococcus* at a concentration of 1 in 1000 (e.g. 1 µl BEZ and 1 µl MPA per 1000 µl) (Both drugs were kindly provided by Professor Chris Bunce, University of Birmingham) Following washing with PBS after infection the new serum free DMEM medium was re supplemented with BAP at the same concentrations as before.

RESULTS

3.1 Phospholipase B is required for in vitro cryptococcal intracellular growth.

Previous studies have reported that *PLB1* deficient *C. neoformans* have an altered phenotype from the wild type that importantly procures reduced virulence. For example in vivo experiments in have mice have shown that mice infected nasally with *PLB1* knockout mutants have a reduced fungal load in the lungs as evidenced by a decreased number of recoverable CFUs over time compared to wild type strains (Chayakulkeeree et al., 2011).

C. neoformans infection in the lung is mainly localised inside macrophages. For this reason we hypothesised that decreased fungal burden in the lungs of mice was due to an intracellular growth deficiency caused by *PLB1* knockout. To test this we performed a macrophage intracellular proliferation assay with PMA activated J774 murine macrophages and opsonised H99, PLB, PLB1 and PLB2 *Cryptococcus* strains. The number of intracellular *C. neoformans* was calculated for each strain at 0 hour, 18 hour and 24 hour time points. The maximum intracellular burden (usually at 18 hours) was divided by the initial intracellular burden counted at 0 hours. This calculation gives the 'IPR' or intracellular proliferation rate. To examine the IPR values for each strain we chose to pre activate the J774 cells with PMA. PMA activation makes the behaviour of the macrophages more consistent as they are all activated to a similar level; thus any differences in IPR seen between strains could be more confidently attributed to differences between the strains and not variations in macrophage state.

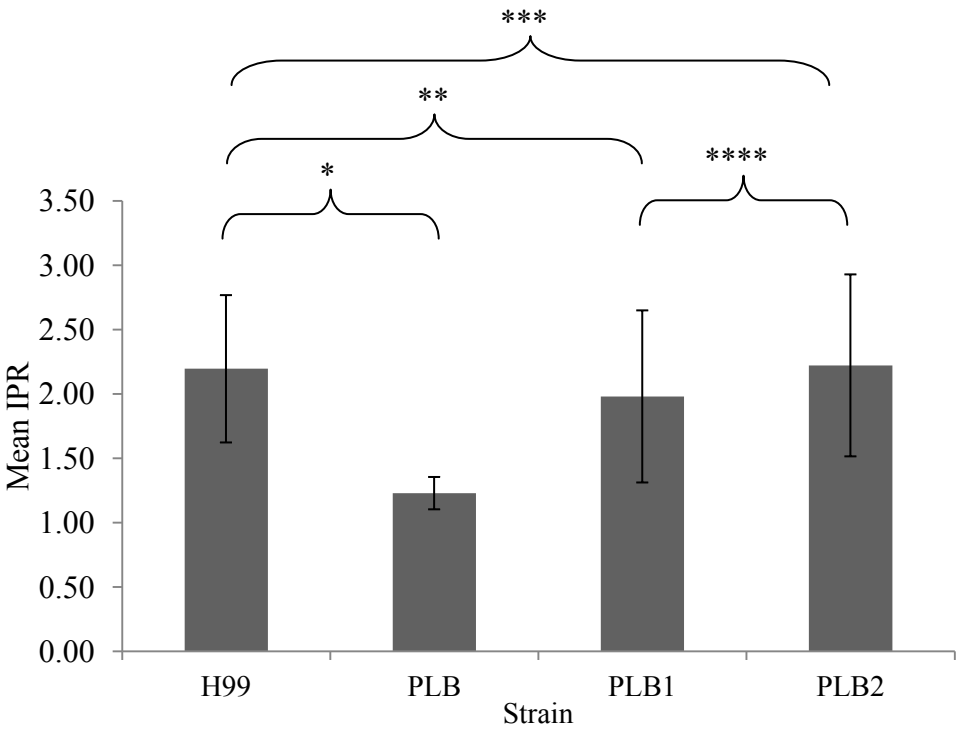

Figure 1: IPR assay with PMA activated J774 macrophages - *The intracellular proliferation rates of C. neoformans stains H99 (wild type, PLB parent), PLB (PLB1 knockout), PLB1 and PLB2 (PLB1 knockout rescues) inside PMA activated J774 macrophage cells were measured using an intracellular proliferation rate (IPR) assay. Briefly 1x10^6 18B7 opsonised C. neoformans was added to 1x10^5 PMA activated J774 macrophages plated in 24 well tissue culture plates in 1ml serum free DMEM. After two hours (0 hours) extracellular Cryptococcus cells were washed away, the number of intracellular Cryptococcus were counted at 0, 18 and 24 hour time points. The IPR was calculated from the maximum intracellular cell number divided by the initial uptake at 0 hour. Filled in bars represent the mean IPR value for each strain (n=5), error bars represent 2x standard error. A two tailed Student's t test was performed for the following groups: H99 vs. PLB (* P= 0.01) H99 vs. PLB1 (** P= 0.64), H99 vs. PLB2 (*** P= 0.95) and PLB1 vs. PLB2 (**** P=0.63) values below 0.05 are considered significant.*

Comparing the IPR for the wild type strain H99 to the knockout mutant PLB (Figure 1) we saw a significant (P= 0.01) decrease in intracellular proliferation of over 50 % for the knockout IPR. As well as H99 and PLB we also analysed two *PLB* rescues (PLB1 and PLB2) which have the *PLB1* gene artificially reintroduced. The IPR results for PLB1 and PLB2 were not significantly different from H99 (P= 0.64 and P= 0.95 respectively) or from each other (P = 0.65) which suggests that the knockout of *PLB1* is responsible for the proliferative deficiency seen in the knockout. Taken together these observations suggest that knockout of the *PLB1* gene produces a cryptococcal phenotype that is less suited to intracellular proliferation than the wild type or knockout rescue strains.

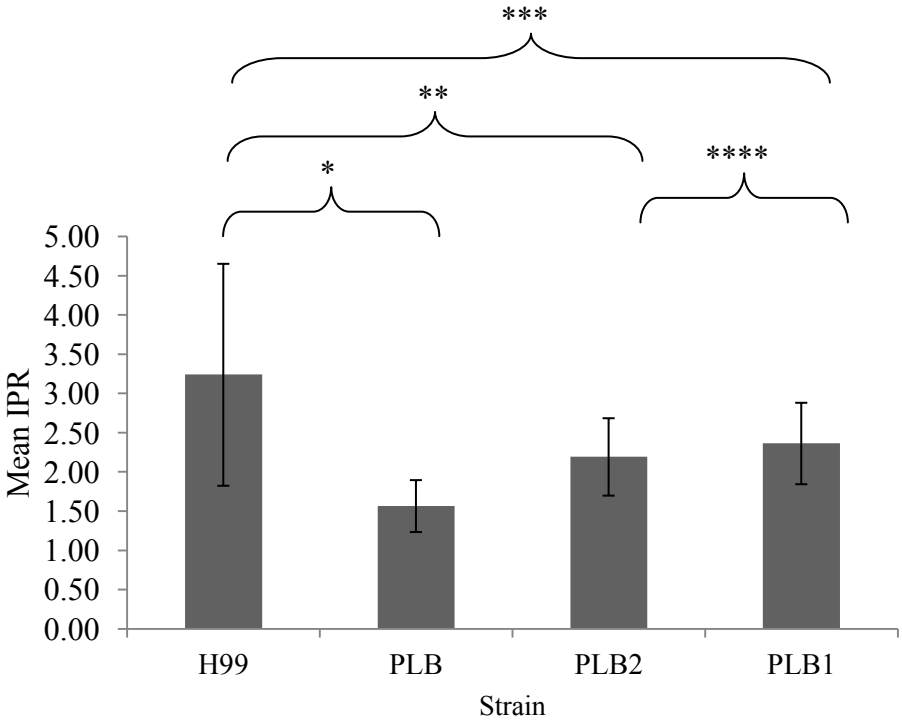

Figure 2: IPR assay with un-activated (no PMA) J774 macrophages - *The intracellular proliferation rates of C. neoformans stains H99 (wild type, PLB parent), PLB (PLB1 knockout), PLB1 and PLB2 (PLB1 knockout rescues) inside un-activated (not PMA pre-activated) J774 macrophage cells were measured using an intracellular proliferation rate (IPR) assay. Briefly 1x10^6 18B7 opsonised C. neoformans was added to 1x10^5 un activated J774 macrophages plated in 24 well tissue culture plates in 1ml serum free DMEM. After two hours (0 hours) extracellular Cryptococcus cells were washed away, the number of intracellular Cryptococcus were counted at 0, 18 and 24 hour time points. The IPR was calculated from the maximum intracellular cell number divided by the initial uptake at 0 hour. Filled in bars represent the mean IPR value for each strain (n=6), error bars represent 2x standard error. A two tailed Student's t test was performed for the following groups: H99 vs. PLB (* P= 0.04) H99 vs. PLB1 (** P= 0.19), H99 vs. PLB2 (*** P= 0.24) and PLB1 vs. PLB2 (**** P=0.77) values below 0.05 are considered significant.*

Activation of macrophages with PMA is an efficient experimental procedure to create conformity within a culture; however it is not a physiological stimulus and in fact produces a very extreme activation state. For these reasons we wanted to confirm that proliferative phenotype displayed by PLB was not an artefact of our experimental conditions, thus we repeated the previous IPR experiment but used J774 macrophages which were not pre activated with PMA (Figure 2). Without PMA activation we saw the same trend that we found with PMA activation; H99, PLB1 and PLB2 showed no significant difference in intracellular proliferation whereas in comparison PLB showed a significant decrease (P= 0.04) in intracellular proliferation. This suggests that the PLB proliferation deficiency seen in activated J774 cells (Figure 1) still occurs in un activated J774 cells (Figure 2), and thus is not a result of PMA activation.

Previous experiments in our lab have shown a correlation between initial uptake (0hr) and the resultant IPR (data unpublished). This correlation suggests that high uptake usually results in a lower IPR and vice versa. We noticed that the initial uptake at 0hr for PLB was higher than the other strains. This was seen especially following PMA pre activation. We found that PMA activation while producing a general increase in initial uptake across all strains boosted the uptake of PLB most significantly. In view of these observations we wondered whether the IPR for PLB was low due to its initial high uptake – we theorised that a high initial uptake could overcrowd macrophages and produce an environment where conditions for *C. neoformans* growth was unfavourable.

To investigate whether the PLB mutant's low proliferative capacity was linked to its high initial uptake we repeated the IPR assay but did not opsonise the *C. neoformans* we used to infect the macrophages. The efficiency of *C. neoformans* phagocytosis is reduced when the

Cryptococcus are not opsonised; thus by infecting the macrophages with un-opsonised *Cryptococcus* we were able to reduce the uptake.

A

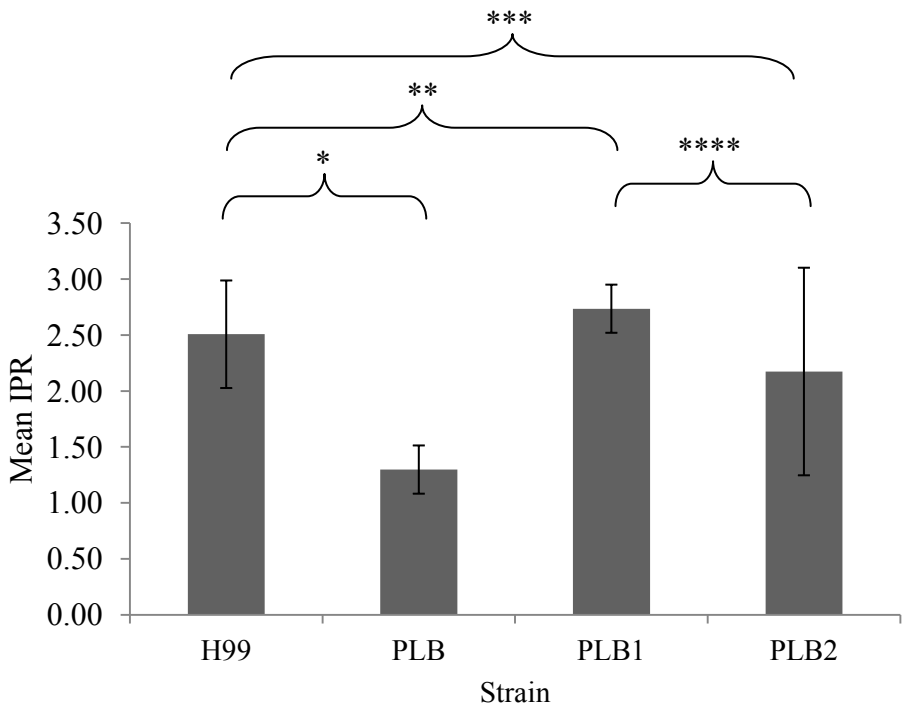

Figure 3A: IPR assay with un opsonised Cryptococcus strains- *The intracellular proliferation rates of un-opsonised C. neoformans stains H99 (wild type, PLB parent), PLB (PLB1 knockout), PLB1 and PLB2 (PLB1 knockout rescues) inside activated J774 macrophage cells were measured using an intracellular proliferation rate (IPR) assay. Briefly $1x10^6$ un opsonised C. neoformans was added to $1x10^5$ PMA activated J774 macrophages plated in 24 well tissue culture plates in 1ml serum free DMEM. After two hours (0 hours) extracellular Cryptococcus cells were washed away, the number of intracellular Cryptococcus were counted at 0, 18 and 24 hour time points. The IPR was calculated from the maximum intracellular cell number divided by the initial uptake at 0 hour. Filled in bars represent the mean IPR value for each strain (n=3), error bars represent 2x standard error. A two tailed Student's t test was performed for the following groups: n=3, H99 vs. PLB (* P= 0.01) H99 vs. PLB1 (** P= 0.43), H99 vs. PLB2 (*** P= 0.56) and PLB1 vs. PLB2 (**** P=0.30) values below 0.05 are considered significant.*

B i

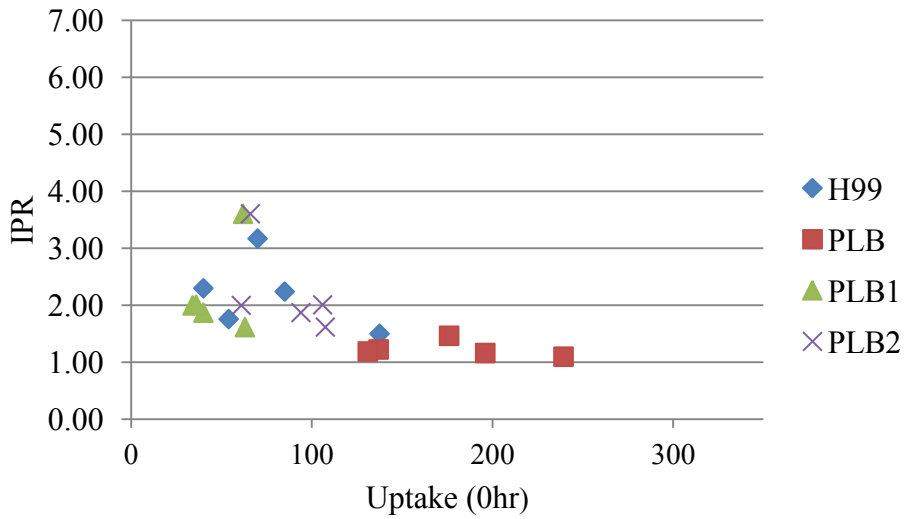
7.00
6.00
5.00
4.00
3.00
2.00
1.00
0.00
IPR
0
100
200
300
Uptake (0hr)
H99
PLB
PLB1
PLB2

ii

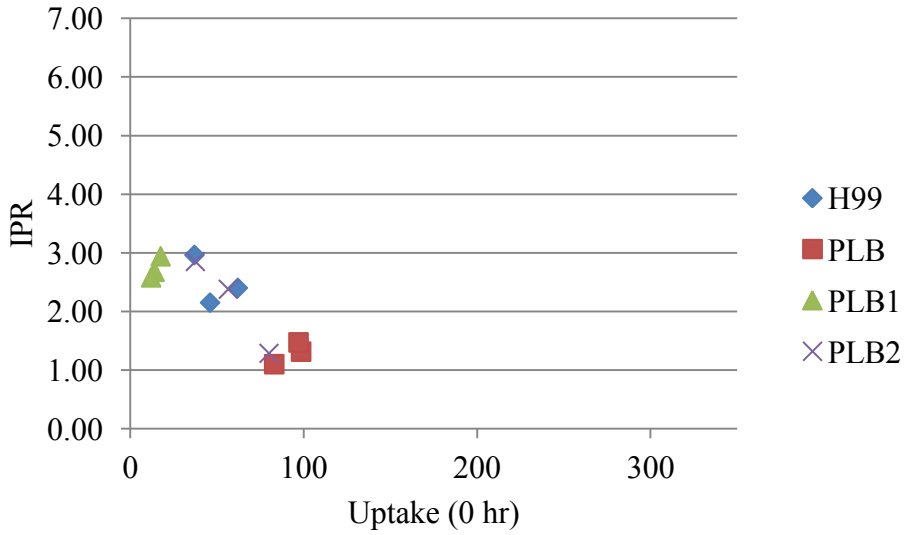
7.00
6.00
5.00
4.00
3.00
2.00
1.00
0.00
IPR
0
100
200
300
Uptake (0 hr)
H99
PLB
PLB1
PLB2

iii

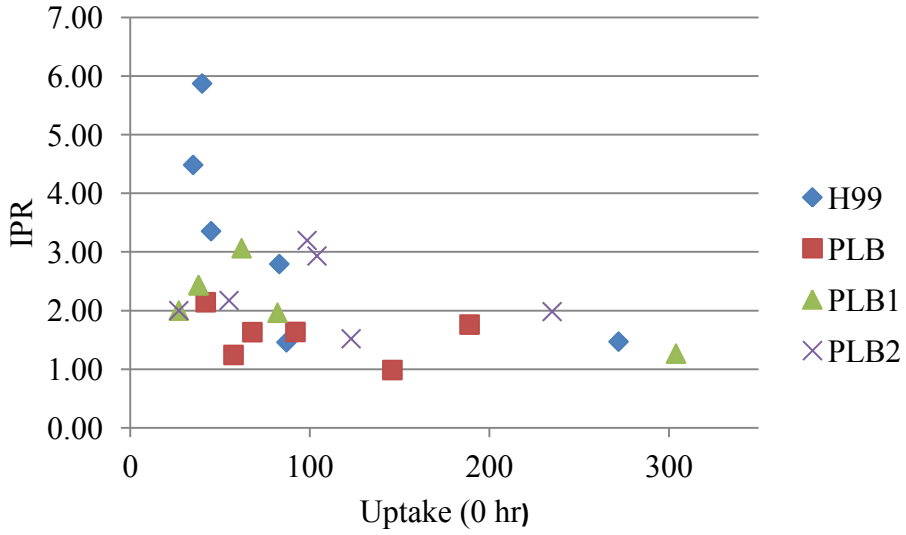
7.00
6.00
5.00
4.00
3.00
2.00
1.00
0.00
IPR
0
100
200
300
Uptake (0 hr)
H99
PLB
PLB1
PLB2

Figure 3B-I to 3B-III: Scatter plots showing the relationship between initial uptake (0 hr) and the resulting IPR – *Scatter plots for each IPR assay – with PMA (Bi), without PMA (B-ii) and with no opsonisation (B-iii) were drawn to compare the initial uptake at 0 hr (X axis) with the resulting IPR (Y axis), for each plot the blue diamonds represent H99, the red squares represent PLB, the green triangles represent PLB1 and the grey crosses represent PLB2.*

The use of un-opsonised yeast reduced the initial uptake at 0 hr for all four strains (Figure 3 B-III) compared to the previous IPR experiments using PMA activated (Figure 3 Bi) and un-activated macrophages (Figure 3 B-iii). In the case of PLB the initial uptake count at 0 hr was reduced by about 50% compared to the first IPR with activated macrophages (Figure 3 B-i and B-iii). Although the uptake was reduced the IPR values for un-opsonised PLB (Figure 3 A) was not significantly different (P = 0.57) from the IPR values obtained with opsonisation and PMA activation (Figure 1). This data suggests that deficiency in intracellular growth is still present when the uptake is reduced and thus the deficiency does not seem to be uptake dependant.

As a whole (Figures 1 – 3) our IPR data identifies a possible proliferation deficiency for PLB which is not seen for H99, PLB1 or PLB2 strains. This suggests that deficiency in Plb expression in *C. neoformans* leads to an aberration in proliferative ability inside infected J774 macrophages.

3.2 *PLB1* knockout produces a distinct, much larger cellular morphology in PLB.

While performing the IPR experiments we observed that PLB was unique among the strains tested in that the physical size of the knockout cells seemed to increase with time; this growth in cell size was not observed for H99 or PLB1 and PLB2.

We wished to quantify this growth in size as we realised that a diversion of energy from cell budding to cell expansion may be an explanation for why PLB appears to proliferate poorly in J774 macrophages. In addition to this an increase in *C. neoformans* cell diameter has previously been reported during in vivo infection, it was suggested that this growth may help protect *C. neoformans* against immune defences during infection but as a trade off the larger size diminishes cryptococcal dissemination from the lungs to the brain (Okagaki et al., 2010).

To quantify the change in *C. neoformans* cell size over time we imaged infected J774 cells using bright field live cell microscopy to create time lapse movies which tracked the expansion of *C. neoformans* cells within macrophages. For this experiment we chose to analyse only one of the rescues – PLB2 to compare with H99 and PLB1. The decision to exclude PLB1 was made following the first experiment. Although we saw that both rescues PLB1 and PLB2 behave like the wild type PLB2 was potentially more like H99 than PLB1. The diameter of all intracellular *C. neoformans* cells in three repeats was measured at 0 hours (2 hours post infection) and 18 hours; two replicates were analysed per strain, per repeat. To avoid counting bias all the intracellular *C. neoformans* cells within a position were counted.

A)

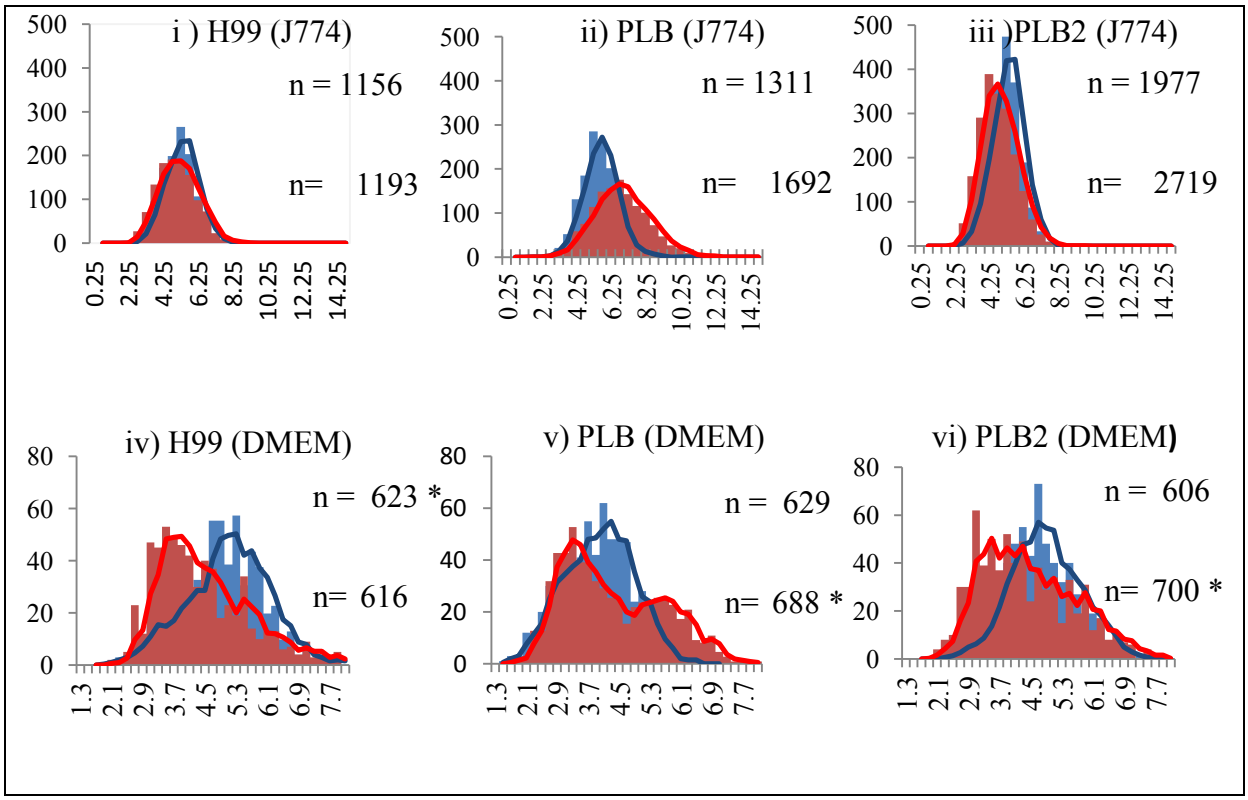

Figure 4 A – Frequency distribution histograms of C. neoformans cell diameter – *The diameter of C. neoformans cells inside infected macrophages (Strain – J774: A-i to A-iii) and in serum free DMEM (Strain –DMEM: A-iv to A-vi) was measured using the ellipse circle measurement tool on NIS elements – the cell diameter was measured in pixels which was then later converted to µm using the appropriate calibration for the 20 X lens used. Overlapping frequency histograms were plotted for each time point, blue histograms were plotted for the 0 hour measurements and red histograms were plotted for the 18 hour time point measurements. Along the X axis is plotted the diameter ranges in µm and along the Y axis is plotted the frequency for each range. The number of cells measured for each time point is given, colour coded for each histogram. The number of cells measured for each time point*

*was not uniform, thus to normalise the frequency distributions the time point where n was the greater was adjusted such that the frequencies plotted were proportional to the time point with the lowest n value (e.g. if 0 hr = 300n and 18 hr = 600n then the frequencies for 18 hours were multiplied by 0.5 to give 18 hr = (600*0.5n). The time point plot normalised for figure is indicated by an asterix whose colour corresponds to the appropriate histogram. Trend lines were drawn using a moving average function with a period of 2.*

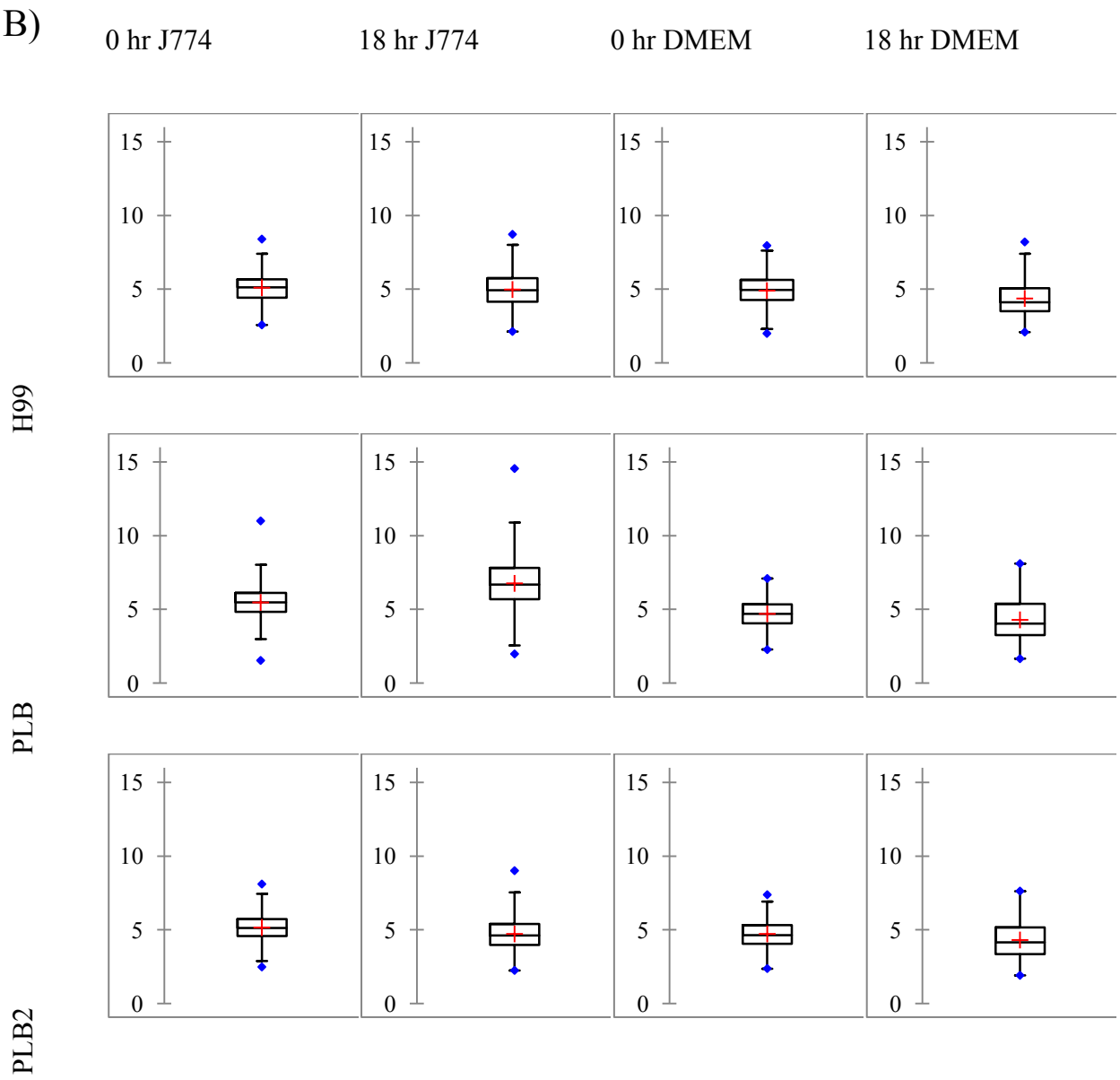

Figure 4 B – Box and whisker plots to show the range distribution of C. neoformans cell diameter – *Box and whisker plots were also produced from the same data shown in figure 4A. The box and whisker plots are arranged in a grid with the corresponding time point and condition (e.g. inside J774 macrophages, extracellular in DMEM) horizontally and the strain vertically .For each plot the red cross marks the mean and the two blue diamonds mark the upper and lower ranges observed. The upper and lower edges of the box represent the upper*

and lower interquartile ranges of the data and the intersecting line represents the median cell diameter.

C) H99 0 hr

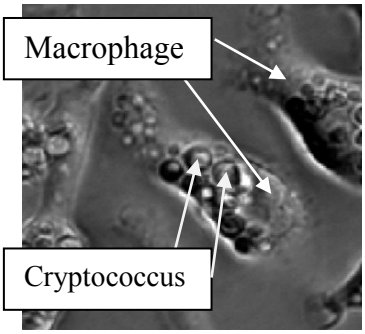

H99 18 hr

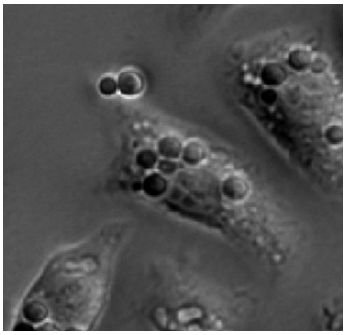

PLB 0 hr

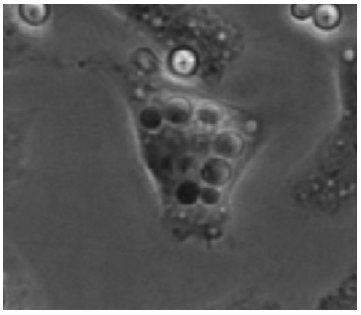

PLB 18 hr

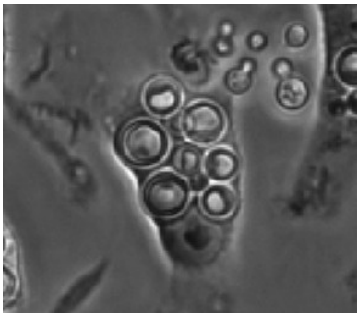

PLB2 0hr

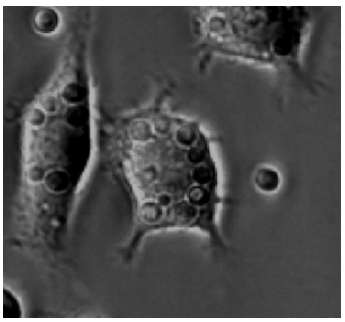

PLB2 18hr

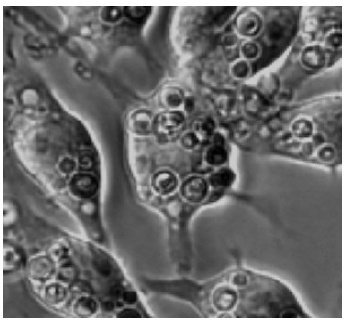

Figure 4C – Bright field images showing Cryptococcus diameter in J774 cells at 0 hour and 18 hour time points – *J774 macrophages were infected with H99, PLB and PLB2 Cryptococcus strains. The cells were imaged using a Digital Sight DS-Qi1MC camera attached to a Nikon TE2000 microscope. Bright field microscopy was used with a 20 x objective lens. Still images were taken every 4 minutes for 20 hours. Still images were*

captured from the movies, for each strain the same macrophage is represented at 0 hours and 18 hours.

C. neoformans strains H99 (figure 4A-i, figure B H99/0 hr J774 and H99/18 hr J774) and PLB2 (figure 4A-iii, figure B PLB2/0 hr J774 and PLB2/18 hr J774) do not show a significant growth in cell diameter within infected macrophages over the 18 hour time scale of the experiment. PLB however did show a significant increase in diameter during the experiment (when $\alpha = 0.05$, $z = -23.88$ (< -1.95), $P < 0.0001$) (figure 4A-ii, figure B PLB/0 hr J774 and PLB/18 hr J774) – the mean cell diameter at 0hr was 5.48μm, this increased to 6.77μm at 18 hours. This suggests that inside infected macrophages a sizeable proportion of PLB cells increase in diameter over time whereas H99 and the knockout rescue do not change in size.

Interestingly there was a significant decrease in the mean cell diameter for H99 (when $\alpha = 0.05$, $z = 3.86$ (> 1.95), $P < 0.0001$) and PLB2 (when $\alpha = 0.05$, $z = 15.94$ (> 1.95), $P < 0.0001$) (figure 4A-i and 4A-iii), this is most likely an indication of active cell proliferation. When *C. neoformans* cells replicate by cell budding smaller daughter cells are produced, thus a increasing rate of proliferation overtime will produce a larger population of small cells – reducing the mean cell diameter.

The discovery that PLB knockout produced markedly different cell morphologies to the wild type was novel to us. As we had only observed this increase in cell diameter within infected macrophages we next wanted to confirm whether it happened to extracellular *C. neoformans* cells.

In order to assess the morphologies of extracellular *C. neoformans* we inoculated serum free DMEM. Briefly 18B7 opsonised H99, PLB and PLB2 cells were plated into 24 well plates at a concentration of $5x10^6$ *Cryptococcus* in 1ml serum DMEM per well. Again time lapse movies were created for each strain over a period of 20 hours. The diameter of approximately 300 cells per position was measured. One position were measured for each strain per repeat, two repeats were measured.

We saw a significant decrease in mean cell diameter over the 18 hour time course for H99 (figure 4A-iv) (when $\alpha = 0.05$, $z = 9.44$ (> 1.95), $P < 0.0001$) and PLB2 (when $\alpha = 0.05$, $z = 7.81$ (> 1.95), $P < 0.0001$) (figure 4 A-vi). Again we attributed this decrease in mean cell diameter to a sign of active cell proliferation. During extracellular growth PLB changed in two ways; active proliferation was observed (figure 4 A-v) and there was also a population of cells at 18 hours with increased diameters (when $\alpha = 0.05$, $z = 7.37$ (> 1.95), $P < 0.0001$). This suggests extracellular PLB both grows in size and proliferates Taken together this data suggests that all three *C. neoformans* strains proliferate better in DMEM than they do inside macrophages. Furthermore PLB is the only strain analysed that shows a significant increase in cell diameter both within and outside macrophages. PLB cells inside macrophages showed a much larger magnitude of expansion than extracellular *Cryptococcus*. This suggests that the conditions which lead to an increase in cell diameter for PLB may be to an extent independent of the macrophage; however there seems to be some factor present in the interplay between the two cells which exacerbates the morphology.

3.3 A high throughput lipidomic analysis of *C. neoformans* infected macrophages

Phospholipase B is a lipid modifying enzyme, for this reason we wanted to analysis the differences in lipid composition between H99 and PLB infected J774 macrophages. Samples from each group were prepared by infecting PMA activated J774 macrophages with H99 and PLB. Following infection the cells were incubated for 24 hours before the whole cell lipid content of both the macrophages and the infecting *Cryptococcus* cells were extracted. Prepared samples were analysed using FT-ICR mass spectroscopy which provides a very high resolution; ideal for lipid analysis where the mass differences between molecules can be very small.

The normalised m/z data was compared to confirmed lipid m/z values contained within the online "Lipids Map Project" (www.lipidmaps.org) database. Two searches were made to identify putative lipids using first the Lipids Map glycerophospholipid database search tool (http://www.lipidmaps.org/tools/ms/glycerophospholipids_batch.html) and secondly the fatty acids database search tool (http://www.lipidmaps.org/tools/ms/fattyacids_batch.html). For each search the mass tolerance for a positive identification was set to +/- 0.001 m/z and the ion type was set to $M\text{-}H^-$ (negative ion).

The phosphoglycerolipid database returned 157 matched masses with a delta value +/- 0.001 from 6352 normalised m/z data values. Some matched masses corresponded to one or more possible lipids with the same mass, as such from 157 matched masses we received 1085 putative phosphoglycerolipid identities with masses ranging between 353.17396 m/z and 951.5977 m/z. The fatty acid database search returned 58 matched masses with a delta value +/- 0.001 from the 6352 raw m/s data values. From these matched masses 94 putative fatty acid identities were given with a mass range between 141.0921m/z and 479.4836 m/z.

This identity data was matched with the corresponding intensity values from each sample to provide an indication of the relative intensities of each putative identity. The mean intensity for each sample group (H99 n=3, PLB n=3) was calculated, a student's T test to calculate the significance of the variability between the two sample groups was also calculated.

Input mass	Matched Mass (M-H$^-$)	Delta	Generic name	Abbreviated name	Formula	H99 mean intensity	PLB mean intensity	P value (H99 vs. PLB)
171.10182	171.1026	0.0008	oxo-methyl-octanoic acid	8:0(Ke,Me)	C9H15O3	1180.233	212.7229	0.0115
171.10182	171.1026	0.0008	hydroxy-nonenoic acid	9:1(OH)	C9H15O3	1180.233	212.7229	0.0115
171.10182	171.1026	0.0008	oxo-nonanoic acid	9:0(Ke)	C9H15O3	1180.233	212.7229	0.0115
331.19139	331.1914	0	epoxy-hydroxy-eicosapentenoic acid	20:5(Ep,OH)	C20H27O4	2494.944	3222.471	0.0437
331.19139	331.1914	0	oxo-hydroxy-prostatetraenoic acid	20:4(Ke,OH)-cyclo	C20H27O4	2494.944	3222.471	0.0437

Table 1 – Putative fatty acid lipid identities which are significantly different between H99 and PLB – *Mass spectrometry m/z data was compared against the 'Lipid Maps' fatty acid database using the fatty acid database search tool, using a delta value cut off of +/- 0.001 m/z. Returned lipid identities were correlated to the original intensity data for each identified mass. The mean intensity for each sample group – H99 and PLB was calculated for the following samples – H99 samples A, B and E – PLB samples A, B and E. A two tailed student's T test was performed to compare the same sample groups.*

Sorting the putative fatty acid identities using the significance of the difference between the two samples returned five putative fatty acids (Table 1) whose intensity was significantly different ($P<0.05$) between the knockout and wild type sample groups. The five fatty acid identities returned represent two matched masses – 171.1026 m/z and 331.1914 m/z.

The three fatty acid identities suggested for the input mass 171.10182 have a matched mass of 171.1026 (table 1); this works out at as different of 0.0008 from the matched m/z. All three putative fatty acids are relatively small chain fatty acids. The relative intensities between the two sample groups (Figure 5 *) suggest that these lipids are more abundant in H99 than they are in PLB.

The two fatty acid identities suggested for the input m/z 331.19139 have a matched mass of 331.1914 m/z which rounds up to give an exact match to the matched mass (e.g. delta = 0). The two putative fatty acids are both 20 carbon fatty acids. The mean mass intensity for the matched m/z is greater in the PLB samples compared to the H99 samples (Figure 5 **) suggesting the lipid is found in greater abundance in PLB than it is in H99 ($p = 0.0437$). The two possible lipids are in fact a part of the same metabolic pathway which is derived from the essential C18 n-3 fatty acid α-Linolenic acid. The "Lipid map" examples for oxo-hydroxy-prostatetraenoic acid are PGA_3, PGJ_3 and PGB_3; all of these molecules are prostaglandin like derivatives of eicosapentenoic acid.

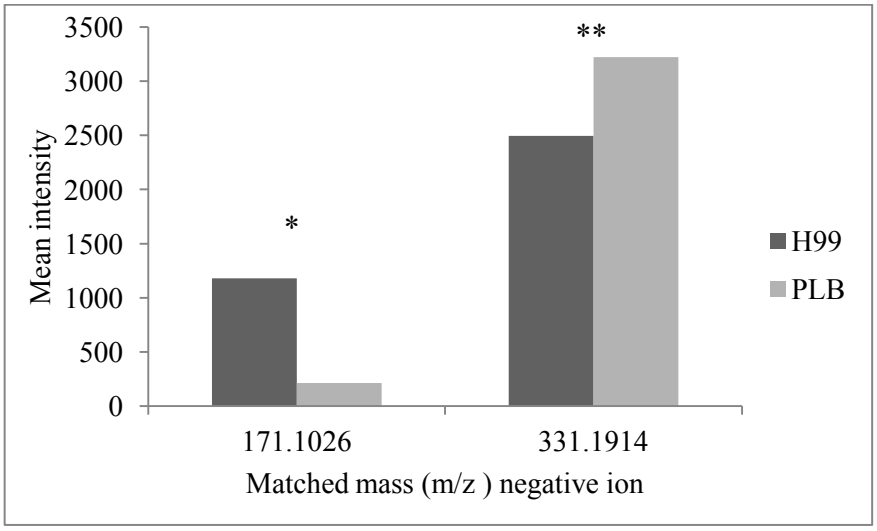

Figure 5 – The intensity of putative fatty acid matched masses between H99 and PLB sample groups - *Mass spectrometry m/z data was compared against the 'Lipid Maps' fatty acid database using the fatty acid database search tool, using a delta value cut off of +/- 0.001 m/z. Returned lipid identities were correlated to the original intensity data for each identified mass. The mean intensity for each sample group – H99 and PLB was calculated for the following samples – H99 samples A, B and E – PLB samples A, B and E. A two tailed student's T test was performed to compare the same sample groups. Significant matched masses (P<0.005) were plotted against mean intensity for H99 and PLB sample groups. * Input mass (m/z) 171.10182 (P=0.0115). ** input mass (m/z) 331.19139 (P=0.0437).*

Input mass	Matched Mass	Delta	Head group	Abbreviated name	Formula	H99 mean intensity	PLB mean intensity	P value (H99 vs. PLB)
645.45019	645.4501	0.0001	PA	PA(12:0/20:1(11Z))	C35H66O8P	46135.24	34317.56	0.014759
645.45019	645.4501	0.0001	PA	PA(10:0/22:1(13Z))	C35H66O8P	46135.24	34317.56	0.014759
645.45019	645.4501	0.0001	PA	PA(16:0/16:1(9Z))	C35H66O8P	46135.24	34317.56	0.014759
645.45019	645.4501	0.0001	PA	PA(15:0/17:1(9Z))	C35H66O8P	46135.24	34317.56	0.014759
645.45019	645.4501	0.0001	PA	PA(14:1(9Z)/18:0)	C35H66O8P	46135.24	34317.56	0.014759
645.45019	645.4501	0.0001	PA	PA(18:0/14:1(9Z))	C35H66O8P	46135.24	34317.56	0.014759
645.45019	645.4501	0.0001	PA	PA(17:1(9Z)/15:0)	C35H66O8P	46135.24	34317.56	0.014759
645.45019	645.4501	0.0001	PA	PA(16:1(9Z)/16:0)	C35H66O8P	46135.24	34317.56	0.014759
645.45019	645.4501	0.0001	PA	PA(22:1(13Z)/10:0)	C35H66O8P	46135.24	34317.56	0.014759
645.45019	645.4501	0.0001	PA	PA(20:1(11Z)/12:0)	C35H66O8P	46135.24	34317.56	0.014759
645.45019	645.4501	0.0001	PA	PA(18:1(9Z)/14:0)	C35H66O8P	46135.24	34317.56	0.014759
645.45019	645.4501	0.0001	PA	PA(14:0/18:1(9Z))	C35H66O8P	46135.24	34317.56	0.014759
671.46605	671.4657	0.0003	PA	PA(14:0/20:2(11Z,14Z))	C37H68O8P	24277.66	19128.41	0.006055
671.46605	671.4657	0.0003	PA	PA(14:1(9Z)/20:1(11Z))	C37H68O8P	24277.66	19128.41	0.006055
671.46605	671.4657	0.0003	PA	PA(12:0/22:2(13Z,16Z))	C37H68O8P	24277.66	19128.41	0.006055
671.46605	671.4657	0.0003	PA	PA(16:0/18:2(9Z,12Z))	C37H68O8P	24277.66	19128.41	0.006055
671.46605	671.4657	0.0003	PA	PA(18:1(9Z)/16:1(9Z))	C37H68O8P	24277.66	19128.41	0.006055
671.46605	671.4657	0.0003	PA	PA(17:2(9Z,12Z)/17:0)	C37H68O8P	24277.66	19128.41	0.006055

Input mass	Matched Mass	Delta	Head group	Abbreviated name	Formula	H99 mean intensity	PLB mean intensity	P value (H99 vs. PLB)
671.46605	671.4657	0.0003	PA	PA(18:2(9Z,12Z)/16:0)	C37H68O8P	24277.66	19128.41	0.006055
671.46605	671.4657	0.0003	PA	PA(17:1(9Z)/17:1(9Z))	C37H68O8P	24277.66	19128.41	0.006055
671.46605	671.4657	0.0003	PA	PA(17:0/17:2(9Z,12Z))	C37H68O8P	24277.66	19128.41	0.006055
671.46605	671.4657	0.0003	PA	PA(16:1(9Z)/18:1(9Z))	C37H68O8P	24277.66	19128.41	0.006055
671.46605	671.4657	0.0003	PA	PA(22:2(13Z,16Z)/12:0)	C37H68O8P	24277.66	19128.41	0.006055
671.46605	671.4657	0.0003	PA	PA(20:2(11Z,14Z)/14:0)	C37H68O8P	24277.66	19128.41	0.006055
671.46605	671.4657	0.0003	PA	PA(20:1(11Z)/14:1(9Z))	C37H68O8P	24277.66	19128.41	0.006055
717.47122	717.4712	0	PG	PG(12:0/20:2(11Z,14Z))	C38H70O10P	81404.68	52576.35	0.029281
717.47122	717.4712	0	PG	PG(10:0/22:2(13Z,16Z))	C38H70O10P	81404.68	52576.35	0.029281
717.47122	717.4712	0	PG	PG(14:0/18:2(9Z,12Z))	C38H70O10P	81404.68	52576.35	0.029281
717.47122	717.4712	0	PG	PG(16:1(9Z)/16:1(9Z))	C38H70O10P	81404.68	52576.35	0.029281
717.47122	717.4712	0	PG	PG(18:2(9Z,12Z)/14:0)	C38H70O10P	81404.68	52576.35	0.029281
717.47122	717.4712	0	PG	PG(17:2(9Z,12Z)/15:0)	C38H70O10P	81404.68	52576.35	0.029281
717.47122	717.4712	0	PG	PG(22:2(13Z,16Z)/10:0)	C38H70O10P	81404.68	52576.35	0.029281
717.47122	717.4712	0	PG	PG(20:2(11Z,14Z)/12:0)	C38H70O10P	81404.68	52576.35	0.029281
717.47122	717.4712	0	PG	PG(15:0/17:2(9Z,12Z))	C38H70O10P	81404.68	52576.35	0.029281
743.48714	743.4868	0.0003	PG	PG(14:0/20:3(8Z,11Z,14Z))	C40H72O10P	46129.72	28957.4	0.03417

Input mass	Matched Mass	Delta	Head group	Abbreviated name	Formula	H99 mean intensity	PLB mean intensity	P value (H99 vs. PLB)
743.48714	743.4868	0.0003	PG	PG(16:0/18:3(9Z,12Z,15Z))	C40H72O10P	46129.72	28957.4	0.03417
743.48714	743.4868	0.0003	PG	PG(16:1(9Z)/18:2(9Z,12Z))	C40H72O10P	46129.72	28957.4	0.03417
743.48714	743.4868	0.0003	PG	PG(18:3(9Z,12Z,15Z)/16:0)	C40H72O10P	46129.72	28957.4	0.03417
743.48714	743.4868	0.0003	PG	PG(17:2(9Z,12Z)/17:1(9Z))	C40H72O10P	46129.72	28957.4	0.03417
743.48714	743.4868	0.0003	PG	PG(17:1(9Z)/17:2(9Z,12Z))	C40H72O10P	46129.72	28957.4	0.03417
743.48714	743.4868	0.0003	PG	PG(20:3(8Z,11Z,14Z)/14:0)	C40H72O10P	46129.72	28957.4	0.03417
743.48714	743.4868	0.0003	PG	PG(18:2(9Z,12Z)/16:1(9Z))	C40H72O10P	46129.72	28957.4	0.03417
879.63422	879.6332	0.001	PI	PI(O-18:0/20:0)	C47H92O12P	11397.68	2238.575	0.034615
879.63422	879.6332	0.001	PI	PI(O-20:0/18:0)	C47H92O12P	11397.68	2238.575	0.034615
879.63422	879.6332	0.001	PI	PI(O-16:0/22:0)	C47H92O12P	11397.68	2238.575	0.034615
937.58129	937.5812	0.0001	PI	PI(20:1(11Z)/22:5(7Z,10Z,13Z,16Z,19Z))	C51H86O13P	3065.072	1743.7	0.007674
937.58129	937.5812	0.0001	PI	PI(22:5(7Z,10Z,13Z,16Z,19Z)/20:1(11Z))	C51H86O13P	3065.072	1743.7	0.007674
937.58129	937.5811	0.0002	PI	PI(20:5(5Z,8Z,11Z,14Z,17Z)/22:1(13Z))	C51H86O13P	3065.072	1743.7	0.007674
937.58129	937.5811	0.0002	PI	PI(20:0/22:6(4Z,7Z,10Z,13Z,16Z,19Z))	C51H86O13P	3065.072	1743.7	0.007674
937.58129	937.5811	0.0002	PI	PI(22:2(13Z,16Z)/20:4(5Z,8Z,11Z,14Z))	C51H86O13P	3065.072	1743.7	0.007674
937.58129	937.5811	0.0002	PI	PI(22:1(13Z)/20:5(5Z,8Z,11Z,14Z,17Z))	C51H86O13P	3065.072	1743.7	0.007674
937.58129	937.5811	0.0002	PI	PI(20:2(11Z,14Z)/22:4(7Z,10Z,13Z,16Z))	C51H86O13P	3065.072	1743.7	0.007674

Input mass	Matched Mass	Delta	Head group	Abbreviated name	Formula	H99 mean intensity	PLB mean intensity	P value (H99 vs. PLB)
937.58129	937.5811	0.0002	PI	PI(22:6(4Z,7Z,10Z,13Z,16Z,19Z)/20:0)	C51H86O13P	3065.072	1743.7	0.007674
937.58129	937.5811	0.0002	PI	PI(22:4(7Z,10Z,13Z,16Z)/20:2(11Z,14Z))	C51H86O13P	3065.072	1743.7	0.007674
937.58129	937.5811	0.0002	PI	PI(20:4(5Z,8Z,11Z,14Z)/22:2(13Z,16Z))	C51H86O13P	3065.072	1743.7	0.007674

Table 2 – Putative phosphoglycerolipid identities which are significantly different between H99 and PLB – *Mass spectrometry m/z data was compared against the 'Lipid Maps' phosphoglycerolipid database using the phosphoglycerolipid database search tool, with a delta value cut off of +/- 0.001 m/z. Returned lipid identities were correlated to the original intensity data for each identified mass. The mean intensity for each sample group – H99 and PLB was calculated for the following samples – H99 samples A, B and E – PLB samples A, B and E. A two tailed student's T test was performed to compare the same sample groups.*

Sorting the phosphogycerolipids by significance in the same way as the fatty acids revealed 55 putative glycerophospholipids which were significantly different between sample groups. The 55 returned lipids represent 6 input m/z values which had matched m/z with delta values between 0 and 0.0003 (Table 2). The matched m/z values were 645.4501 m/z, 671.4657 m/z, 717.4712 m/z, 879.6332 m/z and 937.5811 m/z. Interestingly all the mean intensities for each matched mass were greater in the H99 sample group than they were in the PLB sample group (Figure 6). The 55 putative phosphoglycerolipids identified fell into three different phosphoglycerolipid groups, the three groups were as follows: glycerophosphates (PA), glycerophosphoglycerols (PG) and glycerophosphoinisitols (PI).

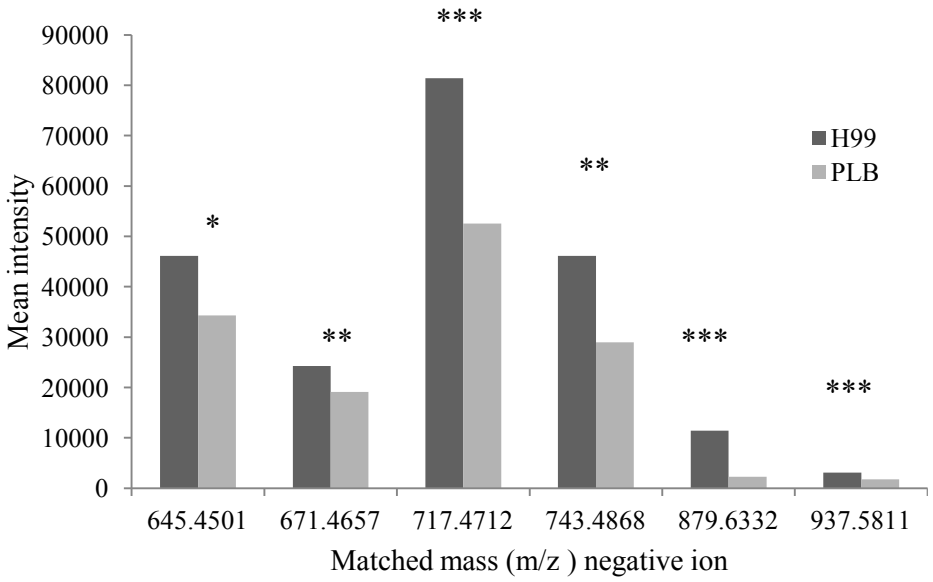

Figure 6 – The intensity of putative phosphoglycerolipids matched masses between H99 and PLB sample groups - *Mass spectrometry m/z data was compared against the 'Lipid Maps' phosphoglycerolipid database using the phosphoglycerolipid database search tool, using a delta value cut off of +/- 0.001 m/z. Returned lipid identities were correlated to the original intensity data for each identified mass. The mean intensity for each sample group – H99 and PLB was calculated for the following samples – H99 samples A, B and E – PLB samples A, B and E. A two tailed student's T test was performed to compare the same sample groups. Significant matched masses (P<0.005) were plotted against mean intensity for H99 and PLB sample groups. * Input mass (m/z) 645.4501 (P=0.014759). ** Input mass (m/z) 671.46605 (P=0.006055). *** Input mass (m/z) 717.47122 (P=0.29281). **** Input mass (m/z) 743.48714 (P=0.3417). ***** Input mass (m/z) 879.634.22 (P=0.034615). ****** Input mass (m/z) 937.58129 (P=0.007674)*

3.4 Cryptococcal intracellular proliferation can be modulated with eicosanoid modifying treatments

Having discovered phenotypic and morphological differences between the *PLB1* gene knockout mutant PLB and the wild type *C. neoformans* strain H99 we next wanted to see whether we could begin elucidate some of the possible biological mechanisms that Plb is a part of during infection. One current theory for the importance of Plb during *C. neoformans* infection of macrophages is that the phospholipase produces a reservoir of arachidonic acid which would allow the production of various bioactive eicosanoids. As well as producing evidence for a putative eicosanoid and arachidonic acid like lipid structures using mass spectrometry in this study it has also been observed in other studies that eicosanoids are produced by *C. neoformans* cells in liquid culture. In addition to this is well established that eicosanoids such as prostaglandins have bioactive roles within macrophages which contribute to the generation of an immune response. Thus it is not such a leap to theorise that the loss of eicosanoid production due to *PLB1* knockout could contribute to some of the differences observed differences between PLB and wild type H99.

To test this theory we decided to see if we could recreate the phenotype observed for PLB in H99 by applying a treatment which is known to modulate eicosanoid metabolism. The treatment we used is a combination of two drugs – bezafibrate (BEZ) and medroxyprogesterone acetate (MPA) which together will be referred to as BAP. We chose this drug combination because they have been reported to alter eicosanoid metabolism within cells (Khanim et al., 2009). We hoped this combination of compounds could help confirm if eicosanoid metabolism contributes to *Cryptococcus* virulence.

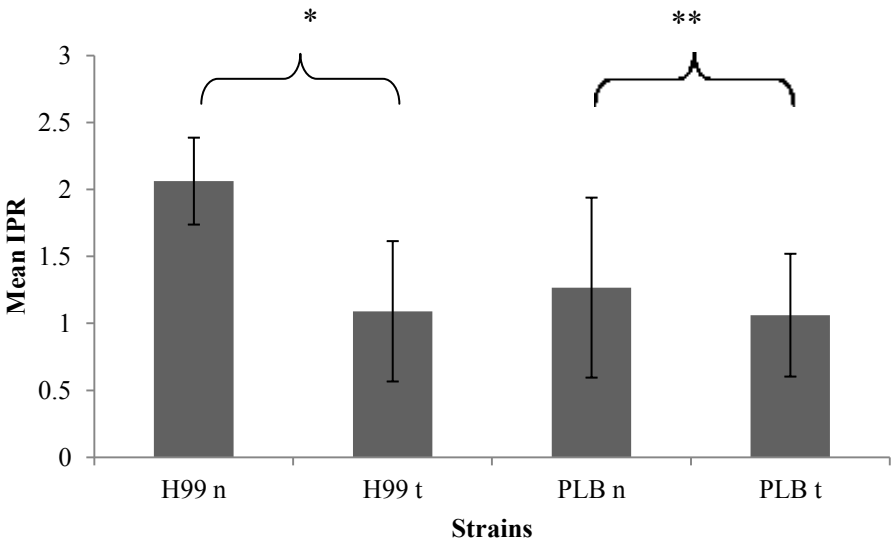

Figure 7 – IPR assay comparing the intracellular proliferation of H99 and PLB with and without BAP treatment – *H99 and PLB infected macrophages were either left untreated (H99n, PLBn) or were treated with bezafibrate and medroxyprogesterone. Briefly 1x10^6 un opsonised C. neoformans strain was added to 1x10^5 PMA activated J774 macrophages plated in 24 well tissue culture plates in 1ml serum free DMEM supplemented with bezafibrate (stock 0.05 M) and medroxyprogesterone (stock 0.5 mM) at a working concentration of 1 in 1000. After two hours (0 hours) extracellular Cryptococcus cells were washed away, the number of intracellular Cryptococcus were counted at 0, 18 and 24 hour time points, the 18 hour and 24 hour time point wells were re supplemented with the same BAP dosage following washing. The IPR was calculated from the maximum intracellular cell number divided by the initial uptake at 0 hour. After two hours (0 hours) extracellular Cryptococcus cells were washed away, the number of intracellular Cryptococcus were counted at 0, 18 and 24 hour time points. The IPR was calculated from the maximum intracellular cell number divided by the initial uptake at 0 hour. Filled in bars represent the mean IPR value for each strain (n=3),*

error bars represent 2x standard error. A two tailed Student's t test was performed for the following groups: H99n vs. H99t (P = 0.03) and PLBn vs. PLBt (**P= 0.64).*

When J774 macrophages were treated with BAP at the same time as H99 infection (Figure 5 - H99 t) there was roughly a 50% decrease in intracellular proliferation compared to H99 in untreated J774 cells (Figure 7 – H99n). Interestingly BAP treatment brought the intracellular proliferation rate of H99 down to the same level untreated PLB (Figure 7 – PLBn). BAP treatment of J774 macrophages infected with PLB (Figure 7 – PLBn) did not significantly affect the intracellular proliferation of PLBt compared to non treatment (Figure 7 – PLBt), however the intracellular proliferation of PLBn was already reduced compared to H99. Taken together this data suggests that the intracellular proliferation rate of the H99 wild type can be brought down to the level of the *PLB1* knockout PLB using BAP which is an eicosanoid altering treatment.

DISCUSSION

Our investigation has described previously unreported phenotypic and morphological observations for the *PLB1* knockout strain PLB which were not observed in the wild type parent strain H99 or in the *PLB1* rescue strains PLB1 and PLB2.

PLB proliferative deficiency

Our finding that PLB appears to grow badly in J774 macrophages compared to H99, PLB1 and PLB2 (Figure 1) indicates that Plb is important for intracellular survival within macrophages. A role for Plb in intracellular survival is supported by previous studies which report a correlation between Plb expression in *C. neoformans* and a greater number fungal burden in the lungs of mice following nasal infection (Chayakulkeeree et al., 2011). Plb could contribute to increased cryptococcal burden inside macrophages possibly by encouraging proliferation and also by providing protection against microbial killing which otherwise would reduce intracellular numbers. Support for Plb's role in proliferation is provided by a study using the same *PLB1* knockout strain as us which reported that PLB had a significantly slower budding rate inside a macrophage cell line than H99, PLB1 or PLB2 (Cox et al., 2001).

Although the molecular basis for PLB's growth deficiency cannot be defined from our data we have seen that the deficiency is not dependant on the cryptococcal burden within macrophages (Figure 3A), or the activation state of macrophages (Figure 2). Further work must be done to characterise PLB's growth within macrophages. This work will include IPR assays within primary human macrophages to ensure that the phenotype observed is not an artefact of our experimental model. Work must also be performed to determine whether the growth deficiency is intrinsic to the *Cryptococcus* or whether something is being produced by the macrophage to halt proliferation.

Cell size

The presence of *C. neoformans* cells which are above average in diameter have been reported *in vitro* as well as *in vivo*, these large cells are often referred to as 'Titan cells' in the literature. The largest PLB cell we measured was 14.56 μm in diameter which is about 2 times bigger than a normal cell (Figure 4B – PLB/18 hr J774). In terms of Titan Cell morphologies previously described this is within the size range for a titan cell but is at the lower end of the size scale. Normal *Cryptococcus* cells grow to be between 5 and 10 μm in diameter, whereas Titan Cells are generally considered to be above 10 μm in diameter, and can grow up to 100 μm in diameter (10 times the normal size) (Okagaki et al., 2010). Although our cells are small compared to some studies it is likely that they were still growing when we measured them at 18 hours and thus if we'd let the experiment run for longer we may have measured even larger cells. It is also possible that our tissue culture model constrained the growth of PLB.

Our measurements only measured the diameter of the cell body and not the diameter of the polysaccharide capsule, as this is hard to measure inside macrophages without specific staining. With the capsule diameter included our cells could in fact be much larger than we have reported. To analyse the absolute diameter of our cells we would have to collect intracellular *Cryptococcus* cells from within J774 cells using a cell lysis step similar to that used in the IPR. *C. neoformans* cells within the cell lysate would then have to be stained to visualise their polysaccharide capsule using a capsule binding monoclonal antibody and an appropriate fluorophore.

Interestingly we observed that inside macrophages PLB grew in size but did not proliferate (Figure 4A). This could provide an explanation for PLB's growth deficiency which was observed in our first experiment (Figure 1); it seems that instead of proliferating like wild type cells PLB cells instead divert their efforts to growing larger.

The reason why only the *PLB1* knockout strain grew larger is unclear but it suggests that deficiency in Plb may be responsible for this morphology. The formation of Titan Cells has been linked to extracellular signalling between *Cryptococcus* cells which are interpreted by G protein receptors on the cell surface (Okagaki et al., 2011). The fact that only the *PLB1* knockout strain and not the knockout grows in size could indicate that something in the normal signalling pathway is being perturbed by Plb deficiency. Plb knockout strains of *C. neoformans* have previously been reported to have abnormal membrane structure (Siafakas et al., 2007). Plb is a phospholipid modifying enzyme so knockout could affect the lipid composition of a cellular membrane and as a result the function of membrane signalling proteins within it.

We report that PLB increases in diameter both inside J774 macrophages and extracellulary in DMEM (Figure 4A). Although PLB cells did increase in size in the negative control the maximum cell diameter did not exceed the 10 μm diameter requirement for Titan Cell morphology. Thus Titan Cell morphology is only seen when PLB is inside J774 macrophages. This leads us to conclude that there must be something which is either present within the macrophage or produced by *C. neoformans* in response to being inside a macrophage which triggers the Titan Cell response. Extracellular Titan Cell formation can be stimulated *in vitro* by reusing medium that has previously been used to grow macrophages (Okagaki et al., 2010), this suggests that there is a molecule produced by macrophages which stimulates Titan Cell development. When this data is taken into consideration with our own data showing that only intracellular cells grow larger this suggests that the development of the observed morphology is due to an interaction between *Cryptococcus* and macrophages.

The Titan Cells morphology is thought to protect *C. neoformans* by increasing the resistance to phagocytosis and also protecting *Cryptococcus* cells from microbial killing mechanism

within the macrophage. Although Titan Cell can protect *C. neoformans* the morphology in fact reduces virulence, this is thought to be because Titan Cells do not appear to disseminate to the brain (Okagaki et al., 2010). A similar inability to disseminate from the lungs has also been reported for a Plb deficient *Cryptococcus* strain (Santangelo et al., 2004), this study found that Plb was required for dissemination from the lungs into the blood in mice but was not required for dissemination from the blood into the brain following intravenous inoculation. Although this study did not report any change in *C. neoformans* morphology it is possible that Titan Cell morphology in the Plb deficient mutant could be an explanation for these results. In addition to this we have previously reported that the PLB mutant has a reduced rate of macrophage escape compared to H99 which could be a compounding factor in reducing dissemination (Chayakulkeeree et al., 2011).

Although PLB produces larger cells we cannot be certain that they are the same as previously described *in vivo* Titan Cells. Thus further work must be performed to firstly define what biochemical factors make Titan cells different from normal *Cryptococcus* cells apart from their size; this could include gene expression analysis as well as lipidomic mass spectrometry to compare the genes and lipids involved in creating a Titan Cell like state. Further work must be done to confirm that PLB cells grow larger with primary human macrophages, we could also analyse cell size in a suitable animal model; this will also allow us to examine dissemination to the central nervous system.

Lipidomic study

To our knowledge we have performed the first whole cell lipidomic study to analyse C. *neoformans* infected macrophages with infecting *Cryptococcus* cells *in situ*. Refinement of this technique in the future will allow us to better examine the host pathogen interaction

between the macrophage and *Cryptococcus* and give us a snapshot of lipid metabolism during fungal infection.

Analysis of the data set generated by the mass spectrometry analysis identified 1143 putative fatty acid and glycerophospholipid identities. Of these 1143 identities 61 were identified as being significantly higher in intensity for either H99 or PLB sample groups (Table 1 and table 2) (The intensity measure although not fully quantitative gives a good indication of the abundance of a lipid in a given sample). PCA analysis of the differences between strains suggest that knockout of Plb did not cause any large scale changes in the lipid composition of the cells (data unpublished). This suggests that perhaps only a few lipids are dependent on Plb's expression; it could also mean that there is a certain level of redundancy – this is understandable as macrophages themselves express phospholipase enzymes when activated (Adams and Hamilton, 1984).

As a preliminary study we feel that the data we have provided proves the concept that differences in lipid composition between macrophages infected with different *Cryptococcus* strains can be compared using mass spectrometry. The main criticism of our study is that it was not really large enough to be conclusive. In future studies we must expand to include more experimental repeats to ensure that any differences we find are due to biological differences and not experimental error and experimental noise. We also hope that with a greater number of repeats we will be able to identify an even greater number of differences between strain sample groups. In the future we must also expand the study to compare more *Cryptococcus* strains such as the *PLB1* rescues PLB1 and PLB2. These two strains are required so that we can more confidently assert that differences between H99 and PLB observed are due to the knockout of the *PLB1* gene. We must also expand the study to include control samples. Desirable controls include uninfected macrophages as well as extracellular

C. neoformans. These extracellular *Cryptococcus* controls would be in the form of *Cryptococcus* cells which have been collected following macrophage infection. These two controls would allow us to begin to determine whether a lipid we have identified is of macrophage or cryptococcal origin. It may also be possible to differentiate between *Cryptococcus* and macrophage lipids by growing our *C. neoformans* overnight cultures in medium in which normal glucose has been substituted for a C^{14} labelled glucose. Growing *Cryptococcus* on this different carbon isotope will allow us to differentiate between lipids of different cellular origin following mass spectrometry analysis; this is because the same lipid molecule from either macrophages or *C. neoformans* cells would have a different but identifiable mass.

Another shortcoming of our lipidomic study is that although we have identified over 1000 putative lipids we cannot definitively confirm a lipid's identity from a m/z match. The reason for this is that there are sometimes multiple lipid molecules for a certain m/z which have the same molecular mass but a different structural configuration. For this reason in future studies we must perform tandem MS/MS analysis. This technique makes use of two mass spectrometers which work in concert with one another. The sample is ionised in the first mass spectrometer to create a mass spectra, ions of interest from this first mass spectrometer are isolated and sent to the second mass spectrometer where fragmentation analysis occurs. Every molecule has a different fragmentation signature, thus using fragmentation analysis one can tell the difference between two molecules even if they have the same molecular mass using their structure. By comparing the fragmentation patterns we observe using MS/MS to an online database such as 'Lipid Maps' we will be able to more definitively confirm lipid identities.

Without knowing the correct identities of the significant lipids we have identified not much can be concluded about their biological significance. We observed that all the significantly different putative glycerophospholipids appeared to have a higher abundance in H99 than they did in PLB. This could be a coincidence. However it may be that the glycerophospholipid lipids measured are a part of the same metabolic pathway, and as such an increase in the uppermost metabolite could lead to a general increase throughout the pathway. Of the putative fatty acids significantly different between the two sample groups (Table 1) we found a group of short chained 8-9 carbon chain fatty acids and two 20 carbon chain fatty acids. The short chain fatty acids we detected are derivatives of octanoic, nonenoic and nonanoic acid; each had the same matched m/z of 171.10182. These fatty acids appeared to be more abundant in H99 than they were in PLB. The two 20 carbon chain fatty acids we detected - epoxy-hydroxy-eicosapentenoic acid and oxo-hydroxy-prostatetraenoic acid are interesting as they are metabolites of α-Linolenic acid, metabolites of this pathway are bioactive molecules which are thought to have opposite effects to prostaglandins in that they are anti inflammatory, thus increased levels of these lipids in PLB may negatively affect wild type virulence by inhibiting eicosanoid production (Singer et al., 2008).

BAP combination treatment

We have found that a combination treatment of BEZ and MPA appears to slow or even inhibit the growth of wild type H99 *Cryptococcus* inside infected J774 macrophages (Figure 7).

BEZ and MPA (BAP) are two existing drugs which have been shown to have bioactive effects on the expression of prostaglandins in mammalian cells. Both drugs are commercially available and off patent; BEZ is an anti-cholesterol drug whereas MPA is a female contraceptive treatment. BAP combination treatment is currently being pioneered as an efficacious treatment for acute myeloid leukaemia (AML). The anti neoplasic effects of these

two drugs is reported to be due to their combined ability to increase the levels of prostaglandin D_2 (PGD_2) in cancer cells via an increase in synthesis and a decrease in metabolism. Increased levels of PGD_2 inside cells leads to a direct increase in PGD_2's dehydrated form called 15 deoxy$\Delta^{12, 14}$ prostaglandin J_2 (15d-PGJ_2) (Khanim et al., 2009). It was due to these eicosanoid modifying effects that we chose to test BAP treatment on *C. neoformans* infected J774 macrophages in order to expand the theory that Plb's contribution to virulence might be because of its ability to influence eicosanoid production within the macrophage. 15d-PGJ_2 is different to most prostaglandins because it does not have a specific extracellular receptor, however it does have an intracellular receptor called PPARγ. This receptor is thought to be the main signalling component which mediates 15d-PGJ_2's bioactivity within cells (Scher and Pillinger, 2005).

We do not know whether infected J774 macrophages treated with BAP produce increased levels of 15d-PGJ_2 so we cannot say for certain that 15d-PGJ_2 is responsible for the decrease in intracellular proliferation observed. If in fact if BAP is acting via 15d-PGJ_2 an exact molecular mechanism would still be hard to deduce; like most eicosanoids 15d-PGJ_2 is complicated and contradictory in nature. In macrophages PPARγ ligation via 15d-PGJ_2 generally produces an anti inflammatory response which is characterised by inhibition of inflammatory cytokines (Jiang et al., 1998), decreased macrophage activation and decreased production of inducible nitric oxide synthase (iNOS) (Ricote et al., 1998). However 15d-PGJ_2 also has pro inflammatory properties (Tontonoz et al., 1998). The diversity of function is probably due to among other things the magnitude of PPARγ activation, the subtype of macrophage and the macrophage's current anatomical location (Scher and Pillinger, 2005) .

To properly elucidate the pharmaceutical effects that BAP has on *Cryptococcus* infected macrophages we must find out what happens when BAP treatment is applied. This will

include analysis of gene expression with and without BAP treatment to observe the transcriptional changes the drug may exert. In addition to this we could examine the activation phenotype of macrophages following treatment, for example we could measure prostaglandin and cytokine secretion as well as cell surface molecule expression on macrophages.

The anti-tumour effects of 15d-PGJ_2 are mainly linked to its ability to induce apoptosis in tumour cells (Date et al., 2003, Khanim et al., 2009). Increased apoptosis is a desirable effect when combating tumours however one of the short comings of the IPR assay is that a drop in intracellular proliferation could be mimicked by increased macrophage cell death; this is because only *Cryptococcus* cells within live macrophages are counted. This potential false positive reading is a viable explanation for our observations as the J774 macrophages we used in our study is an immortalised tumour derived cell line and as such 15d-PGJ_2 might have similar apoptotic effects as it does for other tumour cells. To compound the issue 15d-PGJ_2 has also been reported to cause apoptosis in non neoplasic human macrophages (Chinetti et al., 1998). The question over whether BAP causes apoptosis of macrophages instead of affecting *Cryptococcus* proliferation could be easily answered using an apoptosis assay to quantify the level of apoptosis over time in BAP treated and untreated J774 macrophages.

Even if BAP combination treatment does reduce the proliferation *Cryptococcus* we still cannot state for certain that this is due to specific pharmacological effects of the drug treatment. In addition to the two drug compounds we also in advertently treated the macrophages with DMSO and ethanol which were the solvents for the two drugs. It is possible that these two compounds may have affected either the health of either the macrophages or the *Cryptococcus* cells – this could be via the apoptosis false positive mechanism previously discussed or by signalling in some way to the cells. To remove this potential false positive result we must perform a vehicle control where we compare the

intracellular proliferation of BAP treated macrophages with macrophages treated with DMSO and ethanol only. Further work could also be done to find the minimum effective dose needed to produce a significant decrease in proliferation.

If BAP treatment does in fact inhibit the intracellular growth of *Cryptococcus* then it may be possible to develop the drug combination as a treatment for cryptococcosis. The current treatment for cryptococcosis makes use of the anti fungal drug Fluconazole. A relatively poor prognosis for cryptococcosis even with treatment means there is a demand for effective compounds which could be given alongside Fluconazole to improve treatment. Development of BAP as a supplementary treatment to antifungal drugs would first require *in vitro* IPR experiments comparing the effectiveness of Fluconazole at halting fungal growth with and without additional BAP; it may also be useful to test each BAP drug (BEZ and MPA) on their own to see if both drugs are required or if one or the other is sufficient. Once solid evidence of *in vitro* treatment using BAP alongside Fluconazole is produced we could then move to an *in vivo* model of cryptococcosis using an animal model such as mice. If the drug remains effective and safe in animal models it may be possible to proceed to small scale human trials to test efficacy and safety.

Conclusion

As a result of this study we have reported both phenotypic and morphological differences which appear to correlate to the knockout of phospholipase B expression in *C. neoformans*. These observations point to the conclusion that phospholipase B expression is important for the normal function of *Cryptococcus* cells within murine macrophages. In the future we must expand upon and explore fully the molecular mechanisms behind these novel observations. In doing so we will gain a greater understanding of how phospholipase B and lipid signalling contribute to virulence. This knowledge should help ourselves and others in the mycology

field to better understand the generation of anti fungal immune responses; it will also help us design better treatments for cryptococcosis to improve the prognosis of disease sufferers around the world.

PART TWO

An investigation into the properties of two *Bdellovibrio bacteriovorus* C-di-GMP metabolism proteins – Bd2325 and Bd1971

Supervisor – Dr Andrew Lovering

INTRODUCTION

1.1 Bdellovibrio bacteriovorus

Bdellovibrio bacteriovorus is a small motile bacterium which has evolved to predate gram negative bacteria. Following initial attachment to the prey cell, *B. bacteriovorus* burrows through the cell wall into the periplasmic space where it modifies the prey cell to create an ideal environment for replication. Although *B. bacteriovorus* was appreciated around the time of its discovery for its unique and interesting lifecycle, the full potential of the bacteria has only recently been realised thanks to modern molecular biology techniques. The resurgence of interest surrounding *B. bacteriovorus* can be ascribed partly to its potential use as a 'living antibiotic', and partly to a growing appreciation of the molecular mechanisms regulating its lifecycle; knockout of these mechanisms often cause distinct observable mutant phenotypes and, because many of the same regulatory pathways in *B. Bacteriovorus* can be found across the bacterial kingdom they represent an exciting microbiological research tool (Sockett, 2009).

Strains of *B. bacteriovorus* have been isolated from a variety of different natural habits such as sewage, freshwater (Fry and Staples, 1976), soil (Klein and Casida, 1967) and the guts of animals such as humans (Schwudke et al., 2001). The variety of habitats *B. bacteriovorus* grows in is testament to the wide range of prey cells which *B. bacteriovorus* predates; as each habitat must provide at least one prey species in order for the predator to grow and divide. Predation by *B. bacteriovorus* is confined to gram negative species of bacteria, however within this group a diverse selection of prey species has been identified including important human pathogenic genera e.g. *Escherichia*, *Enterobacter, Vibrio, Shigella, Salmonella* and *Yersinia* to name a few (Dashiff et al., 2011). The potent and wide reaching bactericidal

ability that *B. bacteriovorus* displays has lead some researchers to speculate that a new generation of 'living antibiotics' could be produced using modified *B. bacteriovorus* strains applied directly to infected tissue (Dwidar et al., 2012).

B. bacteriovorus cells are usually found in a predatory 'attack phase', however a host independent (HI) or anexic phase can also be occasionally observed (Sockett, 2009). The cells displaying this HI phenotype are naturally occurring mutants of wild type *B. bacteriovorus* strains. HI cells are capable of forming biofilms in nutrient rich conditions, and disperse back into independent attack phase cells upon the addition of prey cells - in this case *E. coli* (Medina and Kadouri, 2009).The reversible sedentary HI phenotype is assumed to be a mechanism which has evolved to ensure the survival of *B. bacteriovorus* even when prey cells are scarce.

1.2 – Bdellovibrio bacteriovorus lifecycle

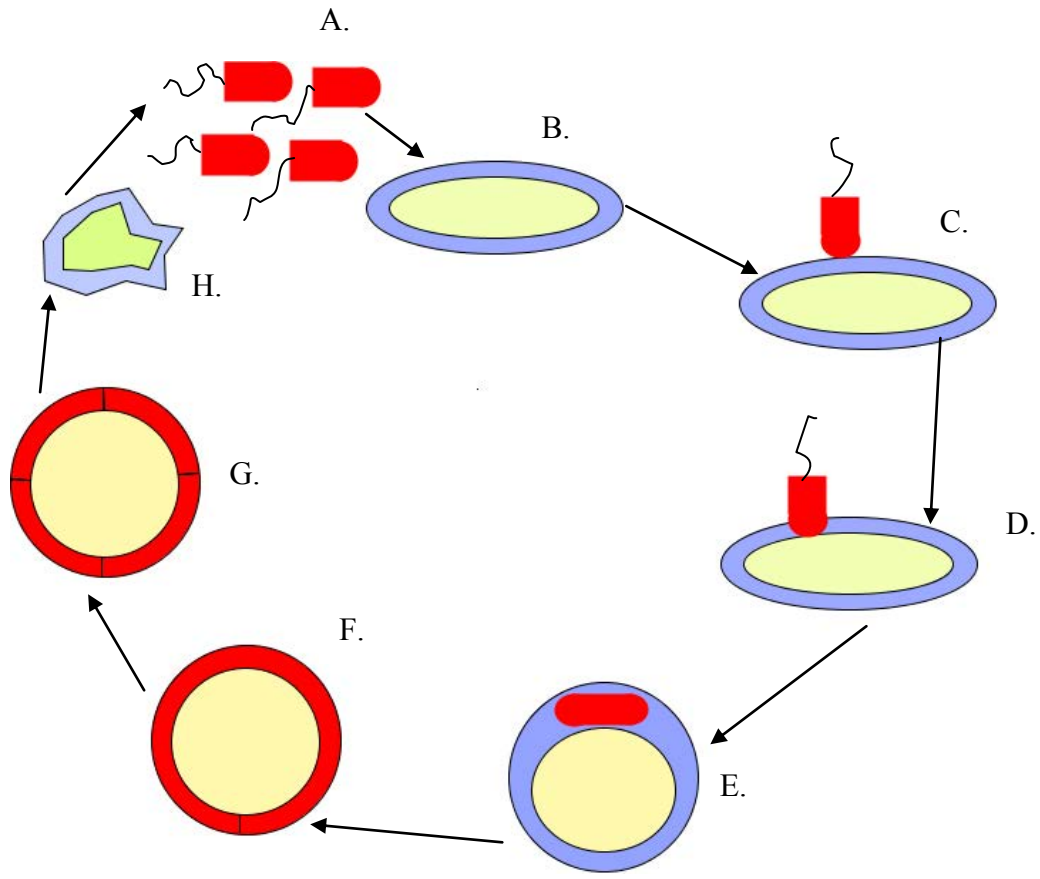

Figure 1: Diagrammatical representation of the B. bacteriovorus predatory lifecycle – ***A)*** *Small, highly motile flagellated attack phase B. bacteriovorus cells hunt for prey via chemotaxic mechanisms.* ***B)*** *Rod shaped gram negative prey cell - the blue outer ring represents the periplasm and the white inner circle represents the cytoplasm.* ***C)*** *An attack phase B. bacteriovorus cell locates a prey cell, initial reversible interactions form between the two cells as they contact. These contacts grow stronger with time until they become irreversible.* ***D)*** *The B. bacteriovorus cell burrows through the cell wall of the prey cell into the periplasm.* ***E)*** *B. bacteriovorus modifies the prey cell using hydrolytic enzymes to create the bdelloplast. These enzymes modify the prey cell wall and membrane and also digest parts*

of the cell as a food source. During bdelloplast formation the rod shape of the prey cell changes to a sphere. ***F)*** *B. bacteriovorus elongates within the periplasm until it forms a long filament the circumference of the bdelloplast.* ***G)*** *During cell division, the long filamented mother cell body septates to produce multiple progeny.* ***H)*** *The new progeny grow flagella, lyse the bdelloplast and then swim away to form new attack phase cells - all that is left of the prey cell is a dead husk.*

Motility and hunting

Motility is very important for *B. bacteriovorus's* predatory life style because the bacterium must search for prey cells to predate before growth and cell division can take place. The major contributor to *B. bacteriovorus* motility is a single sheathed flagellum (Thomashow and Rittenberg, 1985). Using this flagella *B. bacteriovorus* can reach very high speeds of up to 160 μm s^{-1} in liquid culture (Lambert et al., 2006). In addition to flagellar motility *B. bacteriovorus* can also move along solid surfaces using gliding motility; albeit at markedly lower speeds (Lambert et al., 2011).

Studies to discover how *B. Bacteriovorus* locates its prey during the hunt have discovered that attack phase cells are chemotatic towards high concentrations of bacteria (Straley and Conti, 1977). Bacterial products produced by prey cells such as amino acids may also possible chemotactic signals (LaMarre et al., 1977). Molecular studies indicate that chemotaxis proteins in *B. bacteriovorus* such as methyl accepting chemotactic protein (MCP) encoded by the gene *mcp2* may play a role in the hunting of prey (Lambert et al., 2003). Chemotaxis towards high concentrations of bacteria could explain the observed predation of biofilms by *B. bacteriovorus (Núñez et al., 2005)*.

Attachment and invasion

Once a *B. bacteriovorus* attack phase cell has located its prey the intracellular phase of the predatory cycle begins. The first stage of the intracellular phase involves the formation of strong physical attachments to the prey cell surface. It was initially thought that *B. bacteriovorus* made use of its high speed to forcibly ram itself into prey in order to physically attach to the cell wall (Sockett, 2009), however experiments using flagellin subunit (*fliC1-6*) attack phase knockout mutants lacking the motility of the wild type found this not to be the

case. These mutants were less efficient at killing prey due to an inability to seek out prey however when they were applied directly to prey cells predation was unaffected (Lambert et al., 2011). It is now thought that host cell recognition and initial attachment it is mediated by much more specific membrane interactions.

Although the exact nature of the interactions is only starting to be understood, it is known that initial contact with the prey cell is reversible and transient - lasting only a couple of minutes (Lambert et al., 2006). After this initial period however the attachments significantly strengthen and *B. bacteriovorus* becomes committed to the predatory cycle (Burnham et al., 1968). Candidate molecules for these attachments include Type IV pili. Type IV pili are fibre like structures a few microns in length which extend out from the cell wall of some bacteria. Type IV pili are found throughout the bacterial kingdom and have multiple functions including attachment to other cells, motility and disease pathogenesis (Craig et al., 2004). Type IV pili can be found expressed on the surface of around 30% of attack phase *B. bacteriovorus* cells at the opposite end of the cell to the flagellum (Evans et al., 2007). The importance of Type IV pili to the predatory lifecycle of *B. bacteriovorus* has been illustrated via mutation of the gene *PilA* which encodes PilA – the major structural component of Type IV pili fibres. Mutant strains lacking a functional *PilA* gene cannot assemble Type IV pili on the cell surface and are deficient in predation even when applied directly onto the surface of prey cells (Evans et al., 2007).

Once attached to the surface of a prey cell *B. bacteriovorus* creates a small pore within the prey cell wall allowing it to gain entry into the periplasm. The events which create this pore are not fully understood but it is thought that *B. bacteriovorus* might use some of the digestive enzymes which it possesses to weaken structural components of the prey cell wall such as peptidoglycan cross linking (Lambert et al., 2006). The pore, once it is created is not much

larger than *B. bacteriovorus* itself. To enter into the periplasm the predator cell pulls itself through the pore; the pulling force required for this may be generated by the contraction of the Type IV pili previously mentioned. Following entry into the periplasm the site of entry is sealed and *B. bacteriovorus* initiates the next major stage of its lifecycle; the remodelling of the prey cell into the Bdelloplast (Sockett, 2009, Lambert et al., 2006).

Modification and replication

The bdelloplast is the name given to the structure formed by the modification of a prey cell by the invading predator cell. There are thought to be a number of reasons for the formation of the bdelloplast, the first and foremost being the creation of a safe niche in which *B. bacteriovorus* is able to grow and reproduce. During the bdelloplast phase, catabolism of prey cell constituents creates readily available nutrients for cell growth and adjustment of the prey cell's structural integrity occurs which prevents prey cell lysis from osmotic stress (Lambert et al., 2006). The second reason for the bdelloplast may be in order to produce an occupancy signal which is recognisable to other attack phase *B. bacteriovorus* cells (Lerner et al., 2012). This signal is important because a second bacterium attempting to enter an already occupied cell could cause the death of both *B. bacteriovorus* cells.

Modification of the host cell into the bdelloplast occurs via the action of hydrolytic enzymes which are produced by *B. bacteriovorus* upon entry into the periplasm. Some of these enzymes can break apart prey cell wall peptidoglycan cross linking (Thomashow and Rittenberg, 1978b). An effect of this modification seems to be the unification of the periplasm and the prey cell cytoplasm (Cover et al., 1984); this has the effect of allowing small molecules to pass freely between the two spaces, allowing *B. bacteriovorus* access to nutrients usually confined to prey cell cytoplasm. Modification of peptidoglycan cross linking also

increases the tolerance of the prey cell wall to osmotic stresses which may occur during replication, preventing premature bdelloplast lysis (Lambert et al., 2006).

During bdelloplast formation, a change in prey cell shape occurs turning the cell from a rod shaped morphology to a spherical morphology - *N.B. this is assuming that prey cell is a rod shaped bacteria; the standard prey model in B. bacteriovorus research is the rod shaped bacteria Escherichia coli, thus most of what is known about prey cell interaction is based on rod shaped prey cells.* This morphological change firstly increases the volume of the bdelloplast, allowing for increased predator cell growth during replication but in addition it seems to form the cellular occupancy signal that invading *B. bacteriovorus* cells use to stop other attack phase cells entering their prey cell. A recent study identified two *B. bacteriovorus* genes which were responsible for this morphological change – *Bd0816* and *Bd3459*. These genes code for two peptidoglycan modifying proteins which belong to the 'class C penicillin binding protein' (PBP) family; class C PBP proteins remodel peptidoglycan by hydrolysing peptidoglycan crosslinking. The two genes were found to be up regulated during and directly after prey cell invasion. Knockout of the two genes produced *B. bacteriovorus* mutants which took longer to invade prey cells and produced bdelloplasts which remained rod shaped. Importantly these rod shaped bdelloplasts were found to be less efficient at producing an occupancy signal as illustrated by a higher frequency of double occupancy - characterised by a second *B. bacteriovorus* entering the bdelloplast (Lerner et al., 2012).

An ever present issue during formation of the bdelloplast is the balance which must be stuck between breaking down prey cell barriers which hinder the growth of *B. bacteriovorus* and irreparably destabilising the structure of the prey cell - which itself could cause premature bdelloplast lysis. In this respect studies have revealed a *B. bacteriovorus* regulatory system which selectively modifies prey cell wall peptidoglycan via N-deacetylation, protecting it

against cleavage by *B. bacteriovorus* hydrolase enzymes (Thomashow and Rittenberg, 1978a). Using this mechanism *B. bacteriovorus* may be able to control the levels of hydrolysis once the bdelloplast is formed, thus preserving the environment it has created.

It is inside the periplasm of the Bdelloplast that *B. bacteriovorus* replication takes place. The first stage of *B. bacteriovorus* replication involves the elongation of the parent cell until it has formed a long filament spanning the entire circumference of the Bdelloplast. Replication of *B. bacteriovorus,* like replication of any cell, requires the expenditure of significant amounts of energy as new genomes and organelles are produced. All of the energy and nutrients needed for *B. bacteriovorus* replication are obtained from digestion of the prey cell. This mode of replication produces logistical challenges for *B. bacteriovorus*, for instance the size of the *B. bacteriovorus* genome is comparable with that of the prey cell – thus the replication of multiple genomes from a single prey cell requires *de novo* synthesis of nearly all the nucleotides needed. To accomplish this task *B. bacteriovorus* has evolved an array of digestive enzymes to break down prey cell biological macromolecules as well as complex purine and pyrimidine synthesis systems (Lambert et al., 2006) .

Once *B. bacteriovorus* has elongated it begins to septate at multiple points along the filament to form usually four progeny cells (Lambert et al., 2006). Following septation, each progeny cell grows a new flagellum. Finally once the progeny are ready to leave, the bdelloplast is lysed and the new cells burst out to form the next wave of attack phase cells and the predatory cycle beings anew.

1.3 Bdellovibrio bacteriovorus and C-di-GMP signalling

The entire predatory process from initial attachment to bdelloplast lysis takes approximately 3.5 hours (Lambert et al., 2006), each step within the cycle must be dynamically controlled to

ensure the proper progression and timing of events. The molecular basis of these *B. bacteriovorus* control mechanisms are only just being elucidated, one important cellular regulator appears to be the small secondary messenger molecule Bis-(3'-5')-cyclic dimeric guanosine monophosphate (C-di-GMP) (Hobley et al., 2012). The importance of C-di-GMP in the control of cellular processes is not just confined to *B. bacteriovorus* - in fact it is becoming increasing clear that C-di-GMP is a key secondary messenger across the bacterial kingdom. The various signalling pathways which C-di-GMP modulates within bacteria are diverse but are usually linked to important lifecycle decisions (Krasteva et al., 2012) e.g. virulence factor expression, motility vs. senescence, biofilm formation and , in the case of *B. bacteriovorus* ; the control of important decision checkpoints during the predation process (Hobley et al., 2012).

C-di-GMP metabolism

C-di-GMP synthesis and breakdown within bacteria is controlled by the opposing actions of two types of enzymes. Synthesis of C-di-GMP is controlled by a group of diguanylate cyclases which possess a common GGDEF domain while breakdown of C-di-GMP is controlled by phosphodiesterase enzymes which possess either EAL or HD-GYP domains (Krasteva et al., 2012). Homology searches have revealed that GGDEF, EAL and HD-GYP domains proteins are some of the most widely distributed proteins in the bacterial world (Römling et al., 2005). Bacterial genomes can contain multiple genes coding for many different C-di-GMP metabolising proteins, in addition some proteins exist which contain both GGDEF and EAL domains (Tal et al., 1998). It is thought that this diversity is a result of the complexity of C-di-GMP mediated signalling in some bacteria and that the multiple proteins are required for the variety of pathways which C-di-GMP may control within a single cell (Römling et al., 2005) .

A single molecule of C-di-GMP is formed when two guanosine triphosphate (GTP) molecules are fused together via diguanylate cyclase activity. A GGDEF domain is about 180 residues in length and is defined by a Gly–Gly–Asp–Glu–Phe amino acid motif contained within the domain. Each GGDEF domain acts as a binding site for single GTP molecule and in addition possesses half of a catalytic site needed for full diguanylate cyclase activity (Römling et al., 2005). Structural studies of the GGDEF diguanylate cyclase active site have revealed that the mechanism for C-di-GMP synthesis requires the dimerisation of two separate GTP bound GGDEF domain containing proteins; only upon dimerisation is the fully active catalytic site created (Chan et al., 2004).

Degradation of C-di-GMP occurs via a hydrolysis reaction catalysed by the EAL or HD-GYP domain phosphodiesterase enzymes. During this reaction C-di-GMP is degraded into pGpG; further degradation from pGpG to GMP by EAL domain proteins has been observed, although the initial degradation step from C-di-GMP to pGpG is thought to be the rate limiting step of the reaction (Römling et al., 2005). A recent structural study which analysed multiple EAL domain proteins has suggested that the catalytic activity of EAL phosphodiesterases is dependent on the binding of two metal cations to conserved amino acid motifs within the EAL domain, these metal ions help to coordinate the positioning of a water molecule found bound to the active site which is needed for C-di-GMP cleavage (Tchigvintsev et al., 2010). The site which coordinates the binding of these cations is a conserved loop like structure within the EAL domain, metal ions commonly found bound to this loop are Mn^{2+} and Mg^{2+}. The presence of the two coordinating cations helps to position a water molecule which, under catalytic conditions, is deprotonated to give a hydroxide ion (OH^-) - this hydroxide group acts as a nucleophile and participates in a nucleophilic attack during the cleavage of C-di-GMP.

The final components in the C-di-GMP signalling system are the cellular elements which detect changing levels of C-di-GMP within the cytoplasm in order to propagate the signal to downstream processes, resulting ultimately in gene expression changes. Some of these C-di-GMP sensing systems are proteins such as PilZ C-di-GMP receptors and degenerate GGDEF domain proteins. Both groups of protein bind C-di-GMP in order to activate downstream processes – e.g. activation of additional proteins within various signalling pathways (Römling et al., 2005). In addition to these protein based detectors, C-di-GMP signalling is also propagated by a group nucleic acid based detectors called riboswitches; these transcription like elements are regulated by C-di-GMP and facilitate changes in expression for a number of target genes both transciptionally and post transscriptionally (Krasteva et al., 2012).

Bdellovibrio bacteriovorus specific -di-GMP proteins

The *B. bacteriovorus* genome is currently known to encode at least 5 GGDEF domain proteins, 1 EAL domain protein, 5 HD-GYP domain proteins and 15 PilZ domain proteins (Hobley et al., 2012). C-di-GMP signalling in *B. bacteriovorus* offers an exciting opportunity to explore the basis of C-di-GMP signalling mechanisms shared throughout the bacterial kingdom, this is because although C-di-GMP appears to play an important role in *B. bacteriovorus* signalling (as evidenced by the relatively high number of PilZ receptors) the number of C-di-GMP metabolism proteins is relatively low.

Initial knockout studies examining the 5 GGDEF domain proteins produced by *B. bacteriovorus* has been particularly fruitful. The five GGDEF domain proteins found in *B. bacteriovorus* have been designated DgcA (Bd0367), DgcB (Bd0742), DcgC (Bd1434), DgcD (Bd3766) and CdgA (Bd3125). Four of the five proteins, DgcA-D, have confirmed diguanylate cyclase activity as expected, however the fifth protein CdgA is not enzymatically active and may be a degenerative C-di-GMP cellular receptor. Interestingly it was found that

knockout mutants of four of the five genes – *DgcA*, *DgcB*, *DgcC* and *CdgA* – created in the *B. bacteriovorus* strain HD100 produced distinct phenotypes, each of which was related to a different part of the predatory lifecycle (Hobley et al., 2012). DgcA activity for example was found to be required for the control of *B. bacteriovorus* motility. Specifically knockout of *DgcA* rendered attack phase cells unable to swim in liquid culture or glide on solid surfaces (Hobley et al., 2012). Similar to flagella mutants previously discussed (Lambert et al., 2011) *DgcA*$^{-}$ mutants could not hunt prey but could still invade cells if applied directly to the prey. This lack of flagellar or gliding motility also rendered newly septated progeny from exiting the Bdelloplast (Hobley et al., 2012). Unlike *DgcA*$^{-}$ mutants, *DcgB*$^{-}$ mutants did not have any ablation of motility; however they were nonetheless unable to invade prey cells – indicating that DcgB is required for initiation of prey invasion. Study of *DcgC* knockout mutants showed no deficiency in predation as observed with *DgcA* and *DgcB* knockout mutants, instead it was found that the rate at which attack phase cells converted to HI phase cells was significantly decreased. Finally the degenerate GGDEF CdgA was found to play a role in host invasion; unlike *DcgB* knockout mutants, *CdgA* knockout could still invade prey cells but the invasion was significantly slower – nearly doubling the average 30-40 minutes it takes between initial prey encounter and formation of the bdelloplasr (Hobley et al., 2012).

It is surprising that knockout of four proteins which modify the levels of a single cytoplasmic signalling molecule could have such discrete and varied effects within a unicellular organism. A possible explanation for these discrete phenotypes can also be found in the study by Hobley et al., when they used fluorescently tagged versions of each GGDEF protein and found that each protein was localised to a specific area of the bacteria (Hobley et al., 2012). These observations support a model whereby there is not a single global C-di-GMP pool within bacteria, but rather a number of partitioned gradients within the cytoplasm. It is currently

thought that C-di-GMP is not freely diffusible within the cytoplasm but remains sequestered by C-di-GMP binding proteins which are targeted to different parts of the cell (Krasteva et al., 2012). In this way multiple independent C-di-GMP gradients can be curated within the same cytoplasmic space by differentially distributed C-di-GMP metabolising proteins - for the purposes of modulating distinct C-di-GMP signalling pathways.

Compared to what is known about the cellular functions of the 5 GGDEF guanylate cyclases little is known about the functional role of the six phosphodiesterase enzymes found in *B. bacteriovorus.* Although in depth phenotypic studies for these proteins have not yet been produced, a recent study has produced the first complete crystal structure of a *B. bacteriovorus* HD-GYP phosphodiesterase called Bd1817 (Lovering et al., 2011). This structure reveals a protein which possesses a C-terminal active site characterised by the binding of metal ions. The structure for Bd1817 is the first bacterial HD-GYP structure to be published, however Bd1817 in fact a degenerate protein and thus does not possess phosphodiesterase activity. With this in mind, the cellular function of Bd1817 is not known though it is thought it may as a 'decoy' enzyme by diluting out the effects of active enzymes.

1.4 Project aims

This study aims to build on and expand what it known about the functional characteristics for two C-di-GMP phosphodiesterase proteins – Bd2325 and Bd1971, which are found in *B. bacteriovorus*. This is a field of research which has already been advanced in recent years with the publishing of phenotypic and structural studies for *B. bacteriovorus* C-di-GMP related proteins (Hobley et al., 2012). The first of the proteins we propose to study is Bd2325, a 332 amino acid multi-domain HD-GYP protein which shares relatively close sequence homology with the previously mentioned *B. bacteriovorus* HD-GYP protein called Bd1817 (23% identical residues, 47% similar residues). Unlike Bd2325, Bd1817 is an inactive,

degenerative HD-GYP while Bd2325 appears to be fully functional. If a functional structure for Bd2325 were to be determined it would be more biologically relevant compared to Bd1817 in terms of C-di-GMP signalling in *B. bacteriovorus* and also to the field of microbiology as a whole. This is because to our knowledge no complete protein structure for an active bacterial HD-GYP phosphodiesterase protein is currently available.

Preliminary data from collaborators suggests that the biological role of Bd2325 in *B. bacteriovorus* is to control the switch between planktonic growth in liquid media and adherent growth on solid surfaces – this is because knockout mutants which lack Bd2325 expression can only be grown on solid agar. As well as improving our knowledge of C-di-GMP signalling, an understanding of this growth mechanism could prove extremely useful if *B. bacteriovorus* is ever adapted for use as an antibiotic. This is because a strain of *B. bacteriovorus* which can only grow on solid surfaces would allow the bacteria to be applied directly to wounds but would prevent the bacteria from growing within bodily fluids such as the blood which could cause undesirable treatment related complications.

Previous attempts to purify and analyse Bd2325 by our group has been hindered because the full length recombinant protein will not express within *E.coli.* In this study we will therefore attempt to express a truncated form of Bd2325 which has been shortened at the N terminus such that it begins at threonine 22 – this truncation removes a section of Bd2325 sequence which has relatively poor homology to Bd1817 and in addition is not predicted to form any higher protein structures. The reasoning for this truncation is that while Bd1817 could be expressed Bd2325 cannot, therefore removal of this non homologous region from Bd1971 could improve expression. If successful expression is achieved, we will attempt to purify and crystallise the protein with a view to obtaining a crystal structure.

The second protein we propose to study is Bd1971 which is an EAL phosphodiesterase enzyme. Bd1971 is a 400 amino acid 44.97 kDa protein which appears to have a two major domains connected by a linker region. The closest published homologous structure to the N terminal domain is a cyclic adenosine 3',5' monophosphate (cAMP) binding region from a human cGMP dependant protein kinase called 3OCP (Kim et al., 2011) (identical residues 37 %, similar residues 62 %, DOI: 10.2210/pdb3ocp/pdb). The second, C terminal domain however belongs to an unpublished putative EAL / GGDEF protein from *Thiobacillus denitrificans* designated 2R60 (identical residues 37%, similar residues 56%) (DOI: 10.2210/pdb2r6o/pdb). These two homology hits suggest that Bd1971 is a EAL phosphodiesterase protein which seems to be able to bind cAMP. Preliminary findings from phenotypic knockout experiments have found that *B. bacteriovorus* Bd1971 knockout strains clump together into matted structures when grown in suspension, attack phase cells occasionally break off from this structure however and are still fully predatory. As before with Bd2325 If we manage to purify the protein we will first attempt to acquire a crystal for structural determination, in addition to this we will also perform analyses to determine whether cAMP truly interacts with the protein.

A) i.

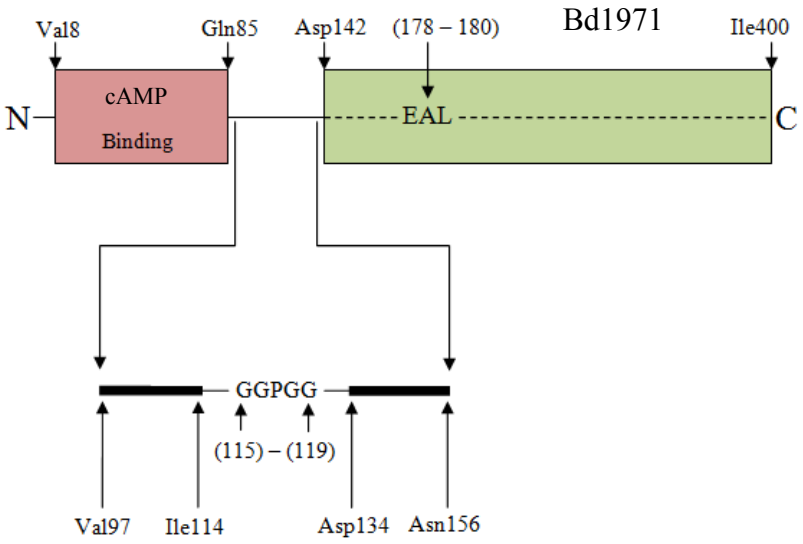

ii.

```
T-COFFEE, Version_9.02.r1228 (2012-02-16 18:15:12 - Revision 1228 - Build 336)
Cedric Notredame
SCORE=98
*
 BAD AVG GOOD
*
Bd1971      :  97
3OCP        :  99
cons        :  98

Bd1971       1 VDIHKDQIIFSEGDAGDCAYIIEKGRVLIYLTKDKEEIPLTILGEGEIFGEMALIDNQNRSASVRALEDVRL   72
3OCP         1 VEYGKDSCIIKEGDVGSLVYVMEDGKVEV----TKEGVKLCTMGPGKVFGELAILYNCTRTATVKTLVNVKL   68

cons         1 *:  **. *:.***.*. .*::*.*:* :  ** : *  :* *::***:*:: * .*:*:*::* :*:*   72


Bd1971      73 AIVTKQ   78
3OCP        69 WAIDRQ   74

cons        73  : :*   78
```

iii.

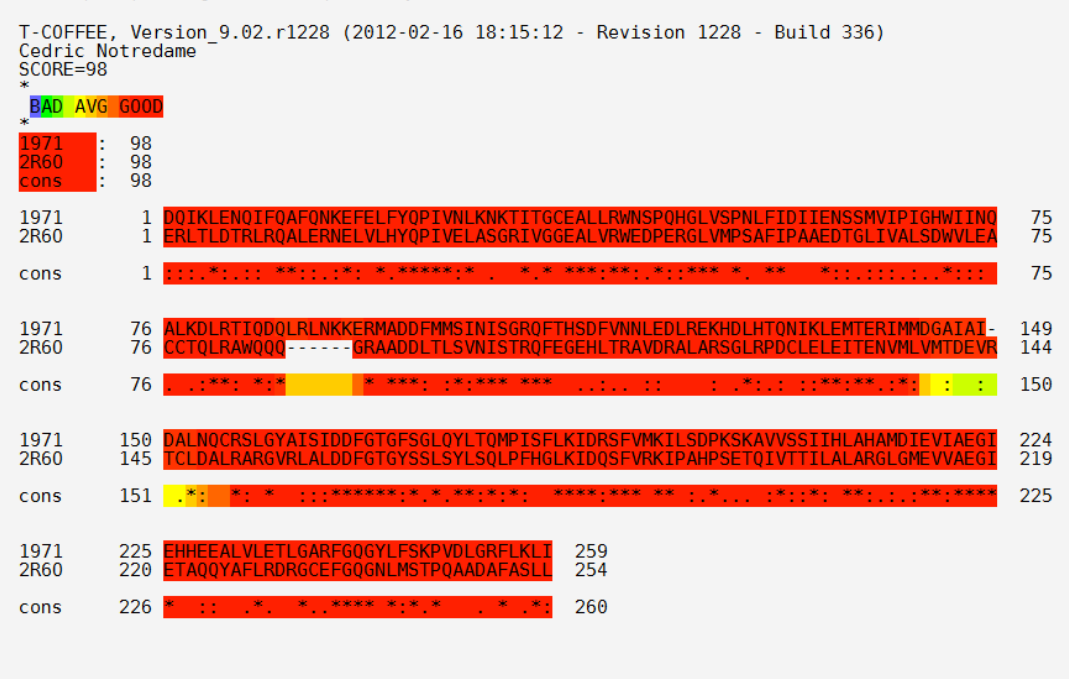

Figure 2: Domain diagrams and sequence alignments for Bd2325 and Bd1971 with their closest homologous partners. ***A) i.*** *Domain diagram for Bd1971. Red domain = N –terminal domain predicted to bind cAMP; this domain has close homology to a cAMP binding domain in a cGMP dependant protein kinase called 3OCP found in humans (Kim et al., 2011) (Identical residues – 23%, similar residues – 46%, DOI:10.2210/pdb3ocp/pdb), residues 8 - 85 in Bd1971 align with residues 122 - 195 in 3OCP. Green domain = C-terminal EAL domain; this domain has close homology to a number of EAL domain containing proteins, the best alignment comes from a GGDEF / EAL co-domain protein from Thiobacillus denitrificans called 2R60 (Identical residues – 37%, similar residues – 56%, DOI: 10.2210/pdb2r6o/pdb), residues 142 - 400 in Bd1971 align with residues 487 - 740 in 2R60 – this region of 2R60 corresponds to its EAL domain. Between the cAMP binding and the EAL domains is a coiled coil region composed of two alpha helix domains (****Bold line****) at residues 97- 114 and 134 – 156, between these two helices at residues 115 - 119 is a flexible linker sequence with the sequence 'GGPGG'.* ***A) ii.*** *Sequence alignment report for Bd1971 (top row) and 2R60 (bottom row), residues 8-85 in Bd1971 align with residues 122-195 in 3OCP.*

Red indicates good sequence homology while green indicates bad sequence homology. ***A) iii.*** *Sequence alignment report for Bd1971 and 2R6O, 2R6) is homologous to the C-terminal domain from Bd1971 (37% identical residues, 56% similar identities), this domain in 2R6O represents an EAL domain. Red indicates good sequence homology while green indicates bad sequence homology.*

B) i.

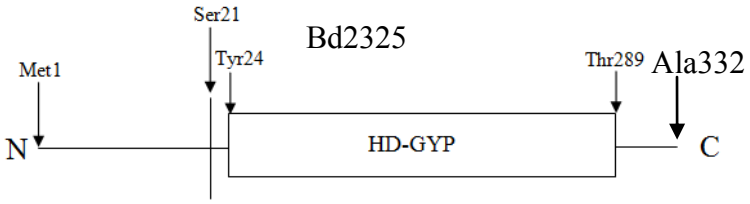

ii.

```
T-COFFEE, Version_9.02.r1228 (2012-02-16 18:15:12 - Revision 1228 - Build 336)
Cedric Notredame
SCORE=94
*
 BAD AVG GOOD
*
Bd2325    :  94
Bd1817    :  95
cons      :  94

Bd2325       1 MFIADLVPSNPLPWQNFPMDSTTYFRIRLSTIRPDKVTSFDIYILVDGKHILYLRAGDKLASGKIKTLHGRD  72
Bd1817       1 M--------------------DYVSIRVSTLRGDQKIDFNAYVKINDKMILYLRRGDSFEGERLKRLKDKK  51

cons         1 *                    *. **:**:* *:  .*: *: ::.* ***** **.: . ::* *:.:.  72


Bd2325      73 TGDSFFVRIEDKQTYRDWVKEEMNSDLLN-----PFDKAKILRESSVALMEDLFENPDVNKALDESRPIITD  139
Bd1817      52 LRK-MYILTDEENSYRTYLQKNIETAYDDTTGKDIQTRADIIQGSQQNNAEEVFENPENVESYNYCKDAAGK  122

cons        73 . :::  :::::** ::::::::  : :  :*.*:: *.    *::****:  :: : .:    .  144


Bd2325     140 FIDLMENAPEAMGFMISLSGHDFYTYNHSLDVSIYSLGLGKALGY-DAKTLEELGVGALFHDIGKRSVSLDI  210
Bd1817     123 YVNFIMSNAQALSAVMNIENTDKTISHHGVTVSTLSIALAQKLGITDPKKTQLLTLGALLHDYGHHHSPLNL  194

cons       145 :::::. .:*:. ::.:.. *    :*.: **  *:.*.: ** *.*. : * :***:** *::  .*::  216


Bd2325     211 LCKKGGLTDAEWEQMKMHPQYGLVIMNNHPNISDAIKAACFEHHESWAGNGYPQQLVAEEIHPFARIVAITD  282
Bd1817     195 NQPLDSMSPEDLALWKKHPIEGAQKVQDKKHFDQTVINIIGQHEETINGTG-PKGLREKDMDPLAVLVSSAN  265

cons       217    ..::  :    * **  *   :::: ::.:::    :*.*:  *.* *: *  :::.*:* :*: ::  288


Bd2325     283 TYDAMTTQRSYNVPMTPMDAVAMMKEKLAGRYDPDMLKAMYSVLFKIKVA  332
Bd1817     266 AMDRLITFE--GVPKAEA--AKKLMIDHVGKHPLQHIQHLNDIL---KGL  308

cons       289 : * : * .  .** :    .  :  . .*:: : :: : .:*   *   338
```

B) ***i.*** *Domain structure for Bd2325. Residues 1 - 21 are not predicted to form any higher structure. Residues 24 – 289 are homologous to a previously published crystal structure for a degenerative B. bacteriovorus HD-GYP protein called Bd1817 (Lovering et al., 2011) (Identical residues – 23% , similar residues – 47%, DOI: 10.2210/pdb3tm8/pdb).* ***B) ii.*** *A sequence alignment report for Bd2325 and Bd1817 (23% identical residues, 47% similar residues). Note the missing tyrosine (Y) residue in Bd1817 at the position 244, this residue is thought to be essential for HD-GYP activity. Red indicates good sequence homology while*

green indicates bad sequence homology. ***Sequence homology report****s (Aii,Aiii and Bii) were generated from the FASTA sequences of each sequence using TCoffee algorithms described here (Di Tommaso et al., 2011).*

MATERIALS AND METHODS

2.1 Bdellovibrio bacteriovorus protein expression

N.B Expression vector construction and 'manual' IPTG induction (but not autoinduction) were kindly performed by Dr A. Lovering prior to the start of the study.

The recombinant protein expression vectors used are given below; each vector was transformed into the lysogenised *E.coli* strain BL21-DE3 prior to recombinant expression.

Bd2325^{LF}**,** expression vector: pET28a, native full length Bd2325 protein with an N-terminal His-tag.

Bd2325^{SF}, expression vector: pET28a, Bd2325 protein, N-terminal truncation such that the protein starts at Thr22, N-terminal His-tag

Bd1971, expression vector: pET41, native full length Bd1971 protein with a C-terminal thrombin cleavable His-tag.

Bd1971^{ALT}, expression vector: pET28a, native full length Bd1971 with a N-terminal His-tag.

Manual induction

The protocol used for these expressions is similar to one published previously (Lovering et al., 2011). Briefly 1 litre of culture medium was used for each expression run; this volume was split between two, two litre conical flasks – e.g. 500 ml per flask. The culture medium used was LB broth; each flask was supplemented with 500 µl kanamycin (Sigma Aldrich) (stock concentration - 50 mg per ml) to select for the growth of successfully transformed cells. Each culture was inoculated with the relevant *E. coli* strain - transformed with the above expression constructs. Inoculation was performed using overnight 10 ml mini cultures grown at 37 ^{o}C in half strength LB broth, 5 ml of this culture was added to 500 ml of LB broth (Sigma Aldrich) media. After inoculation the cultures were incubated first at 37 ^{o}C until they

reached an optical density of approximately 0.6 at 600 nm; expression was then induced via the addition of IPTG to the cultures which were then incubated overnight at 20 ^{o}C – throughout both incubations the flasks were shaken to promote aeration. After overnight incubation the cellular fraction of the culture media was extracted using centrifugation, the cell pellet was removed to a 50 ml plastic centrifuge tube and frozen at -80 ^{o}C for at least 24 hours before being prepared for lysis and purification.

Autoinduction

The transformed *E. coli* strains (containing the recombinant expression vectors) used for the autoinduction protocol were the same as those used for the manual induction protocol described above. The composition of the media used for the autoinduction expression protocol was as follows: Yeast Extract 5 g/l, Tryptone 10 g/l , Na_2HPO_4 25 mM, KH_2PO_4 25 mM, NH_4Cl 50 mM, $MgCl_2$ 2mM, 0.5 % glycerol, 0.05 % glucose, 0.2 % lactose, 0.5 ml / 100 ml trace metal stock solution for the full recipe, including the trace metal stock see (Studier, 2005).

Each expression was carried out in a total volume of 800 ml; this volume was split equally between two, two litre conical flasks. To inoculate the cultures, for each flask containing 400 ml of media 4 ml of inoculate was added from a mini overnight culture of the relevant transformed *E. coli* strain – this mini culture was grown up in 10 ml half strength LB broth supplemented with 10 µl kanamycin (50 mg per ml) inside mini 25 ml conical flasks, inoculation of the transformed *E. coli* was performed from frozen glycerol stocks. The mini culture was left to grow over night at 37 ^{o}C with constant shaking.

Following inoculation the flasks were warmed in a 37 ^{o}C incubator with constant shaking for 2.5 hours for the cells to reach high density, they were then placed in a second incubator

cooled to 20 ^{o}C overnight – again with constant shaking. After overnight incubation the cellular fraction of the culture media was extracted using centrifugation, the cell pellet was removed to a 50 ml plastic centrifuge tube and frozen at -80 ^{o}C for at least 24 hours before being prepared for lysis and purification.

2.2 Pre purification lysate preparation

Cell lysis

The cell pellet was removed from -80^{o}C storage and left to thaw at room temperature, this thawing process was accelerated by the addition of approximately 40 ml room temperature lysis buffer – the lysis buffer was composed of our standard binding buffer or 'Buffer A' as it will be referred to, this buffer contained 30 mM Tris-HCL, 250 mM NaCl, 20 mM imidazole, 5 % w/v glycerol and 5 % w/w sucrose, pH adjusted to give an overall pH of 7.95, with an additional 0.125 mg/ml lysozyme (Sigma Aldrich) and a single protease inhibitor cocktail tablet (Roche) added. Following addition of the lysis buffer, the tubes containing the lysate were left mixing on an automated tumbler for 45 minutes at room temperature. After this thawing period the lysate was chilled for 10 minutes on ice. Once chilled the cells within the lysate were lysed via sonication using a 'Heat Systems – ultrasonic sonicator' (Model W-25) tuned to give a total power output of 40 %. Sonication was performed in short bursts of 20 seconds, leaving the cells to rest on ice between bursts to prevent unwanted heating of the cells and potential degradation of protein, this process was repeated a total of eight times.

Lysate preparation

Following cell lysis the lysate was clarified to remove cell debris and insoluble protein fractions. The chilled lysate then was decanted equally into two centrifuge tubes and centrifuged for 25 minutes at 15,000 g, 4 ^{o}C in a Beckman JA20 rotor fitted to a 'Beckman

Coulter Avanti J-25 centrifuge. This first centrifuge step was to remove heavy cell debris and will be referred to as the 'soft spin'. Following centrifugation, supernatant from the soft spin was decanted equally into new centrifuge tubes and spun at 50,000 g, 4 ^{o}C in a Beckman type 70-ti rotor fitted to a Beckman XL-90 Ultracentrifuge for 60 minutes - this faster centrifuge step referred to as the 'hard spin' was to remove much finer cell debris such as residual membrane fragments. The supernatant from the hard spin was carefully decanted off using a pipette into clean glassware and placed on ice - while removing the supernatant care was taken to avoid any disturbance of the pellet. This supernatant from step final step – the clarified lysate – will be referred to as the 'onto'.

2.3 Protein purification

IMAC column purification

Purification of the His-tagged recombinant protein – now referred to as the ' target protein' – from the onto was achieved by passing the onto through a pre-prepared 1ml HisTrap HP immobilised metal affinity chromatography (IMAC) column (GE Healthcare Life Sciences, Product code: 17-5247-01), which had been equilibrated with 20 column volumes of Buffer A.

The entire onto volume (usually 40 ml) was passed through the column using a peristaltic pump (GE Healthcare Lifesciences, model – Pump P-1) , a steady flow rate of around 1 ml a minute passing though the column was maintained to ensure that it was not subject to excessive pressure which would crush the sepharose resin. While the onto was being applied to the top of the column we collected what came off the bottom, we referred to this run off as the 'flow through' and it was reserved as a control for future analysis to ensure the target protein from the onto had bound to the column during purification. Once all of the onto had

been passed through the column we removed it from the pump and placed in the FPLC ÄKTA Prime (GE Healthcare Life Sciences) protein purification system.

The FPLC was preloaded and pump washed with the 'Buffer A' previously mentioned and 'Buffer B' – Buffer B being the same composition as Buffer A but with 300 mM imidazole instead of 20 mM. Throughout the FPLC purification procedure the relative magnitude of protein eluted from the column was measured using UV absorbance and all fractions eluted from the column were collected in 5 ml plastic test tubes. The pump was set to pump a volume of 1 ml buffer through the column per minute at a pressure of 0.5 MPa , we collected 4.5 ml of eluted buffer per fraction (e.g. one 5 ml test tube with 4.5 ml elution buffer = one fraction).

In the first step the column was washed with a Buffer A to B ratio of 100 % to 0 % respectively until the absorbance peak reached a steady state – this was to ensure that all unbound protein was eluted from the column. Once the absorbance was once again level we upped the concentration of imidazole running through the column by altering the ratios of Buffer A and B to 87% and 13 % respectively – this helped to clean column of any protein which can bind weakly to the resin, again we waited until the change in absorbance peaked and then fell to a steady state. Once the column had been clean the ratios of Buffer A to B was altered to give a ratio of 0% to 100 % respectively. In these high imidazole conditions the His-tagged target protein was assumed to be eluted from the column – thus any peak in absorbance during the elution of these fractions inferred purified His-tagged protein.

2.4 Analysis of purified protein

Preparation of purified protein

Following elution from the HisTrap column, fractions containing the desired protein were further analysed using SDS-PAGE, the fractions which were assumed to contain protein were those that showed a peak in UV absorbance (as measured by the FPLC) under His-tag elution conditions – e.g. 100% Buffer B. Briefly samples from each elution peak were taken and loaded on an SDS-PAGE gel with an appropriate molecular weight marker (Fermentas, Thermo Scientific Catalogue No# SM0672). Fractions inferred to contain the desired protein were then determined by comparing the position of the protein bands with the markers to find the fractions whose band profile matched the molecular weight of the *B. bacteriovorus* protein.

The fractions which were determined to contain the purified protein using UV absorbance and SDS-PAGE analysis were pooled and dialysed to remove imizazole before being concentrated. The selected fractions were pipetted into dialysis tubing and placed in the dialysis buffer – unless specifically stated this buffer consisted of 1 litre of 'A' binding buffer but with no imidazole added (e.g. 30 mM Tris-HCL, 250 mM Nacl, 5 % w/v glycerol and 5 % sucrose – pH 7.95). Dialysis was performed at 4 ^{o}C for a minimum of 3 hours. Following dialysis the solution was concentrated to an appropriate volume in order to give a protein concentration of between 10 – 20 mg per ml as determined by the Bradford protein concentration assay, comparing against a BSA standard. Concentration was performed using a spin concentrator (Vivaspin, 15ml)

Size exclusion chromatography

To perform size exclusion chromatography, 4 ml of un-dialysed eluted fraction from FPLC protein purification was passed onto a gel filtration column loaded with sepharose. Following loading, filtered dialysis buffer (e.g. Buffer A with 0 mM imidazole) was passed through the column. Eluted fractions coming from the column were analysed for UV absorbance to indicate the presence of protein, those fractions which were determined to contain protein were analysed with SDS-PAGE. Fractions eluted during the 'dead volume' phase of elution from the column were assumed to be aggregated.

Protein crystallisation screening

To assess a broad range of different crystallisation conditions we used a number of commercially available crystallisation screens. Generally as an initial screen to judge the protein's behaviour we used the Molecular Dimensions 'Mini Screen' which is largely based on the precipitant polyethylene glycol (PEG). If the protein appeared to behave well in this screen (e.g. limited protein aggregation) we proceeded to screen using the Molecular Dimensions 'JCSG^{+}' screen which is also based largely on PEG as a precipitant. If the purified protein showed excessive aggregation in the 'Mini Screen' we instead moved to the Molecular Dimensions 'Midas' screen which screens against a number of alternative precipitants to PEG. Protein crystallisation of purified protein samples was performed using the hanging drop crystallisation method. Briefly 500 µl of each screening condition was loaded into the corresponding reservoir. On a plastic cover slip 1.5 µl of the purified protein was then mixed with 1.5 µl of the reservoir contents, this coverslip was then sealed over the reservoir with vacuum grease and the completed tray was left at 18 ^{o}C and check periodically for crystal growth.

Analytical ultracentrifuge analysis

To prepare samples for analytical ultracentrifuge (AUC), the purified protein was diluted with dialysis buffer (e.g. Buffer A with 0 mM imidazole) to a protein concentration which gave an OD of 0.5 at 280 nm – this measurement was performed in a quartz cuvette. Samples with and without cAMP were measured using AUC, each sample was prepared to a volume of 500 µl. For samples with additional cAMP, we added cAMP (Sigma Aldrich, dissolved in sterile distilled water), to give a final concentration of 10 mM. Prepared samples were provided with blank controls (buffer only or buffer and cAMP) to the Birmingham Biophysical Characterisation Facility (BBCF) on the 7th floor of Birmingham University Biosciences building to be analysed by sedimentation velocity AUC using a Beckman XL-I analytical ultracentrifuge.

2.5 Inclusion body resolubilisation and refolding

Inclusion body resolubilisation

Insoluble protein fractions from the initial Soft Spin step of lysate preparation which were deemed to contain inclusion bodies were resolubilised in high concentrations of denaturant – either guanidine HCl or urea. The composition of these resolubilisation buffers was the same as Buffer A but with additional 6 M guanidine HCl or 8 M urea respectively.

The resolubilsation buffer was added directly to the centrifuge tubes containing the pellet, the pellet was then mashed into small pieces using a metal spatula and then fully homogenised using a glass plunger homogeniser. Once fully homogenised the mixture was left to mix at room temperature for at least 12 hours on an automated tumbler. After this mixing period the mixture was centrifuged for 25 minutes at 15,000 g, 4 ^{o}C in a Beckman JA20 rotor fitted to a

‘Beckman Coulter Avanti J-25 centrifuge to remove any protein which still remained insoluble.

Protein refolding

We went about refolding the contents of the inclusion bodies by dialysing out the denaturant in two ways – we will refer to the first method as ‘shock dialysis’ and the second method as ‘step dialysis’.

Shock dialysis refolding first involved placing the supernatant from the final centrifuge step of inclusion body resolubilsation into dialysis tubing. This filled tubing was then placed in 1 litre of dialysis buffer which contained no denaturant – this buffer was essentially Buffer A. Dialysis was performed in a two litre glass beaker with constant stirring of the dialysis buffer via a magnetic rod and stirrer at a constant temperature of 4 ^{o}C for at least 18 hours. After this time period the contents of the dialysis tubing were removed and centrifuged or 25 minutes at 15,000g, 4^{o}C in a Beckman JA20 rotor fitted to a ‘Beckman Coulter Avanti J-25 centrifuge to separate the soluble fraction of the mixture from the insoluble aggregates which may have formed during removal of the denaturant.

Step dialysis was similar to shock dialysis in that the supernatant from inclusion body resolubilsation was placed in dialysis tubing and then placed into dialysis buffer within a beaker with constant stirring. The difference however was that multiple dialysis conditions were used which reduced the molarity of denaturant in the dialysis buffer incrementally with each condition. In this protocol the amount of denaturant in the dialysis buffer was reduced by 1 mole per step – e.g. 8 M → 7 M → 6 M etc. For each incremental step the contents of the dialysis tubing were allowed to sit for at least 2 and a half hours in each dialysis condition in order to fully equilibrate.

RESULTS

3.1 – Bd2325 expression

Previous attempts to purify recombinant full length Bd2325^{LF} (LF = "Longform") from transformed *E.coli* culture have not been successful as the vector cannot be made to express Bd2325^{LF} in detectable quantities. Bd2325^{LF} has close sequence homology to another *B. bacteriovorus* protein Bd1817 which has been successfully in purified and crystallised previously (Lovering et al., 2011). Although the two proteins are similar, the first 21 N-terminal residues in Bd2325^{LF} have relatively low similarity to Bd1817 (Figure 2B.ii). As this sequence is not found in Bd1817 - which does express in *E.coli* - it was reasoned that its removal from Bd2325^{LF} may improve recombinant expression, in addition this tail was not predicted form any higher structure so it was felt that its removal would not necessarily affect the global structure of Bd2325^{LF}. The shortened version of Bd2325^{LF} was created prior to this study and shall be referred to as Bd2325^{SF} (SF = "shortform") – this construct, kindly provided by Dr A. Lovering, is what we initially attempted to purify.

Cell pellets from the Bd2325^{SF} pET28a expression construct transformed into *E.coli* were kindly provided pre-prepared for this study by Dr A, Lovering. The cells were cultured in 1 litre of LB broth split between two, two litre conical flasks. The cells were grown at 37 ^{o}C until their density reached an OD of 0.6 at 600 nm, expression was then induced via the addition of IPTG to give a final concentration of 0.2 mM. Putative expression of Bd2325^{SF} was detected using SDS-PAGE analysis of the cell lysates (data not provided).The cultures were then incubated at 20 ^{o}C overnight before the cell pellet was extracted using centrifugation.

3.2 Recombinant Bd2325^{SF} appears to be sequestered in insoluble inclusion bodies following expression in E. coli.

Initial attempts to purify soluble Bd2325^{SF} from the prepared lysate onto were not successful. Following the initial 'soft spin' centrifuge step while preparing the cell lysate we observed that the insoluble pellet was large and had a very pale, almost white colour which is indicative of inclusion body formation. Inclusion bodies are cellular organelles that can sometimes form during recombinant protein expression; these structures sequester the recombinant protein within the normally insoluble lysate fraction, most often in an unfolded or mis-folded state (Tsumoto et al., 2003) . The absence of Bd2325^{SF} from the onto was confirmed following an unsuccessful purification attempt which elicited no significant bands in the elution fractions (Figure 3, lanes #10,#11 and #12), SDS-PAGE analysis of the onto lysate experimental control confirmed that there was no detectable Bd2325^{SF} within the soluble fraction of the cell lysate (Figure 3 , lane OT). Taken together this indicates that while the Bd2325^{SF} construct does express within *E.coli*, it is highly likely that most of the recombinant protein is insoluble and in a mis-folded state within inclusion bodies.

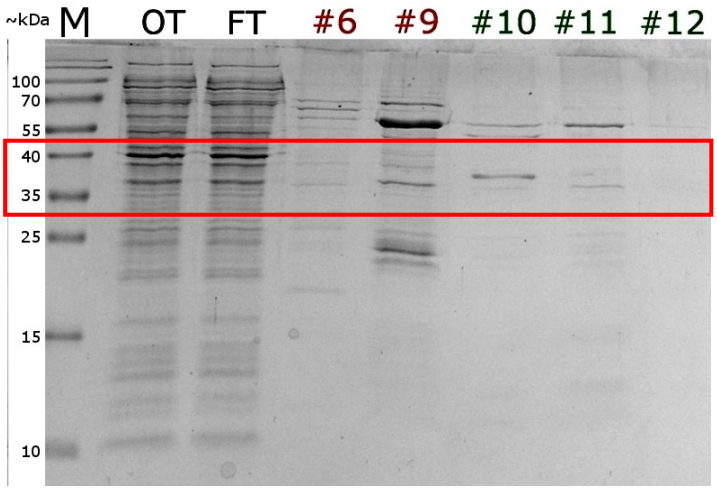

Figure 3: SDS-PAGE analysis following IMAC purification of Bd2325^{SF} from the soluble lysate fraction. *Lane identities **M** = molecular weight marker, **OT**= 'onto', the lysate composition before passing onto the column, **FT** = 'flow through', the lysate composition after passing through the column, **#n** = the nth elution fraction from the column – Red #n = 13 % Buffer B vs. 87 % Buffer A. Green #n = 100% Buffer B vs. 0 % Buffer A. Loading volumes – M = 2.5 µl, OT and FT = 10 µl loaded into lane (1 in 20 dilution sample vs. SDS-PAGE loading buffer), #n = 10 µl loaded into lane (1 in 10 dilution - sample vs. SDS-PAGE loading buffer). The red box indicates the bands of interest in the approximate weight range of Bd2325^{SF} (~38kDa) as indicated by the molecular weight marker control.*

3.3 Bd2325^{SF} inclusion bodies can be solubilised in highly denaturing conditions.

In an effort to purifiy Bd2325^{SF} from the insoluble pellet we next attempted to resolubilise the inclusion bodies under denaturing conditions before attempting to refold their protein contents *in vitro* into the correct conformation. To maximise our chances of successfully extracting Bd2325^{SF} from the inclusion bodies we chose to compare two commonly used denaturants – urea and guanidine hydrochloride (Gu-HCl) to ascertain which was the most effective at extracting Bd2325^{SF}. Insoluble inclusion body pellets which were roughly the same weight (8 M urea pellet – 2.17 g, 6 M Gu-HCl pellet – 2.49 g) from the 'soft spin' step of lysate preparation were resolubilised in Buffer A containing either 8 M urea or 6 M Gu-HCl. Following solubilisation for at least 18 hours the suspensions were centrifuged to remove all material within the lysate which still remained insoluble. Examination of the pellets produced by this step indicated to us that 6 M Gu-HCl seemed to be better at resolubilising the pellet compared to 8 M urea – as evidenced by the much smaller insoluble pellet following 6 M Gu-HCl solubilisation compared to 8 M urea solubilisation (Figure 4A.i).

3.4 Bd2325SF protein refolding shows varying success using different methods

Following resolubilisation of the inclusion bodies we attempted to refold Bd2325^{SF} *in vitro* by gradually reducing the concentration of denaturant in the protein buffer. Preliminary attempts by us to refold Bd2325^{SF} via shock dialysis e.g. by placing the denatured protein (within dialysis tubing) straight into dialysis buffer with 0 M denaturant were not successful for either denaturant condition (data not shown). Near to the end of the dialysis time (roughly 16 hours out of 18) we observed large scale aggregation of the solubilised protein – indicative of unsuccessful folding due to the denatured protein being unable to cope with the removal of denaturing conditions. As a result of these initial experiments we adapted our technique and used a method taken from a study (Gupta et al., 2010) which managed to solubilise and refold

C-di-GMP metabolism proteins from *E.coli* inclusion bodies. This technique which, in this study will be termed ‘step dialysis’, differed from our initial refolding method as the denatured protein was incrementally dialysed in a series of dialysis conditions - each with a slightly lower concentration of denaturant. Utilising this technique meant that we could better control the rate at which the denaturant was removed, and also if precipitation did occur we could pinpoint the concentration of denaturing agent at which it occurred much more readily.

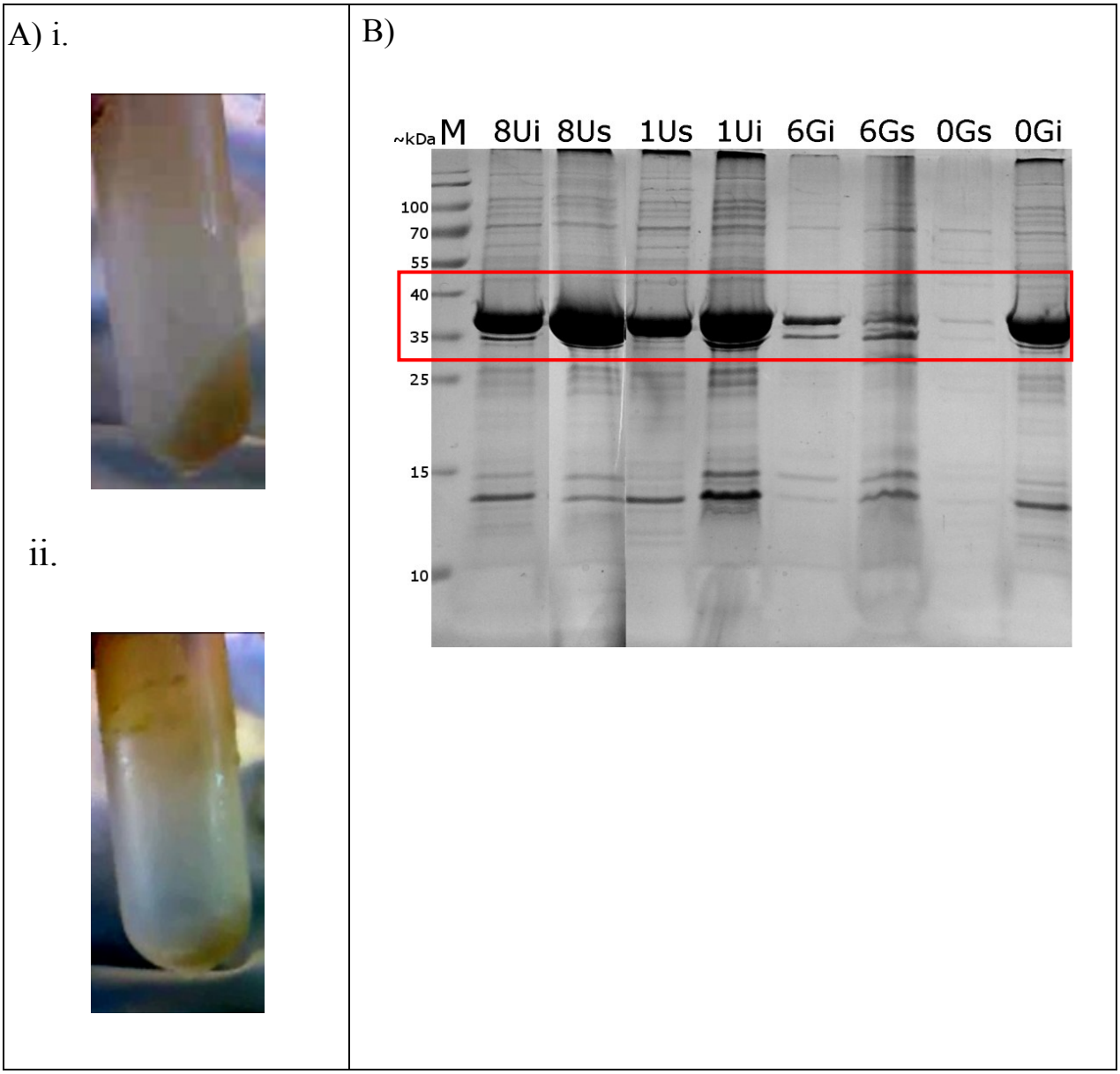

Figure 4: Comparison of Bd2325^{SF} inclusion body resolubilisation using 8 M urea and 6 M Gu-HCl. ***A)*** *Two equally sized inclusion body pellets were resolubilised in 8 M urea (**A.i**) and 6 M Gu-HCl (**A.ii**) respectively.* ***B)*** *SDS-PAGE analysis of samples taken before and after step dialysis from 8 M urea and 6 M Gu-HCl experimental conditions. Lane identities –* ***M*** *= Molecular weight marker control,* ***8Ui*** *= The remaining insoluble pellet following resolubilisation of inclusion body with 8 M urea,* ***8Us*** *= Soluble sample taken following inclusion body resolubilisation with 8 M urea (e.g. the sample which went on to be dialysed),*

1Us *= Sample of the protein which remained soluble following step dialysis from 8 M urea to 1 M urea,* ***1Ui*** *= Sample of the protein which did not remain soluble following step dialysis from 8 M urea to 1 M urea,* ***6Gi*** *= The remaining insoluble pellet following resolubilisation of inclusion body with 6 M Gu-HCl,* ***6Gs*** *= Soluble sample taken following inclusion body resolubilisation with 6 M Gu-HCl (e.g. the sample which went on to be dialysed),* ***0Gs*** *Sample of the protein which remained soluble following step dialysis from 6 M Gu-HCl to 1 M Gu-HCl,* ***0Gi*** *= Sample of the protein which did not remain soluble following step dialysis from 8 M urea to 1 M urea. Loading volumes – M = 2.5 µl, 8Ui, 8Us, 1Us, 1Ui, 0Gs and 0Gi = 10 µl loaded into lane (1 in 20 dilution, sample vs. SDS-PAGE loading buffer), 6Gi, 6Gs = 10 µl loaded into lane (1 in 40 dilution, sample vs. SDS-PAGE loading buffer). The red box indicates the bands of interest in the approximate weight range of Bd2325^{SF} as indicated by the molecular weight marker control.*

Our preliminary experiments showed that if protein mis-folding and aggregation occur it usually did so in the final stages of shock dialysis (e.g. in the 1 M to 0 M denaturant range). To reduce the risk of aggregation during step dialysis we decided to remove the final traces of denaturant as quickly as possible. For this reason we decided to perform the final molar step (e.g. 1 M to 0 M urea) an IMAC column. To do this 'on column' refolding as it is called; the 1 M protein solution is bound onto a column equilibrated with a binding buffer with an equal denaturant concentration. Once the His-tagged protein is bound to the column a 0 M denaturant containing buffer is washed through the column to remove the final traces of denaturant. The bound protein is then eluted in 0 M denaturant conditions. This 'on column' refolding technique could only be used for the 1 M urea condition as we found that Gu-HCl interferes with the binding of $Bd2325^{SF}$ to the IMAC column. Therefore in the case of the Gu-HCl condition we fully dialysed the solution to 0 M using the 'step dialysis' method.

Following the completion of step dialysis (e.g. 8 M urea → 1 M urea and 6 M Gu-HCl → 0 M Gu-HCl) we observed a difference in the level of protein precipitation. Whereas the 1M urea solution a showed only minor clouding, the 0 M Gu-HCl condition was found to have large solid white clumps of aggregated protein floating within it – indicative of protein mis-folding. Both solutions were centrifuged to remove insoluble matter and then analysed using SDS-PAGE to assess the amount of soluble protein left within either solution compared to that before dialysis. From this analysis we observed that for 8 M urea resolubilisation, although a significant amount of $Bd2325^{SF}$ remained insoluble in 8 M urea (Figure 4.B Lane 8Ui) some of the protein was resolubilised (Figure 4.B Lane 8Us), and importantly a lot of this resolubilised protein remained soluble following step dialysis down to 1 M urea denaturant conditions. In comparison the $Bd2325^{SF}$ which was resolubilised by 6 M Gu-HCl (Figure 4.B Lane 6Us) did not remain soluble following step dialysis down to 0 M Gu-HCl (Figure 4.B

Lane 0Us) and became mostly insoluble (Figure 4.B Lane 0Ui). *N.B. The samples loaded into lanes 6Ui and 6Us, (Figure 4.B) had a twofold greater dilution factor than the other lanes on the gel – this is because high concentrations of Gu-HCl adversely reacted with the SDS-PAGE loading buffer causing the sample to congeal; this meant a greater volume of SDS-PAGE loading buffer was needed to sufficiently thin the sample for loading. Therefore the band sizes for 6Ui and 6Us are not directly comparable to the other lanes in the gel.*

Taken together our observations suggest that for $Bd2325^{SF}$ inclusion bodies 8 M urea is the more suitable resolubilisation agent than 6 M Gu-HCl; this is because while 6 M Gu-HCl did manage to resolubilise the inclusion body pellet more efficiently than 8 M urea (Figure 4.A), protein denatured in Gu-HCl was more prone to aggregation and precipitation than urea when the denaturant was removed. Due the complete loss of soluble $Bd2325^{SF}$ from the 0 M Gu-HCl sample following step dialysis we chose to abandon this sample and concentrate on the 1 M urea sample - which still contained detectable amounts of $Bd2325^{SF}$ (Figure 4.B Lane 1Us).

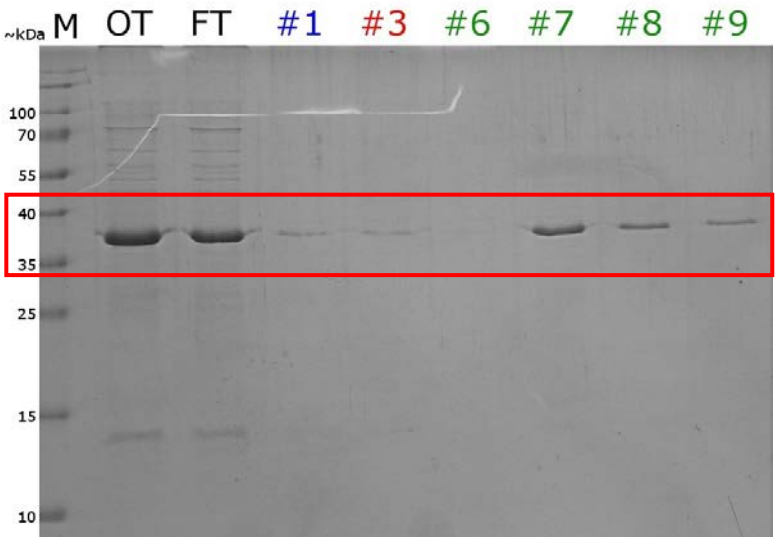

Figure 5 – SDS-PAGE analysis of the on column refold and purification of Bd2325^{SF} from inclusion bodies resolubilised in 8 M urea. *Lane identities M = molecular weight marker, OT= 'onto', the lysate composition before passing onto the column (1 M urea denaturing conditions), FT = 'flow through', the lysate composition after passing through the column (0 M urea denaturing conditions), #n = the nth elution fraction from the column – Blue #n = 0 % Buffer B vs.100 % Buffer A, Red #n = 13% Buffer B vs.87 % Buffer A, Green #n = 100% Buffer B vs.0 % Buffer A. Loading volumes – M = 2.5 µl , OT and FT = 10 µl loaded into lane (1 in 20 dilution, sample vs. SDS-PAGE loading buffer), #n = 10 µl loaded into lane (1 in 10 dilution, sample vs. SDS-PAGE loading buffer). The red box indicates the bands of interest in the approximate weight range of Bd2325^{SF} as indicated by the molecular weight marker control.*

As mentioned previously we chose to remove the final traces of urea (e.g. 1 M → 0 M) using 'on column' refolding. Following this on column refolding, the bound protein was eluted from the column and analysed using SDS-PAGE to determine if Bd2325^{SF} remained in the eluted fractions. This analysis firstly revealed that much of the Bd2325^{SF} which was present in the onto and was passed onto the column (Figure 5, Lane OT) did not bind to the column; this is because it could also be detected in the flow through control (Figure 5, Lane FT). Although not all of the protein had bound to the column, the SDS-PAGE analysis did show bands corresponding to the molecular weight of Bd2325^{SF} in three of the elution fractions (Figure 5, Lanes #7, #8 and #9). This indicates that we did manage to extract some soluble recombinant protein from the initial insoluble inclusion bodies – although the efficiency of the protocol was not great.

Although this recovered protein remained soluble this was not sufficient evidence to prove that it had correctly refolding during removal of the denaturant. For this reason we subjected one of the eluted fractions (fraction #7) to size exclusion chromatography to see if the protein within the sample was the correct molecular weight for Bd2325^{SF}, this result would indicate that the protein was properly folded and not aggregated. Unfortunately this analysis revealed that all of the protein within the sample could only be found at a molecular weight much greater than that predicted for Bd2325^{SF} and thus we concluded that mis-folding and aggregation had occurred.

At this point we concluded that our attempts to resolubilise the contents of the inclusion bodies and refold them correctly were not likely to be successful. We have shown that it is possible to resolubilise the Bd2325^{SF} inclusion bodies using buffers containing 8 M urea and 6 M Gu-HCl, however it appeared that the later removal of these denaturants caused protein mis-folding and aggregation – the opposite to what was needed. It may have been possible to

further refine our refolding protocols but given time restraints on the study we instead opted to change the initial protein expression conditions for $Bd2325^{SF}$ in order to stop the formation of the inclusion bodies in the first place.

3.5 An autoinduction expression protocol allows the expression of $Bd2325^{LF}$ and improves the solubility of $Bd2325^{SF}$

To try and stop the formation of inclusion bodies, we decided to switch from induced expression protocol to a different technique called autoinduction. Induced expression protocols rely on an individual judging the right moment to induce recombinant protein expression by adding ITPG to the culture; in contrast to this, autoinduction allows the bacteria within the culture to induce recombinant protein expression themselves when the time is exactly right. This technique often improves protein yield as well as solubility of the recombinant protein.

In addition to attempting soluble $Bd2325^{SF}$ expression we also decided to test whether autoinduction would allow successful expression of the $Bd2325^{LF}$ expression construct – a feat which could not be accomplished using the standard induced expression protocol. Following autoinduction, SDS-PAGE analysis of cell lysate from $Bd2325^{SF}$ and $Bd2325^{LF}$ autoinduction cultures both showed thick protein bands corresponding to the approximate weights of $Bd2325^{SF}$ and $Bd2325^{LF}$ respectively. Interestingly the band in the $Bd2325^{SF}$ lysate lane ran slightly further into the gel than the corresponding band in $Bd2325^{LF}$, this observation agrees with the fact that $Bd2325^{SF}$ is shorter than $Bd2325^{LF}$ and as such has a lower molecular weight. This is quite convincing evidence that both of the expression constructs expressed Bd2325 during autoinduction which is especially significant for $Bd2325^{LF}$ as it is the first time the expression construct has properly worked.

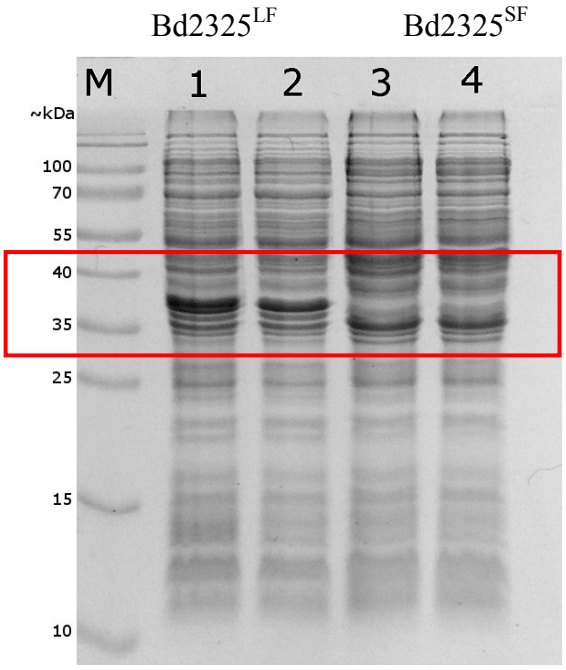

Figure 6: SDS-PAGE analysis of cell lysate from two Bd2325 autoinduction expression experiments. *Lysates from Bd2325^{LF} (lane 1 and 2) and Bd2325^{SF} (lane 3 and 4) autoinduction expression runs. Lane identities:* ***M****= molecular weight marker,* ***1*** *= raw cell lysate from Bd2325^{LF} culture, lysed in 400 µl bugbuster per 3 ml of pelleted culture.* ***2*** *= soluble fraction from Bd2325^{LF} raw cell lysate following centrifugation,* ***3*** *= raw cell lysate from Bd2325^{SF} culture, lysed in 400 µl Bugbuster Protein Extraction Reagent (Novagen) per 3 ml of pelleted culture,* ***4*** *= soluble fraction from Bd2325^{SF} raw cell lysate following centrifugation. Loading volumes: M = 2.5 µl loaded into lane, 1-4 = 10 µl loaded into lane (1 in 4 dilution. Sample vs. SDS-PAGE loading buffer). The red box indicates the bands of interest in the approximate weight range of both Bd2325 versions as indicated by the molecular weight marker control.*

Following two promising protein expression experiments we went on to attempt to purify Bd2325^{LF} and Bd2325^{SF} from their respective cell lysates. We first attempted to purify Bd2325^{LF} which, until the use of autoinduction we had not managed to express successfully in *E.coli.* During elution of Bd2325^{LF} from the IMAC column we did not see any significant peaks in UV absorbance in the fractions where you would expect His-tagged protein elution to occur (e.g. 100% Buffer B). SDS-PAGE analysis of these eluted fractions confirmed to us that we had been unsuccessful in isolating Bd2325^{LF} from the onto (Figure 7A.ii Lanes #15, #16, #17 and #18); as there were no visible bands in these fractions corresponding to the molecular weight of Bd2325^{LF}. To determine at which point during the protocol we 'lost' Bd2325^{LF}, we studied the onto and flow through controls (Figure 7A.ii. Lanes OT and FT) as well as sample controls which were taken during the preparation of the cell lysate for purification (Figure 7A.i). These controls suggested that the majority of initially expressed Bd2325^{LF} remained in the insoluble fractions of the lysate e.g. the pellets following the soft spin and hard spin steps of lysate preparation (Figure 7A.i. Lanes Si and OTi). Thus the absence of Bd2325^{LF} in the eluted fractions was due to there being no Bd2325^{LF} within the onto which was pumped onto the IMAC column (Figure 7A.ii. Lane OT). From this failed purification we can conclude that although autoinduction allowed successful expression of the Bd2325^{LF} construct in *E.coli,* the recombinant protein expressed was in some way insoluble and thus could not be extracted using IMAC purification.

Following our attempts to purify Bd2325^{LF} we next tried the prepared Bd2325^{SF} lysate from the autoinduced cells. During lysate preparation we observed that we did not get the large pale insoluble inclusion body pellets which occurred following manual expression induction; this observation suggested to us that autoinduction had improved the solubility of Bd2325^{SF}. SDS-PAGE analysis of samples taken during lysate preparation confirmed that solubility of

Bd2325^{SF} had improved (Figure 7B.i); this was illustrated by a thick clear band corresponding to the molecular weight of Bd2325^{SF} which could be seen in the soluble fraction of the lysate, following the initial soft spin centrifuge step (Figure 7B.i. Lane Ss). Furthermore this band was not present in the insoluble pellet from the same centrifugation step (Figure 7B.i. Lane Si). Taken together this indicated that when expressed using autoinduction Bd2325^{SF} seemed to remain soluble during lysate preparation – a different fate to previous manual induction attempts which saw Bd2325^{SF} remain sequestered inside insoluble inclusion bodies.

Although the solubility of Bd2325^{SF} seemed to have been improved by autoinduction, when we progressed to attempting to purify the protein using IMAC the results were not so promising. SDS-PAGE analysis of the purification attempt (Figure 7B.ii.) revealed a thick band of protein at the right molecular weight for Bd2325^{SF} in the onto control (Figure 7B.ii. Lane OT) suggesting that soluble Bd2325^{SF} entered the column, in addition this same band was not detectable in the flow through control (Figure 7B.ii. Lane FT) suggesting the His-tagged protein bound to the column once it was applied. Due to the fact that Bd2325^{SF} was applied to the column and was not present in the flow through, it was surprising that we could not detect any traces of the protein in our elution fractions, which corresponded to the peak in UV absorbance during 100% Buffer B elution conditions (Figure 7B.ii. Lanes #13 and #14). From this analysis we can only conclude that Bd2325^{SF} must for some reason remain bound to the column even under conditions which normally would have eluted a His-tagged protein from the Ni^{+} charged HisTrap column.

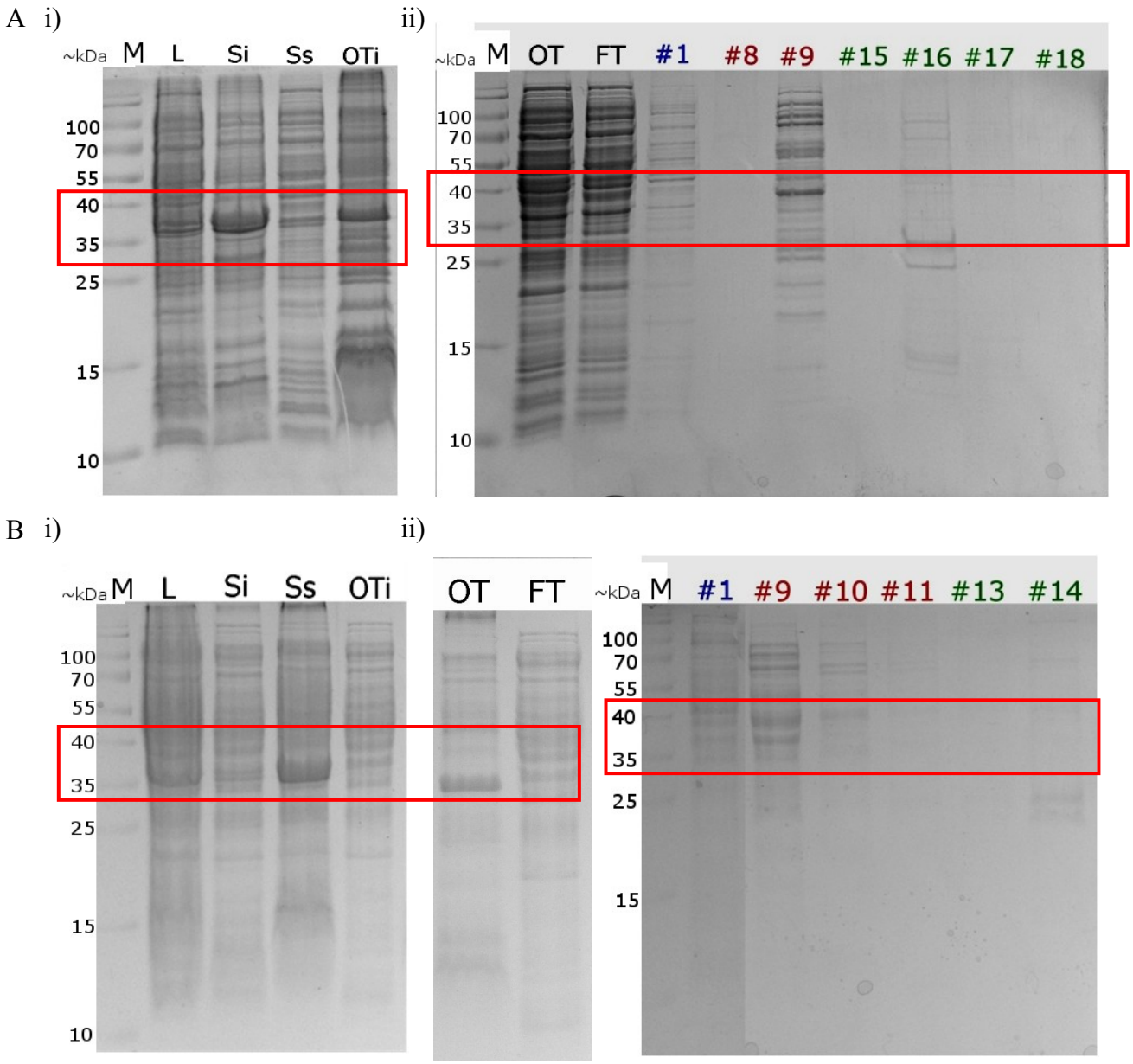

Figure 7: SDS-PAGE analysis of IMAC purification experiments for Bd2325^{LF} and Bd2325^{SF}- ***A)*** *SDS-PAGE analysis of autoinduced Bd2325^{LF} purification.* ***B)*** *SDS-PAGE analysis of autoinduced Bd2325^{SF} purfication.* ***A.i)*** *and* ***B.i)*** *- Samples taken during lysate preparation. Lane identities:* ***M*** *= Molecular weight marker control,* ***L*** *= lysate sample – taken following sonication of cell pellet,* ***Si*** *= Soft spin insoluble fraction – taken from the pellet following the initial soft spin centrifuge step,* ***Ss*** *= Soft spin soluble fraction – taken from the supernatant following the initial soft spin centrifuge step,* ***OTi*** *= Onto insoluble fraction – taken from the insoluble pellet following the final hard spin centrifuge step.*

Loading volumes – M = 2.5 µl loaded. L, Si, Ss and OTi 10 µl loaded (1 in 4 dilution sample vs. SDS-PAGE loading buffer) ***A.ii)*** *and* ***B.ii)*** *- Samples taken during IMAC purification. Lane identities:* ***M****= Molecular weight marker control,* ***OT****= 'onto', the lysate composition before passing onto the column,* ***FT*** *= 'flow through', the lysate composition after passing through the column,* ***#n*** *= the* n^{th} *elution fraction from the column – Blue = 0 % Buffer B vs. 100 % Buffer A. Red = 13% Buffer B vs. 87% Buffer A. Green = 100% Buffer B vs. 0% Buffer A. Loading volumes – M = 2.5 µl loaded , OT and FT = 10 µl loaded into lane (1 in 4 dilution sample vs. SDS-PAGE Loading buffer), #n = 10 µl loaded into lane (1 in 2 dilution sample vs. SDS-PAGE Loading buffer). The red box indicates the bands of interest in the approximate weight range of* $Bd2325^{SF}$ *as indicated by the molecular weight marker control.*

3.6 – Bd1971 expression

Previous attempts by our group to purify Bd1971 have not been successful; although the initial expression and purification appears to work well the protein does not remain stable once it is eluted from the IMAC column and the imidazole is dialysed away. These purification attempts used the expression vector pET41 which gave the recombinant protein a C-terminal His-tag. To ascertain if the position of the His-tag was interfering with the stability of Bd1971 we decided to use an alternative expression construct using the vector pET28a which gave Bd1971 an N-terminal His-tag (This construct was kindly provided by Dr A. Lovering) – the recombinant protein produced with this alternative tag was called $Bd1971^{ALT}$ to differentiate it from our initial construct.

3.7 An alternatively positioned His-tag does not improve the stability of Bd1971

We attempted to purify the His-tagged protein from the onto prepared from the crude cell pellet (Cell pellet again kindly provided by Dr A. Lovering) by the aforementioned protocol. During elution from the column under 100% Buffer B conditions we observed a very high peak in UV absorbance which was indicative of large amounts of eluted protein from the column. SDS-PAGE analysis of these eluted fractions showed a very clean, thick band of protein in the fractions from the 100% Buffer B elution peak, at the correct molecular weight for $Bd1971^{ALT}$; as indicated by the molecular weight marker control lane. Taken together this data provided very convincing evidence to us that we had managed to purify $Bd1971^{ALT}$ from the cell lysate.

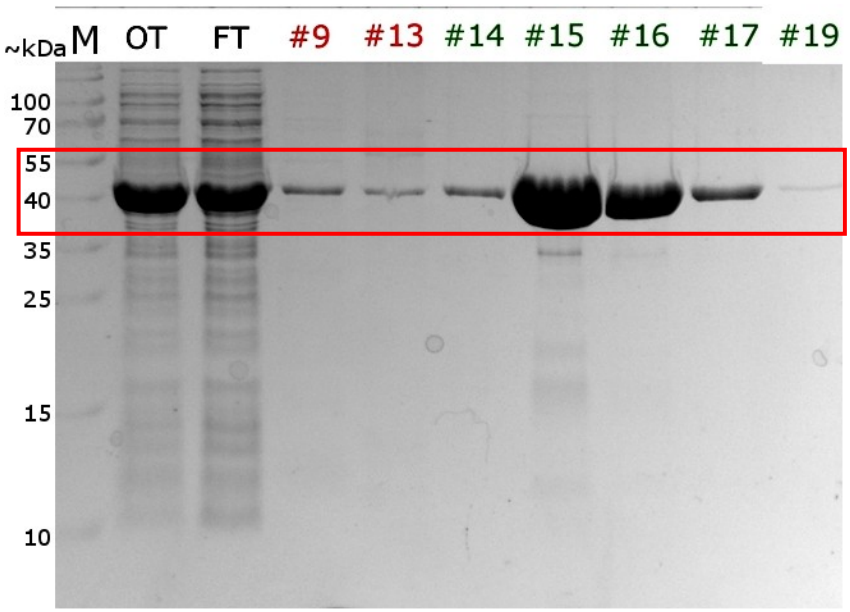

Figure 8: SDS-PAGE analysis following IMAC purification of Bd1971^{ALT} from the soluble lysate fraction - *Lane identities **M** = molecular weight marker, **OT**= 'onto', the lysate composition before passing onto the column, **FT** = 'flow through', the lysate composition after passing through the column, **#n** = the nth elution fraction from the column - red = 13% Buffer B vs. Buffer A, green = 100% Buffer B vs. Buffer A. Loading volumes – M = 2.5 µl , OT and FT = 10 µl loaded into lane (1 in 20 dilution, sample vs. SDS-PAGE loading buffer), #n = 10 µl loaded into lane (1 in 10 dilution , sample vs. SDS-PAGE loading buffer). The red box indicates the bands of interest in the approximate weight range of Bd2325 as indicated by the molecular weight marker control.*

Of the three elution fractions which we had previously determined to contain purified Bd1971^{ALT} (Figure 8, lanes #15, #16 and #17) we decided to prepare fractions #15 and #16 for protein crystallisation e.g. dialysis to remove imidazole and spin concentration whereas fraction #17 would be analysed using size exclusion chromatography to determine if the eluted protein was properly folded or composed of mis-folded aggregates. Unfortunately while handling fractions #15 and #16 we found that the instability which plagued our earlier experiments remained; the protein within the pooled fractions precipitated firstly during dialysis and then again during concentration of the remaining soluble fraction leaving us with negligible amounts of protein – we therefore abandoned our attempts to perform analyses using this sample. Size exclusion analysis of the remaining fraction #17 indicated to us that the protein within the fraction was in a single, large molecular weight clump much larger than the expected size of Bd1971^{ALT} – indicative of protein aggregation. Through consideration of both the inherent protein instability post elution and this size exclusion data we concluded that the use of an alternatively located His-tag had not improved the structural stability of Bd1971.

The size exclusion analysis of Bd1971^{ALT} indicated to us that the problems we'd encountered with Bd1971 thus far may have been due to mis-folding and or aggregation of Bd1971. Our earlier successes with getting soluble Bd2325 expression using the autoinduction method lead us to wonder if, by applying this expression method again we could improve the stability of Bd1971.

3.8 Autoinduction expression of Bd1971 significantly improves protein stability

For autoinduction expression we chose to use the original expression construct with a C-terminal tag, this was because the C-terminal His-tag had the potential of being cleaved from the protein using thrombin if the purification was successful, which we saw as another possible avenue to improve protein stability. SDS-PAGE analysis of the raw cell lysates

following autoinduction suggested that expression of soluble Bd1971 using this method was possible, as illustrated by the large protein band corresponding to the rough molecular weight of Bd1971 on the gel.

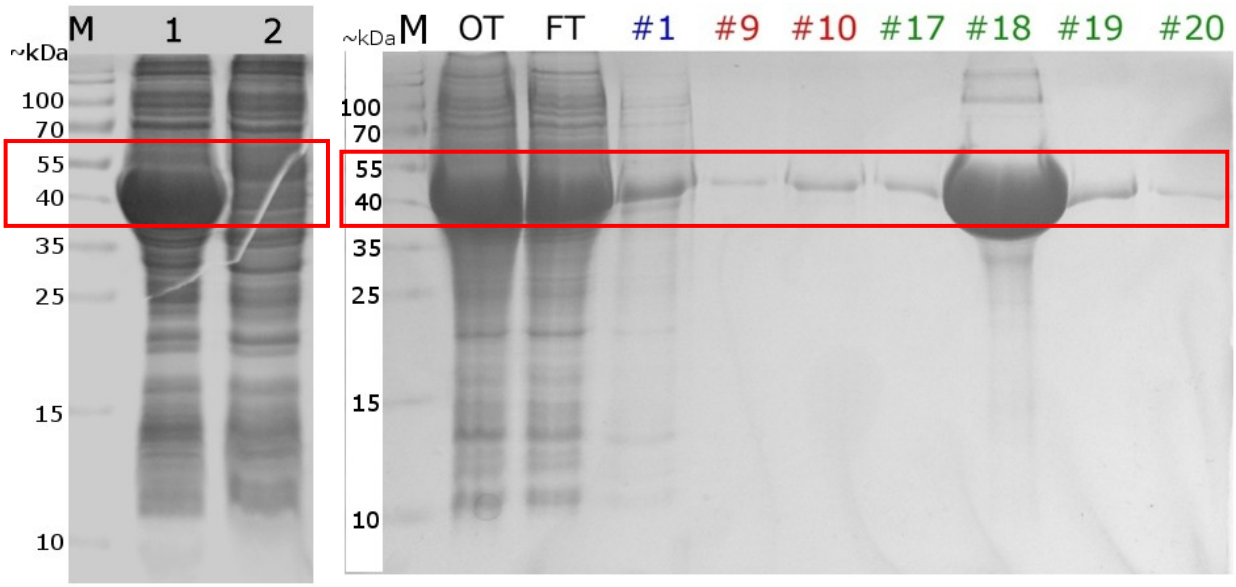

Figure 9 – *SDS-PAGE analysis of Bd1971 expression using autoinduction and its subsequent purification using IMAC purification. A) SDS-PAGE Analysis of lysate from the Bd1971 autoinduction expression run. Lane identities = M = Molecular weight marker control, 1 = raw cell lysate from Bd1971 autoinduction culture, lysed in 400 µl bugbuster per 3 ml of pelleted culture. 2 = soluble fraction from Bd1971 raw cell lysate following centrifugation. B) SDS-PAGE analysis of Bd1971 purification following autoinduced expression. Lane identities, M = molecular weight marker, OT= 'onto', the lysate composition before passing onto the column, FT = 'flow through', the lysate composition after passing through the column, #n = the n^{th} elution fraction from the column – Blue = 0 % Buffer B vs. 100 % Buffer A, Red = 13% Buffer B vs. Buffer A, Green = 100% Buffer B vs. Buffer A. Loading volumes – M = 2.5 µl , OT and FT = 10 µl loaded into lane (1 in 2 dilution, sample vs. SDS-PAGE loading buffer), #n = 10 µl loaded into lane (1 in 2 dilution, sample vs. SDS-PAGE loading*

buffer). The red box indicates the bands of interest in the approximate weight range of Bd1971 as indicated by the molecular weight marker control.

The presence of large amounts of soluble Bd1971 was further suggested following a successful IMAC column purification in which we observed a high UV absorbance upon target protein elution conditions e.g. 100% Buffer B – SDS-PAGE analysis of the eluted fractions detected a very large single band of protein at the correct molecular weight for Bd1971. Taken together this is compelling evidence that using autoinduction expression we were able to purification large amounts of relatively pure Bd1971. Importantly the protein within the eluted fractions remained stable throughout imidazole dialysis – a feat which could not be claimed for Bd1971 produced using manual induction. Following complete removal of imidazole from the sample, we used a Bradford's protein concentration assay to determine the protein concentration within the sample which was already 20 mg per ml. Due to the concentration of the sample already being sufficient for protein crystallisation concentration of the sampe was not needed – omission of the concentration step is highly unusual and empathises the very large amounts of protein which were produced during autoinduction expression.

3.9 Bd1971 – purified protein analysis

We next attempted to crystallise the purified protein using a number of commercially available chemical screen kits. Crystallisation was attempted using the hanging drop method, each reservoir was filled with 500 µl screening solution and a drop composed of 1.5 µl undiluted (e.g. 20 mg/ml) protein and 1.5 µl screening solution was suspended above on a plastic coverslip, sealed down with vacuum grease. We first tried the 24 well 'Mini Screen' from Molecular dimensions; this screen largely uses polyethylene glycol (PEG) as a precipitant. No crystal hits were obtained from this screen and in addition many of the conditions produced a thick brown precipitate in the drop. The magnitude of precipitation indicated to us that Bd1971 crystal formation was not likely to occur in PEG, so we next

switched to the Molecular Dimensions 'Midas' screen which tests for many different precipitating compounds, unfortunately again no crystal hits were acquired and as before the majority of screening conditions produced thick brown precipitates.

The unstable nature of Bd1971 during our crystallisation screens led us to think that perhaps the C-terminal His-tag attached to the protein to facilitate purification may be interfering with crystal formation by preventing ordered molecular alignment in the crystal. Fortunately the C-terminal His-tag that was attached to Bd1971 was cleavable using thrombin, we therefore treated an aliquot of our protein sample with restriction grade thrombin (EMD Millipore, catalogue). To ensure excess thrombin we added 0.5 µl of the stock enzyme for every 100 µl of protein sample.

To assess the success of His-tag cleavage we ran SDS-PAGE analysis of samples taken from the protein sample before thrombin addition, 24 hours after thrombin addition and 72 hours after thrombin addition – we reasoned that cleavage of the His-tag would reduce the molecular weight of Bd1971 and thus could assess His-tag cleavage using SDS-PAGE by comparing how far into the gel each sample had run. From this analysis we determined that complete cleavage of the His-tag had not occurred by 24 hours (Figure 10 lane 3), however by 72 hours the majority of protein within the sample appeared to be of a smaller molecular weight (Figure 10 lane 4).

Following successful cleavage of the His-tag from Bd1971 we repeated the same crystallisation screens that we used before, we observed that the performance of the protein improved slightly e.g. it did not precipitate in as many screening conditions as before. Unfortunately however we did not manage to obtain any crystal hits in the screens which we performed.

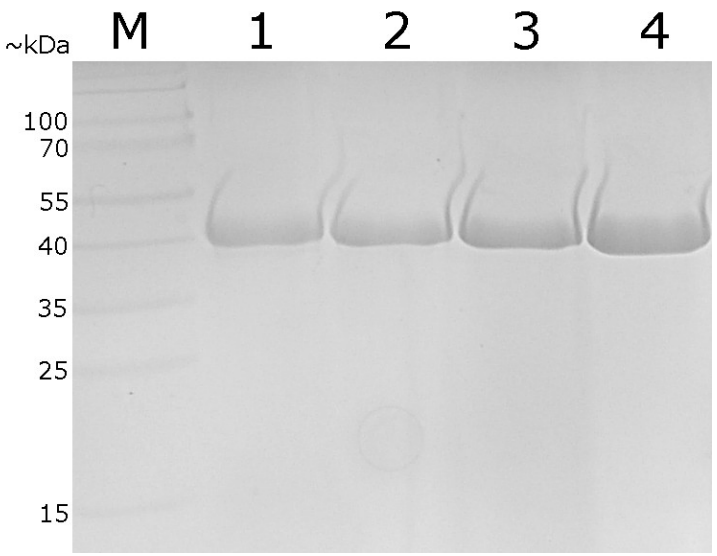

Figure 10 – SDS-PAGE analysis of Bd1971 before and after His-tag cleavage with thrombin. *The C-terminal His-tag attached to purified Bd1971 was cleaved using thrombin, to assess the success of cleavage protein samples were taken before and after the addition of thrombin – successful cleavage is assumed for samples which have a lower molecular weight than the pre thrombin control. Lane identities –* ***M)*** *Molecular weight marker control,* ***1)*** *Bd1971 pre thrombin control 1 – sample taken immediately following protein purification and imidazole dialysis.* ***2)*** *Bd1971 pre thrombin control 2 – sample taken just before the addition of thrombin, this sample is approximately 24 hours older than lane 1.* ***3)*** *Bd1971 + thrombin – sample taken 24 hours after the addition of thrombin.* ***4)*** *Bd1971 + thrombin – sample taken 72 hours after the addition of thrombin. Loading volumes – M = 2.5 µl loaded, 2, 3 and 4 = 10 µl loaded (1 in 20 dilution, sample vs. SDS-PAGE loading buffer).*

3.10 Preliminary AUC analysis of Bd1971 shows possible oligomeric state changes in the presence of cAMP

It has been stated previously that an N-terminal region of Bd1971 from residue 8-85 is highly homologous to a cAMP binding domain from a human cGMP dependant protein kinase designated 3OCP (Kim et al., 2011) (Figure 2A.ii). This homology leads us postulate that cAMP may in some way interact with Bd1971 and somehow modulate its function. With this in mind we wished to determine whether the addition of cAMP to Bd1971 could lead to a change in oligomerisation e.g. the change from a monomer to a dimer or vice versa. To perform this analysis we chose to use sedimentation equilibrium analytical ultracentrifugation which allows the molecular weight of protein complexes in solution to be determined – as each Bd1971 monomer has a molecular weight of ~45 kDa; therefore oligomerisation can be inferred by mass peaks which are multiples of this weight.

AUC samples containing purified Bd1971 were prepared both with and without cAMP at varying concentrations. It must be noted that the addition of cAMP to the samples seemed to interfere with data acquisition, for this reason we were only able to successfully process data for two conditions – one un thrombinised Bd1971 sample (e.g. with His-tag attached) with 10 mM cAMP and one thrombinised Bd1971 sample (e.g. without His-tag attached) without any additional cAMP added. For this reason and because of the aggregative unstable nature of Bd1971 this AUC data is considered preliminary.

A)

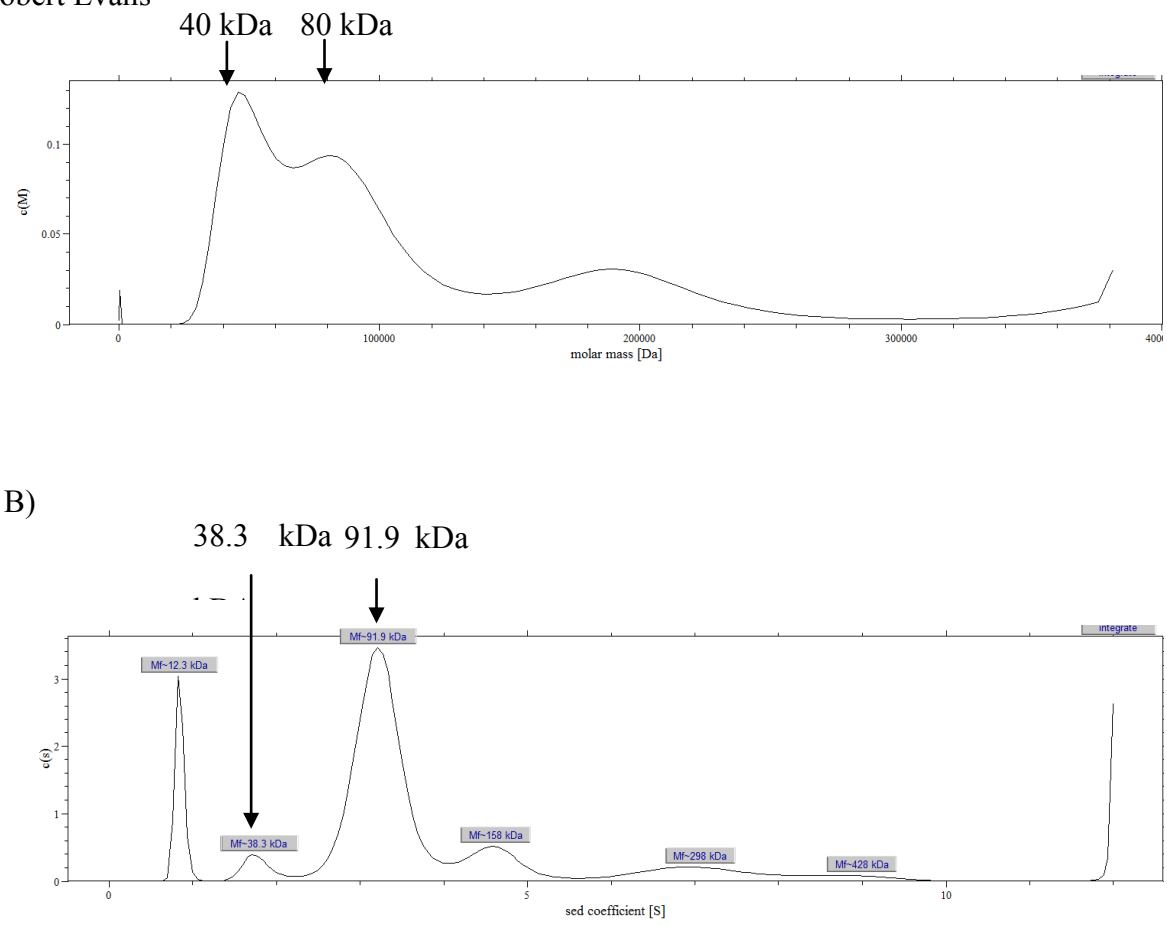

Figure 11 – AUC analysis of Bd1971 with and without the addition of cAMP. ***A)*** *AUC analysis of Bd1971 (with His-tag) without the addition of cAMP, peaks along the x-axis correspond to populations within the solution with different molar masses (Da). The two arrows mark the peaks of interest with ~45 kDa and ~90 kDa molar masses respectively – these two peaks may represent monomeric and dimeric Bd1971 respectively.* ***B)*** *AUC analysis of Bd1971 (without His- tag) with additional cAMP added (10 mM). The X-axis represents the sedimentation coefficient of different populations within the solution, to allow peak comparison with A) the molar masses for the peaks have been calculated, the two peaks of interest are marked with arrows and annotated.*

Although we cannot currently infer definitive conclusions from the AUC analysis it is possible to discern distinct populations of protein within the sample which correspond to the

molar masses 45 kDa and 90 kDa respectively (figure 11). It is therefore possible that the 45 kDa peak represents Bd1971 in a monomeric form and the 90 kDa peak in its dimeric form. Importantly the size of the respective populations seems to change between the sample which has additional cAMP and the control sample which does not. This indicates that the oligomeric state of Bd1971 may change when cAMP is present.

The data presented above seems to indicate that Bd1971 may form into a dimeric state when cAMP is added to the solution (figure 11.B); this conflicts with data which was acquired by Dr A Lovering following completion of the experimental stages of this study. This analysis used small angle x-ray scattering to analyse Bd1971 and produced evidence to suggest that in fact Bd1971 naturally forms a dimer in solution which is broken apart upon the addition of cAMP. With this in mind and considering the unstable nature of purified Bd1971 we can only conclude at this point that cAMP may cause a switch between monomeric and dimeric states, however the direction of this state switch is yet to be conclusively determined.

DISCUSSION

4.1 Bd2325

Bd2325^{LF} and Bd2325^{SF} expression using manual induction

In this study we found that N-terminal truncation of the native length Bd2325^{LF} from Met1 to Thr21 allowed expression of the recombinant protein (albeit mis-folded) where before no expression could be detected. This success suggests that something about the full length Bd2325^{LF} - and more specifically the 21 amino acid sequence which was removed from it, somehow prevents recombinant expression. It must be noted however that although truncation improved Bd2325 expression, the protein produced remained within inclusion bodies - most likely in a mis-folded form. Thus the truncation of Bd2325^{LF} to Bd2325^{SF} may have allowed for recombinant expression but it did not allow us to easily purify the protein later on (Figure 3). The reason for inclusion body formation is unclear; it could be that truncated Bd2325^{SF} expressed too highly leading to overloading of translational machinery. The stress this may have put on the *E.coli* could have lead to the recombinant protein being sequestered into inclusion bodies – this is a very likely outcome for recombinant expression when it is too high (Singh and Panda, 2005). It is possible that the truncation lead to structural instability in the protein, leading to mis-folding and inclusion body formation. With the latter theory in mind, a possible model exists which nicely tying together both forms of Bd2325 - it could be that both Bd2325^{LF} and Bd2325^{SF} can be expressed in *E.coli* but only Bd2325^{SF} is produced in detectable quantities. This is because biologically active Bd2325^{LF} is toxic to *E.coli* and as such kills the cells which express it while conversely Bd2325^{SF} can accumulate in culture because it is mis-folded, functionally inactive and thus is not toxic to *E.coli*

Inclusion body resolubilisation and *in vitro* refolding

Our attempt to resolubilise the inclusion bodies formed as a result of Bd2325^{SF} expression was partly successful. Through comparison of two denaturing conditions – 8 M urea and 6 M Gu-HCl – we found that 6 M Gu-HCl was possibly more effective at solubilising the inclusion bodies compared to 8 M urea (Figure 4A). When we later went on to refold the denatured protein by removing the denaturants however we found that protein solubilised in 6 M Gu-HCl was more prone to aggregation at lower molar ranges of denaturant compared to 8 M urea. This lead us to conclude that overall 8 M urea was a better candidate for Bd2325^{SF} inclusion body resolubilsation. While the recovery of protein from the inclusion body pellet was lower for urea than Gu-HCl we were nonetheless able to isolate some soluble protein from the urea solubilised sample following removal of the denaturant (Figure 4B Lane 1Us) – a result which could not be achieved for Gu-HCl (Figure 4B Lane 0Gs).

Following inclusion body resolubilisation and *in vitro* refolding via 'step dialysis' we found that we had soluble protein remaining in the sample which had been solubilised in 8 M urea (Figure 4B lanes 1Us). This sample was passed onto a IMAC column and relatively pure His-tagged Bd2325^{SF} was eluted (Figure 5). Unfortunately size exclusion analysis for one of the eluted fractions revealed that even though the eluted protein was soluble it was still mis-folded and aggregated. From these results we concluded that resolubilisation of inclusion bodies was possible using 8 M urea but currently the denatured protein could not made to refold correctly.

Although we did not manage to properly refold the contents of the inclusion bodies in this study, it is conceivable that further work to optimise the *in vitro* refolding protocol could prove fruitful. One of the improvements which could be made to our protocol would be the supplementation of the dialysis buffer with additional compounds to facilitate refolding. The

purpose of these additives could either be to prevent protein aggregation or to encourage correct protein re-folding. Our dialysis buffer did in fact contain sucrose (5 % w/v) which is known to encourage formation of the stable fully folded protein structures, thus the addition of an aggregation inhibitor such as polyethylene glycol or arginine HCl could have reduced the level of protein aggregation which we observed during refolding. These aggregation inhibitors function by preventing interactions between partial refolded protein molecules which can disrupt refolding and lead to aggregation (Tsumoto et al., 2003). Another improvement which could be made is to optimise the mode of dialysis used to remove the denaturant. In this study we found that quickly dialysing the denaturant using 'shock dialysis' lead to protein aggregation during refolding so we switched to a slower, more controlled 'step dialysis' method - however this method also lead to aggregation. It is possible that a middle ground exists between the two dialysis methods – this method would remove the denaturant at the correct rate to stimulate protein refolding while also preventing aggregation. With this in mind, one route of optimisation could be to adjust our step dialysis to find the correct dialysis speed. For instance the dialysis process could be sped by increasing the molar step between each dialysis condition e.g. to 2 M per step (e.g. 8 M → 6 M → 4 M etc.).

Bd2325^{SF} and Bd2325^{LF} expression using autoinduction

Following our failure to isolate Bd2325^{SF} from inclusion bodies we went back to our initial expression protocol to see if we could improve recombinant expression such that the inclusion bodies would not form in the first place. In this respect we found that switching manual induction expression for autoinduction improved recombinant expression for both forms of Bd2325 quite noticeably in this study - firstly it allowed us for the first time to express Bd2325^{LF} (Figure 6 lanes 1 and 2) and secondly it improved the solubility of Bd2325^{SF} by ablating the formation of inclusion bodies (Figure 7B.i lane Si). It must be noted however that

we were still unable to purify either form of Bd2325 from prepared lysate; Bd2325^{LF} autoinduction allowed protein expression but the recombinant protein remained in some way insoluble during lysate preparation (Figure 7A.i lane OTi), while for Bd2325^{SF} the protein appeared soluble but could not eluted from the IMAC column (Figure 7B.ii). From this we conclude that the fate of both forms of Bd2325 following autoinduction indicate that the protein is still mis-folded following recombinant expression.

The principles of autoinduction

The question still remains though how switching to autoinduction improved protein expression - to explain this, an understanding of autoinduction and the inducible *lac* operon (used in our expression vectors) is needed. Autoinduction expression relies on the principle that *E.coli* can utilise different energy sources, switching from a preferred substrate to a less preferred substrate once the first is fully utilised – this is called diauxic growth. In the case of *E.coli* this means that glucose is metabolised in preference to lactose which is only metabolised when glucose is depleted- this is because lactose requires more energy investment to metabolise. Diauxic growth in *E.coli* is controlled by the *lac* operon. Briefly when glucose is being metabolised, expression of the lactose metabolising enzyme β-galactosidase - coded for by the gene *lacZ* - is suppressed by a constitutively expressed gene repressor protein coded by *lacI* – another *lac* operon gene. When *E.coli* runs out of glucose, allolactose – a metabolite of lactose - causes *lacI* inhibition of *lacZ* to be circumvented allowing *lacZ* expression thus allowing *E.coli* to utilise lactose in its environment. Expression of *lacZ* is further stimulated by a spike in cellular cAMP levels triggered by the lack of glucose in the medium. This cAMP starvation response activates the 'cAMP receptor protein' (CRP); CRP is an activator protein which binds to the *lac* operon, further boosting *lacZ* expression (Wilson et al., 2007).

Recombinant protein expression technology has taken the *lac* operon and modified it to create an inducible expression system. Many expression vectors (including those used in this study) contain a modified copy of the *lac* operon which has had the coding region of *lacZ* replaced with a cloned gene for the recombinant protein to be expressed. The expression vector is cloned into an *E.coli* strain which is then grown in bulk culture. When the culture has reached the correct stage of growth – usually the log phase – expression of the recombinant gene is activated by the addition of IPTG; IPTG is an artificial analogue of allolactose and thus activates expression of the modified *lacZ* gene. This 'manual' IPTG induction method is what was initially used to produce the recombinant *B. bacteriovorus* proteins for this study. IPTG induction was initially used because it generally produces successful results and uses standard commercially available culture media – in our case LB broth. However this method does not faithfully replicate wild type *lac* induction as IPTG is added when glucose is still available in the medium. This means that the normal cAMP response is not activated and in addition one must judge the correct time point to add IPTG. The result of misjudged IPTG induction is that the expressing cells are often unnaturally shocked into expression at the incorrect time – thus this method requires careful optimisation to obtain good results.

Switching to autoinduction allowed us to produce a more natural *lac* operon induction process. Autoinduction uses a defined media into which carefully controlled ratios of glucose, lactose and glycerol are added. Unlike IPTG induction glucose is not in excess in autoinduction media, this means that during *E.coli* culture growth glucose is depleted meaning cells must switch to lactose metabolism – when this occurs recombinant expression of the modified *lacZ* gene occurs. This diauxic switch is controlled on an individual cell basis meaning cells in culture only start producing recombinant protein when they are ready

producing a much more natural induction, in addition because glucose in the media depletes cAMP levels rise activating CRP.

As stated previously 'Manual' IPTG induction did not seem to work with either form of Bd2325 produced for this study, however a switch to autoinduction did seem to improve the expression of both proteins. We attribute this improvement to the gentler induction of recombinant expression that autoinduction can produce. Even though the use of autoinduction did not allow us to purify either form of Bd2325 it nonetheless improved some properties of the protein post expression, thus in future studies refinement of the autoinduction could be the route to the expression of soluble Bd2325. For instance by changing the ratio of glucose to lactose in the autoinduction media one can alter the point at which the *lacZ* cloned gene is activated – optimisation of this time point such that it occurs exactly when the *E.coli* cells are ready to express could improve the outcome of the expression.

4.2 Bd1971

Bd1971 manual induction

Unlike Bd2325, manual induction using IPTG did not seem to hinder the solubility or expression of Bd1971 (Figure 8) – instead the protein had problems with stability in solution meaning it could not be handled post purification without causing precipitation.

Bd1971 autoinduction

Once again switching from manual induction to autoinduction seemed to improve some properties of Bd1971. Using autoinduction the stability of Bd1971 improved significantly meaning that although we did not manage to crystallise the purified protein we did manage to perform some preliminary analytical tests to elucidate some of its properties. In addition we

managed to obtain a much higher yield of recombinant protein using autoinduction compared to IPTG induction.

An intriguing explanation for the increased stability of Bd1971 following autoinduction could be linked to our findings that Bd1971 interacts with cAMP (Figure 11). As discussed previously, during *E.coli's* diauxic switch from glucose to lactose, a rise in intracellular cAMP occurs which helps to induce expression of the *lacZ* gene via CRP. This rise in cAMP is likely to be mirrored during autoinduction when the *E.coli* exhausts the limited glucose in the media. It could be this spike in intracellular cAMP helps to stabilise Bd1971 via the putative interactions observed in this study. This is of course assuming that Bd1971 interacts with cAMP and that this interaction somehow promotes protein stability. With this in mind, it is conceivable that the high levels of cAMP produced during autoindction remains associated with Bd1971 during lysate preparation and IMAC purification – thus improving the stability of purified Bd1971. Corroborating this theory is the fact that recombinant Bd1971 obtained via IPTG induction was less stable, if our theory is correct this fits because IPTG induction does not produce the same cellular spike in cAMP, this is because IPTG induction is performed in glucose rich conditions and therefore the cAMP starvation response is not reproduced as it is in autoinduction.

Purified Bd1971 - protein analysis

Putative findings from analyses using analytical ultracentrifuge (AUC) suggest that Bd1971 can exist as either a monomer or dimer in solution, and interestingly switches between the two conformations when cAMP is introduced to the sample. Due to the preliminary nature of our current data we cannot confidently state whether cAMP induces dimer formation from Bd1971 monomers, or conversely induces monomer formation from naturally forming Bd1971 dimers. The data from our preliminary AUC analysis suggests that cAMP may induce

dimer formation because the addition of cAMP seems to increase the ~ 90 kDa population in solution which is the weight inferred for a Bd1971 dimer. Conflicting data from an experiment performed by Dr A Lovering using small angle x-ray diffraction however suggests that the natural state of Bd1971 in solution is in a dimer and cAMP induces monomer formation. In view of the uncertainty produced by these conflicting data sets, and the inherent aggregative nature of purified Bd1971 and the interference of glycerol in the sample buffer we can currently only conclude that cAMP may change the oligomeric state of Bd1971.

It will be essential in the future to ascertain the correct contribution of cAMP to Bd1971 quaternary structure if we are to fully understand the function of Bd1971. This will firstly require establishment of how exactly cAMP changes the oligomerisation of Bd1971 – e.g. dimer to monomer or monomer to dimer. Following this work it will be also be important to ascertain whether cAMP binds to the N-terminal cAMP receptor like domain previously discussed. If it does in fact bind to this domain it is possible that cAMP acts as an allosteric regulator of Bd1971 C-di-GMP hydrolysis. If Bd1971 is allosterically regulated by cAMP it is possible that the switch in oligomeric state may play a role. Oligomeric state switches have been been shown to improve EAL phosphodiesterase activity in another EAL protein called YkuI from *Bacillus subtillis (Minasov et al., 2009)* where dimerisation is induced from protein monomers. Conversely to this example, a naturally forming Bd1971 dimer could be inactive until cAMP binding breaks it apart into active monomers.

Bd1971 and cAMP

Compelling evidence which would likely clear up any uncertainties as to the relationship between Bd1971 quaternary structure and cAMP could be gained by obtaining a crystal structure for Bd1971, especially if a crystal could be formed with cAMP and or C-di-GMP bound *in situ*. Our preliminary attempts to crystallise Bd1971 in this study were not

successful – for every condition tried we observed either no crystal formation or protein precipitation. It must be noted however these attempts were made before we discovered that Bd1971 may interact with to cAMP. With this in mind it is possible that a repeat of the crystallisation screening with additional cAMP or C-di-GMP added to the purified protein sample could provide the stability needed for formation of an ordered crystalline structure. This crystal could give us information as to whether cAMP does bind to Bd1971 and also where on the protein it binds, if the protein is crystallised in a dimerised form we could also determine what areas of the protein are involved in dimerisation and whether cAMP is implicated in this process.

If the interaction between cAMP and Bd1971 can be established it will contribute to existing research which is gradually revealing close links between cAMP and C-di-GMP signalling systems in bacteria. An example of this link between the two signalling system comes from the bacteria *Vibrio cholerae* where it was found that cAMP was a negative regulator of biofilm formation and worked in opposition to C-di-GMP which positively regulated biofilm formation. Most significantly however was the discovery that cAMP directly controlled the activity of diguanylate cyclase and phosdiesterase enzymes within *V. cholerae* via transcriptional regulation (Fong and Yildiz, 2008). This *V. cholerae* study is especially relevant to our study because initial phenotypic knockout experiments examining Bd1971's functional role in *B. bacteriovorus* suggest that its knockout leads to biofilm like pellicle formation. With this in mind it is possible that a theme has evolved in the bacterial world whereby specific cAMP and C-di-GMP signalling systems work together to control switches between the formation and dispersal of bacterial biofilms. It is therefore possible that Bd1971 – which has a potential role in *B. bacteriovorus* biofilm formation – is affected by the cAMP

starvation response, in this way perhaps cAMP can help to trigger a less energy intensive form of lifecycle in *B. bacteriovorus* when energy sources such as glucose are low.

4.3 Conclusion

In conclusion to our study we have firstly improved upon existing methods for the expression and purification of our two *B. bacteriovorus* proteins – Bd2325 and Bd1971. The improvements we recommend include the use of autoinduction expression technqiues to facilitate improved recombinant expression as well as the use of different expression constructs – e.g. truncation of $Bd2325^{LF}$. In addition to these experimental optimisations we also present the first successful isolation of recombinant Bd1971 from *E.coli* expression cultures and initial analysis of its properties. In this respect we have identified a potential interaction between cAMP and Bd1971, more specifically we suggest that this interaction may result in an oligomeric change between a monomer and dimer formation in solution. Although these findings are exciting we realise that further work must be done in order to establish and expand upon what we have found. In this respect we hope that the findings presented here, and any future findings which may come as a result of this study contribute in some way to our understanding of the unusual predacious bacterium *Bdellovibrio bacteriovorus* and its place in the bacterial kingdom as an important utiliser of C-di-GMP signalling.

BIBLIOGRAPHY

ADAMS, D. O. & HAMILTON, T. A. 1984. The cell biology of macrophage activation. *Annu Rev Immunol,* 2**,** 283-318.

ALVAREZ, M. & CASADEVALL, A. 2006. Phagosome extrusion and host-cell survival after Cryptococcus neoformans phagocytosis by macrophages. *Curr Biol,* 16**,** 2161-5.

BARTLETT, K. H., KIDD, S. E. & KRONSTAD, J. W. 2008. The emergence of Cryptococcus gattii in British Columbia and the Pacific Northwest. *Curr Infect Dis Rep,* 10**,** 58-65.

BOSE, I., REESE, A. J., ORY, J. J., JANBON, G. & DOERING, T. L. 2003. A yeast under cover: the capsule of Cryptococcus neoformans. *Eukaryot Cell,* 2**,** 655-63.

BUCHANAN, K. L. & MURPHY, J. W. 1998. What makes Cryptococcus neoformans a pathogen? *Emerg Infect Dis,* 4**,** 71-83.

BURNHAM, J. C., HASHIMOTO, T. & CONTI, S. F. 1968. Electron microscopic observations on the penetration of Bdellovibrio bacteriovorus into gram-negative bacterial hosts. *J Bacteriol,* 96**,** 1366-81.

CHAN, C., PAUL, R., SAMORAY, D., AMIOT, N. C., GIESE, B., JENAL, U. & SCHIRMER, T. 2004. Structural basis of activity and allosteric control of diguanylate cyclase. *Proc Natl Acad Sci U S A,* 101**,** 17084-9.

CHANG, Y. C. & KWON-CHUNG, K. J. 1994. Complementation of a capsule-deficient mutation of Cryptococcus neoformans restores its virulence. *Mol Cell Biol,* 14**,** 4912-9.

CHANG, Y. C. & KWON-CHUNG, K. J. 1998. Isolation of the third capsule-associated gene, CAP60, required for virulence in Cryptococcus neoformans. *Infect Immun,* 66**,** 2230-6.

CHANG, Y. C. & KWON-CHUNG, K. J. 1999. Isolation, characterization, and localization of a capsule-associated gene, CAP10, of Cryptococcus neoformans. *J Bacteriol,* 181**,** 5636-43.

CHANG, Y. C., PENOYER, L. A. & KWON-CHUNG, K. J. 1996. The second capsule gene of cryptococcus neoformans, CAP64, is essential for virulence. *Infect Immun,* 64**,** 1977-83.

CHANG, Y. C., STINS, M. F., MCCAFFERY, M. J., MILLER, G. F., PARE, D. R., DAM, T., PAUL-SATYASEELA, M., KIM, K. S., KWON-CHUNG, K. J. & PAUL-SATYASEE, M. 2004. Cryptococcal yeast cells invade the central nervous system via transcellular penetration of the blood-brain barrier. *Infect Immun,* 72**,** 4985-95.

CHAYAKULKEEREE, M., JOHNSTON, S. A., OEI, J. B., LEV, S., WILLIAMSON, P. R., WILSON, C. F., ZUO, X., LEAL, A. L., VAINSTEIN, M. H., MEYER, W., SORRELL, T. C., MAY, R. C. & DJORDJEVIC, J. T. 2011. SEC14 is a specific requirement for secretion of phospholipase B1 and pathogenicity of Cryptococcus neoformans. *Mol Microbiol,* 80**,** 1088-101.

CHEN, S. C., MULLER, M., ZHOU, J. Z., WRIGHT, L. C. & SORRELL, T. C. 1997a. Phospholipase activity in Cryptococcus neoformans: a new virulence factor? *J Infect Dis,* 175**,** 414-20.

CHEN, S. C., WRIGHT, L. C., GOLDING, J. C. & SORRELL, T. C. 2000. Purification and characterization of secretory phospholipase B, lysophospholipase and lysophospholipase/transacylase from a virulent strain of the pathogenic fungus Cryptococcus neoformans. *Biochem J,* 347**,** 431-9.

CHEN, S. C., WRIGHT, L. C., SANTANGELO, R. T., MULLER, M., MORAN, V. R., KUCHEL, P. W. & SORRELL, T. C. 1997b. Identification of extracellular phospholipase B, lysophospholipase, and acyltransferase produced by Cryptococcus neoformans. *Infect Immun,* 65**,** 405-11.

CHINETTI, G., GRIGLIO, S., ANTONUCCI, M., TORRA, I. P., DELERIVE, P., MAJD, Z., FRUCHART, J. C., CHAPMAN, J., NAJIB, J. & STAELS, B. 1998. Activation of proliferator-activated receptors alpha and gamma induces apoptosis of human monocyte-derived macrophages. *J Biol Chem,* 273**,** 25573-80.

COVER, W. H., MARTINEZ, R. J. & RITTENBERG, S. C. 1984. Permeability of the boundary layers of Bdellovibrio bacteriovorus 109J and its bdelloplasts to small hydrophilic molecules. *J Bacteriol,* 157**,** 385-90.

COX, G. M., MCDADE, H. C., CHEN, S. C., TUCKER, S. C., GOTTFREDSSON, M., WRIGHT, L. C., SORRELL, T. C., LEIDICH, S. D., CASADEVALL, A., GHANNOUM, M. A. & PERFECT, J. R. 2001. Extracellular phospholipase activity is a virulence factor for Cryptococcus neoformans. *Mol Microbiol,* 39**,** 166-75.

CRAIG, L., PIQUE, M. E. & TAINER, J. A. 2004. Type IV pilus structure and bacterial pathogenicity. *Nat Rev Microbiol,* 2**,** 363-78.

DASHIFF, A., JUNKA, R. A., LIBERA, M. & KADOURI, D. E. 2011. Predation of human pathogens by the predatory bacteria Micavibrio aeruginosavorus and Bdellovibrio bacteriovorus. *J Appl Microbiol,* 110**,** 431-44.

DATE, M., FUKUCHI, K., MORITA, S., TAKAHASHI, H. & OHURA, K. 2003. 15-Deoxy-delta12,14-prostaglandin J2, a ligand for peroxisome proliferators-activated receptor-gamma, induces apoptosis in human hepatoma cells. *Liver Int,* 23**,** 460-6.

DI TOMMASO, P., MORETTI, S., XENARIOS, I., OROBITG, M., MONTANYOLA, A., CHANG, J. M., TALY, J. F. & NOTREDAME, C. 2011. T-Coffee: a web server for the multiple sequence alignment of protein and RNA sequences using structural information and homology extension. *Nucleic Acids Res,* 39**,** W13-7.

DWIDAR, M., MONNAPPA, A. K. & MITCHELL, R. J. 2012. The dual probiotic and antibiotic nature of Bdellovibrio bacteriovorus. *BMB Rep,* 45**,** 71-8.

EVANS, K. J., LAMBERT, C. & SOCKETT, R. E. 2007. Predation by Bdellovibrio bacteriovorus HD100 requires type IV pili. *J Bacteriol,* 189**,** 4850-9.

FELDMESSER, M., KRESS, Y., NOVIKOFF, P. & CASADEVALL, A. 2000. Cryptococcus neoformans is a facultative intracellular pathogen in murine pulmonary infection. *Infect Immun,* 68**,** 4225-37.

FONG, J. C. & YILDIZ, F. H. 2008. Interplay between cyclic AMP-cyclic AMP receptor protein and cyclic di-GMP signaling in Vibrio cholerae biofilm formation. *J Bacteriol,* 190**,** 6646-59.

FROMTLING, R. A., SHADOMY, H. J. & JACOBSON, E. S. 1982. Decreased virulence in stable, acapsular mutants of cryptococcus neoformans. *Mycopathologia,* 79**,** 23-9.

FRY, J. C. & STAPLES, D. G. 1976. Distribution of Bdellovibrio bacteriovorus in sewage works, river water, and sediments. *Appl Environ Microbiol,* 31**,** 469-74.

GARCIA-HERMOSO, D., JANBON, G. & DROMER, F. 1999. Epidemiological evidence for dormant Cryptococcus neoformans infection. *J Clin Microbiol,* 37**,** 3204-9.

GILES, S. S., DAGENAIS, T. R., BOTTS, M. R., KELLER, N. P. & HULL, C. M. 2009. Elucidating the pathogenesis of spores from the human fungal pathogen Cryptococcus neoformans. *Infect Immun,* 77**,** 3491-500.

GOLDMAN, D. L., LEE, S. C., MEDNICK, A. J., MONTELLA, L. & CASADEVALL, A. 2000. Persistent Cryptococcus neoformans pulmonary infection in the rat is associated with intracellular parasitism, decreased inducible nitric oxide synthase expression, and altered antibody responsiveness to cryptococcal polysaccharide. *Infect Immun,* 68**,** 832-8.

GRANGER, D. L., PERFECT, J. R. & DURACK, D. T. 1985. Virulence of Cryptococcus neoformans. Regulation of capsule synthesis by carbon dioxide. *J Clin Invest,* 76**,** 508-16.

GUPTA, K., KUMAR, P. & CHATTERJI, D. 2010. Identification, Activity and Disulfide Connectivity of C-di-GMP Regulating Proteins in <italic>Mycobacterium tuberculosis</italic>. *PLoS ONE,* 5**,** e15072.

HARIZI, H., CORCUFF, J. B. & GUALDE, N. 2008. Arachidonic-acid-derived eicosanoids: roles in biology and immunopathology. *Trends Mol Med,* 14**,** 461-9.

HILL, J. O. 1992. CD4+ T cells cause multinucleated giant cells to form around Cryptococcus neoformans and confine the yeast within the primary site of infection in the respiratory tract. *J Exp Med,* 175**,** 1685-95.

HOBLEY, L., FUNG, R. K., LAMBERT, C., HARRIS, M. A., DABHI, J. M., KING, S. S., BASFORD, S. M., UCHIDA, K., TILL, R., AHMAD, R., AIZAWA, S., GOMELSKY, M. & SOCKETT, R. E. 2012. Discrete cyclic di-GMP-dependent control of bacterial predation versus axenic growth in Bdellovibrio bacteriovorus. *PLoS Pathog,* 8**,** e1002493.

HULL, C. M. & HEITMAN, J. 2002. Genetics of Cryptococcus neoformans. *Annu Rev Genet,* 36**,** 557-615.

IDNURM, A., BAHN, Y. S., NIELSEN, K., LIN, X., FRASER, J. A. & HEITMAN, J. 2005. Deciphering the model pathogenic fungus Cryptococcus neoformans. *Nat Rev Microbiol,* 3**,** 753-64.

JIANG, C., TING, A. T. & SEED, B. 1998. PPAR-gamma agonists inhibit production of monocyte inflammatory cytokines. *Nature,* 391**,** 82-6.

KHANIM, F. L., HAYDEN, R. E., BIRTWISTLE, J., LODI, A., TIZIANI, S., DAVIES, N. J., RIDE, J. P., VIANT, M. R., GUNTHER, U. L., MOUNTFORD, J. C., SCHREWE, H.,

GREEN, R. M., MURRAY, J. A., DRAYSON, M. T. & BUNCE, C. M. 2009. Combined bezafibrate and medroxyprogesterone acetate: potential novel therapy for acute myeloid leukaemia. *PLoS One,* 4**,** e8147.

KIM, J. J., CASTEEL, D. E., HUANG, G., KWON, T. H., REN, R. K., ZWART, P., HEADD, J. J., BROWN, N. G., CHOW, D. C., PALZKILL, T. & KIM, C. 2011. Co-crystal structures of PKG Iβ (92-227) with cGMP and cAMP reveal the molecular details of cyclic-nucleotide binding. *PLoS One,* 6**,** e18413.

KLEIN, D. A. & CASIDA, L. E. 1967. Occurrence and enumeration of Bdellovibrio bacteriovorus in soil capable of parasitizing Escherichia coli and indigenous soil bacteria. *Can J Microbiol,* 13**,** 1235-41.

KOZEL, T. R. & GOTSCHLICH, E. C. 1982. The capsule of cryptococcus neoformans passively inhibits phagocytosis of the yeast by macrophages. *J Immunol,* 129**,** 1675-80.

KRASTEVA, P. V., GIGLIO, K. M. & SONDERMANN, H. 2012. Sensing the messenger: The diverse ways that bacteria signal through c-di-GMP. *Protein Sci,* 21**,** 929-48.

KRONSTAD, J. W., ATTARIAN, R., CADIEUX, B., CHOI, J., D'SOUZA, C. A., GRIFFITHS, E. J., GEDDES, J. M., HU, G., JUNG, W. H., KRETSCHMER, M., SAIKIA, S. & WANG, J. 2011. Expanding fungal pathogenesis: Cryptococcus breaks out of the opportunistic box. *Nat Rev Microbiol,* 9**,** 193-203.

KWON-CHUNG, K. J. & RHODES, J. C. 1986. Encapsulation and melanin formation as indicators of virulence in Cryptococcus neoformans. *Infect Immun,* 51**,** 218-23.

LAMARRE, A. G., STRALEY, S. C. & CONTI, S. F. 1977. Chemotaxis toward amino acids by Bdellovibrio bacteriovorus. *J Bacteriol,* 131**,** 201-7.

LAMBERT, C., FENTON, A. K., HOBLEY, L. & SOCKETT, R. E. 2011. Predatory Bdellovibrio bacteria use gliding motility to scout for prey on surfaces. *J Bacteriol,* 193**,** 3139-41.

LAMBERT, C., MOREHOUSE, K. A., CHANG, C. Y. & SOCKETT, R. E. 2006. Bdellovibrio: growth and development during the predatory cycle. *Curr Opin Microbiol,* 9**,** 639-44.

LAMBERT, C., SMITH, M. C. & SOCKETT, R. E. 2003. A novel assay to monitor predator-prey interactions for Bdellovibrio bacteriovorus 109 J reveals a role for methyl-accepting chemotaxis proteins in predation. *Environ Microbiol,* 5**,** 127-32.

LERNER, T. R., LOVERING, A. L., BUI, N. K., UCHIDA, K., AIZAWA, S., VOLLMER, W. & SOCKETT, R. E. 2012. Specialized peptidoglycan hydrolases sculpt the intra-bacterial niche of predatory Bdellovibrio and increase population fitness. *PLoS Pathog,* 8**,** e1002524.

LEVITZ, S. M., NONG, S. H., SEETOO, K. F., HARRISON, T. S., SPEIZER, R. A. & SIMONS, E. R. 1999. Cryptococcus neoformans resides in an acidic phagolysosome of human macrophages. *Infect Immun,* 67**,** 885-90.

LOVERING, A. L., CAPENESS, M. J., LAMBERT, C., HOBLEY, L. & SOCKETT, R. E. 2011. The structure of an unconventional HD-GYP protein from Bdellovibrio reveals the roles of conserved residues in this class of cyclic-di-GMP phosphodiesterases. *MBio,* 2.

MA, H., CROUDACE, J. E., LAMMAS, D. A. & MAY, R. C. 2006. Expulsion of live pathogenic yeast by macrophages. *Curr Biol,* 16**,** 2156-60.

MA, H. & MAY, R. C. 2009. Chapter 5 Virulence in Cryptococcus Species. *In:* ALLEN I. LASKIN, S. S. A. G. M. G. (ed.) *Advances in Applied Microbiology.* Academic Press.

MEDINA, A. A. & KADOURI, D. E. 2009. Biofilm formation of Bdellovibrio bacteriovorus host-independent derivatives. *Res Microbiol,* 160**,** 224-31.

MINASOV, G., PADAVATTAN, S., SHUVALOVA, L., BRUNZELLE, J. S., MILLER, D. J., BASLÉ, A., MASSA, C., COLLART, F. R., SCHIRMER, T. & ANDERSON, W. F. 2009. Crystal structures of YkuI and its complex with second messenger cyclic Di-GMP suggest catalytic mechanism of phosphodiester bond cleavage by EAL domains. *J Biol Chem,* 284**,** 13174-84.

MONARI, C., BISTONI, F. & VECCHIARELLI, A. 2006. Glucuronoxylomannan exhibits potent immunosuppressive properties. *FEMS Yeast Res,* 6**,** 537-42.

NOSANCHUK, J. D., RUDOLPH, J., ROSAS, A. L. & CASADEVALL, A. 1999. Evidence that Cryptococcus neoformans is melanized in pigeon excreta: implications for pathogenesis. *Infect Immun,* 67**,** 5477-9.

NOVERR, M. C., COX, G. M., PERFECT, J. R. & HUFFNAGLE, G. B. 2003. Role of PLB1 in pulmonary inflammation and cryptococcal eicosanoid production. *Infect Immun,* 71**,** 1538-47.

NOVERR, M. C., PHARE, S. M., TOEWS, G. B., COFFEY, M. J. & HUFFNAGLE, G. B. 2001. Pathogenic yeasts Cryptococcus neoformans and Candida albicans produce immunomodulatory prostaglandins. *Infect Immun,* 69**,** 2957-63.

NÚÑEZ, M. E., MARTIN, M. O., CHAN, P. H. & SPAIN, E. M. 2005. Predation, death, and survival in a biofilm: Bdellovibrio investigated by atomic force microscopy. *Colloids Surf B Biointerfaces,* 42**,** 263-71.

OKAGAKI, L. H., STRAIN, A. K., NIELSEN, J. N., CHARLIER, C., BALTES, N. J., CHRÉTIEN, F., HEITMAN, J., DROMER, F. & NIELSEN, K. 2010. Cryptococcal cell morphology affects host cell interactions and pathogenicity. *PLoS Pathog,* 6**,** e1000953.

OKAGAKI, L. H., WANG, Y., BALLOU, E. R., O'MEARA, T. R., BAHN, Y. S., ALSPAUGH, J. A., XUE, C. & NIELSEN, K. 2011. Cryptococcal titan cell formation is regulated by G-protein signaling in response to multiple stimuli. *Eukaryot Cell,* 10**,** 1306-16.

PARK, B. J., WANNEMUEHLER, K. A., MARSTON, B. J., GOVENDER, N., PAPPAS, P. G. & CHILLER, T. M. 2009. Estimation of the current global burden of cryptococcal meningitis among persons living with HIV/AIDS. *AIDS,* 23**,** 525-30.

RICOTE, M., LI, A. C., WILLSON, T. M., KELLY, C. J. & GLASS, C. K. 1998. The peroxisome proliferator-activated receptor-gamma is a negative regulator of macrophage activation. *Nature,* 391**,** 79-82.

RIVERA, J., FELDMESSER, M., CAMMER, M. & CASADEVALL, A. 1998. Organ-dependent variation of capsule thickness in Cryptococcus neoformans during experimental murine infection. *Infect Immun,* 66**,** 5027-30.

RODRIGUES, M. L., NIMRICHTER, L., OLIVEIRA, D. L., FRASES, S., MIRANDA, K., ZARAGOZA, O., ALVAREZ, M., NAKOUZI, A., FELDMESSER, M. & CASADEVALL, A. 2007. Vesicular polysaccharide export in Cryptococcus neoformans is a eukaryotic solution to the problem of fungal trans-cell wall transport. *Eukaryot Cell,* 6**,** 48-59.

ROSAS, A. L., NOSANCHUK, J. D., FELDMESSER, M., COX, G. M., MCDADE, H. C. & CASADEVALL, A. 2000. Synthesis of polymerized melanin by Cryptococcus neoformans in infected rodents. *Infect Immun,* 68**,** 2845-53.

RÖMLING, U., GOMELSKY, M. & GALPERIN, M. Y. 2005. C-di-GMP: the dawning of a novel bacterial signalling system. *Mol Microbiol,* 57**,** 629-39.

SANTANGELO, R., ZOELLNER, H., SORRELL, T., WILSON, C., DONALD, C., DJORDJEVIC, J., SHOUNAN, Y. & WRIGHT, L. 2004. Role of extracellular phospholipases and mononuclear phagocytes in dissemination of cryptococcosis in a murine model. *Infect Immun,* 72**,** 2229-39.

SANTANGELO, R. T., CHEN, S. C., SORRELL, T. C. & WRIGHT, L. C. 2005. Detection of antibodies to phospholipase B in patients infected with Cryptococcus neoformans by enzyme-linked immunosorbent assay (ELISA). *Med Mycol,* 43**,** 335-41.

SCHER, J. U. & PILLINGER, M. H. 2005. 15d-PGJ2: the anti-inflammatory prostaglandin? *Clin Immunol,* 114**,** 100-9.

SCHWUDKE, D., STRAUCH, E., KRUEGER, M. & APPEL, B. 2001. Taxonomic studies of predatory bdellovibrios based on 16S rRNA analysis, ribotyping and the hit locus and characterization of isolates from the gut of animals. *Syst Appl Microbiol,* 24**,** 385-94.

SHEA, J. M., HENRY, J. L. & DEL POETA, M. 2006. Lipid metabolism in Cryptococcus neoformans. *FEMS Yeast Res,* 6**,** 469-79.

SIAFAKAS, A. R., SORRELL, T. C., WRIGHT, L. C., WILSON, C., LARSEN, M., BOADLE, R., WILLIAMSON, P. R. & DJORDJEVIC, J. T. 2007. Cell wall-linked cryptococcal phospholipase B1 is a source of secreted enzyme and a determinant of cell wall integrity. *J Biol Chem,* 282**,** 37508-14.

SINGER, P., SHAPIRO, H., THEILLA, M., ANBAR, R., SINGER, J. & COHEN, J. 2008. Anti-inflammatory properties of omega-3 fatty acids in critical illness: novel mechanisms and an integrative perspective. *Intensive Care Med,* 34**,** 1580-92.

SINGH, S. M. & PANDA, A. K. 2005. Solubilization and refolding of bacterial inclusion body proteins. *J Biosci Bioeng,* 99**,** 303-10.

SOCKETT, R. E. 2009. Predatory lifestyle of Bdellovibrio bacteriovorus. *Annu Rev Microbiol,* 63**,** 523-39.

STRALEY, S. C. & CONTI, S. F. 1977. Chemotaxis by Bdellovibrio bacteriovorus toward prey. *J Bacteriol,* 132**,** 628-40.

STUDIER, F. W. 2005. Protein production by auto-induction in high density shaking cultures. *Protein Expr Purif,* 41**,** 207-34.

TAL, R., WONG, H. C., CALHOON, R., GELFAND, D., FEAR, A. L., VOLMAN, G., MAYER, R., ROSS, P., AMIKAM, D., WEINHOUSE, H., COHEN, A., SAPIR, S., OHANA, P. & BENZIMAN, M. 1998. Three cdg operons control cellular turnover of cyclic di-GMP in Acetobacter xylinum: genetic organization and occurrence of conserved domains in isoenzymes. *J Bacteriol,* 180**,** 4416-25.

TCHIGVINTSEV, A., XU, X., SINGER, A., CHANG, C., BROWN, G., PROUDFOOT, M., CUI, H., FLICK, R., ANDERSON, W. F., JOACHIMIAK, A., GALPERIN, M. Y., SAVCHENKO, A. & YAKUNIN, A. F. 2010. Structural insight into the mechanism of c-di-GMP hydrolysis by EAL domain phosphodiesterases. *J Mol Biol,* 402**,** 524-38.

THOMASHOW, L. S. & RITTENBERG, S. C. 1985. Isolation and composition of sheathed flagella from Bdellovibrio bacteriovorus 109J. *J Bacteriol,* 163**,** 1047-54.

THOMASHOW, M. F. & RITTENBERG, S. C. 1978a. Intraperiplasmic growth of Bdellovibrio bacteriovorus 109J: attachment of long-chain fatty acids to escherichia coli peptidoglycan. *J Bacteriol,* 135**,** 1015-23.

THOMASHOW, M. F. & RITTENBERG, S. C. 1978b. Intraperiplasmic growth of Bdellovibrio bacteriovorus 109J: solubilization of Escherichia coli peptidoglycan. *J Bacteriol,* 135**,** 998-1007.

TONTONOZ, P., NAGY, L., ALVAREZ, J. G., THOMAZY, V. A. & EVANS, R. M. 1998. PPARgamma promotes monocyte/macrophage differentiation and uptake of oxidized LDL. *Cell,* 93**,** 241-52.

TSUMOTO, K., EJIMA, D., KUMAGAI, I. & ARAKAWA, T. 2003. Practical considerations in refolding proteins from inclusion bodies. *Protein Expr Purif,* 28**,** 1-8.

VAN DER POUW KRAAN, T. C., BOEIJE, L. C., SMEENK, R. J., WIJDENES, J. & AARDEN, L. A. 1995. Prostaglandin-E2 is a potent inhibitor of human interleukin 12 production. *J Exp Med,* 181**,** 775-9.

VOELZ, K., LAMMAS, D. A. & MAY, R. C. 2009. Cytokine signaling regulates the outcome of intracellular macrophage parasitism by Cryptococcus neoformans. *Infect Immun,* 77**,** 3450-7.

WILSON, C. J., ZHAN, H., SWINT-KRUSE, L. & MATTHEWS, K. S. 2007. The lactose repressor system: paradigms for regulation, allosteric behavior and protein folding. *Cell Mol Life Sci,* 64**,** 3-16.